# EXPERIMENTAL AND THEORETICAL STUDY OF SURFACTANT-BASED ACID DIVERTING MATERIALS

A Dissertation

by

ABDULWAHAB HUSSAIN A. ALGHAMDI

Submitted to the Office of Graduate Studies of
Texas A&M University
in partial fulfillment of the requirements for the degree of

DOCTOR OF PHILOSOPHY

December 2010

Major Subject: Petroleum Engineering

# EXPERIMENTAL AND THEORETICAL STUDY OF SURFACTANT-BASED ACID DIVERTING MATERIALS

A Dissertation

by

ABDULWAHAB HUSSAIN A. ALGHAMDI

Submitted to the Office of Graduate Studies of
Texas A&M University
in partial fulfillment of the requirements for the degree of

DOCTOR OF PHILOSOPHY

Approved by:

| | |
|---|---|
| Co-Chairs of Committee, | A. Dan Hill |
| | Hisham Nasr-El-Din |
| Committee Members, | David S. Schechter |
| | Victor Ugaz |
| | Peter Valko |
| Head of Department, | Stephen A. Holditch |

December 2010

Major Subject: Petroleum Engineering

# ABSTRACT

Experimental and Theoretical Study of Surfactant-Based Acid Diverting Materials.

(December 2010)

Abdulwahab Hussain A. Alghamdi, B.S., King Fahd University of Petroleum & Minerals; M.S., Texas A&M University

Co-Chairs of Advisory Committee: Dr. A. Dan Hill
Dr. Hisham Nasr-El-Din

The purpose of matrix stimulation in carbonate reservoirs is to bypass damaged zones and increase the effective wellbore area. This can be achieved by creating highly conductive flow channels known as wormholes. A further injection of acid will follow a wormhole path where the permeability has increased significantly, leaving substantial intervals untreated. Diverting materials such as surfactant-based acids plays an important role in mitigating this problem. In this study and for the first time, 20-inch long cores were used to conduct the acidizing experiments in two configurations, single coreflood and parallel coreflood.

The major findings from performing single coreflood experiments can be summarized as follows: The acid injection rate was found to be a critical parameter in maximizing the efficiency of using surfactant-based acids as a diverting chemical, in addition to creating wormholes. The maximum apparent viscosity, which developed during viscoelastic surfactant acid injection, occurred over a narrow range of acid injection rates. Higher injection rates were not effective in enhancing the acidizing

process, and the use of diverting material produced results similar to those of regular acids. The amount of calcium measured in the effluent samples suggests that, if the acid was injected below the optimum rate, it would allow the acid filtrate to extend further ahead of the wormhole; at some point, it would trigger the surfactant and form micelles. When the acid injection rate was lowered further to a value of 1.5 $cm^3$/min, the fluid front developed in more progressive fashion and the calcium concentration was more significant, continuing to increase until wormhole breakthrough

On the other hand, the parallel coreflood tests show several periods that can be identified from the shape of the flow rate distribution entering each core. The acid injection rate was confirmed as influencing the efficiency of the surfactant to divert acid. Acid diversion was noted to be most efficient at low rates (3 $cm^3$/min). No significant diversion was noted at high initial permeability ratios, at least for the given core length. The use of surfactant-based acid was also found to be constrained by the scale of the initial permeability ratio. For permeability ratios greater than about 10, diversion was insufficient.

# DEDICATION

This work is dedicated

To my father, who taught me that the best kind of knowledge to have is that which is learned for its own sake;

To my mother, who taught me that even the largest task can be accomplished if it is done one step at a time;

To my beloved wife, who offered me unconditional love and support throughout the course of this thesis;

To my daughter, Yara, the source of my inspiration.

To all my brothers and sisters, thanks for all you did for me and wishing you all good health.

## ACKNOWLEDGEMENTS

From the formative stages of this thesis to the final draft, I owe an immense debt of gratitude to the chairman of my graduate advisory committee, Dr. Dan Hill. His sound advice and careful guidance were invaluable.

Thank you to the co-chairman of my graduate advisory committee, Dr. Hisham Nasr-El-Din, for his endless support and continuous assistance in helping me to bring this research to completion.

Thank you to Dr. David Schechter, Dr. Victor Ugaz, and Dr. Peter Valko for serving as members of my advisory committee and for the knowledge I gained from them.

Thank you to my colleague Mohamed Nasr-El-Din for his assistance during the course of this research.

Thanks also to faculty and staff of the Harold Vance Department of Petroleum Engineering at Texas A&M University for providing the facilities and accommodations to conduct my research.

Finally, I would also like to thank the sponsors of the Middle East Carbonate Stimulation joint industry project at Texas A&M University for support of this work. Also, I would like to thank Saudi Aramco for giving me this opportunity to pursue my Ph.D. at a premier university in the petroleum engineering field.

# TABLE OF CONTENTS

Page

## LIST OF FIGURES

Page

Page

Page

## LIST OF TABLES

# CHAPTER I

# INTRODUCTION

## 1.1 Background

### 1.1.1 Surfactant-Based Acid as Diverting Material

The stimulation process starts by injecting an acid into a formation below the fracture pressure, which dissolves the carbonate minerals. The dissolution patterns created are known as wormholes. A relatively close permeability ratio is essential to ensure the proper placement of acid to stimulate the target zones. When such a condition is not present in the candidate formation, diversion is necessary for better acid placement. In this case, diverting materials play an important role in equalizing the flow, allowing untreated zones to be stimulated and thus, benefiting the overall productivity of the treated well. Historically, several techniques have been implemented for the aim of diverting the stimulation fluid to the target zones. These procedures can be classified into two main categories: mechanical and chemical.

Extensive laboratory testing has been conducted to evaluate the diversion of a viscoelastic surfactant-based acid system. Chang *et al.* (2001) conducted multi-core flood testing, incorporating a post acidizing computed tomography (CT) scan, which showed that self-diverting acid successfully diverted acid from the high permeability core into lower permeability core. Also, they observed that the rock face remained clean with no trace of residue.

---

This dissertation follows the style of *SPE Journal.*

The cores were 1-inch in diameter by 4-inches in length, and injection rates ranging from 5 to 10 $cm^3$/min were used simultaneously through all three cores. Lungwitz *et al.* (2006) demonstrated the diverting ability of the acid as a function of initial permeability, characterized by introducing the concept of maximum pressure ratio ($dP_{max}/dP_o$) supported by core-flow tests. They showed that the surfactant exhibits better clean-up behavior as demonstrated by the low flow initiation pressure (FIP) and high regained permeability, using gas or brine as a displacement fluid. Nasr-El-Din *et al.* (2006, 2009) conducted parallel flow testing on a similar type of surfactant material. In addition to what has been observed in the literature, they noticed that in all cases, the effluent volume through the lower permeability core was greater than through the higher permeability core. As a result, acid breakthrough occurred first with the lower permeability core. Tardy *et al.* (2007) developed a new set of parameters characterizing the reactive flow of a self-diverting acid, which were used later to model the process. They found that self-diverting acids are characterized by two parameters that can be expressed in terms of wormhole penetration and zonal coverage. Their experimental set-up combined multiple pressure taps along the core in an attempt to assess the displacement pattern in the core. They concluded that wormholes are virtually infinitely conductive and the build-up in viscosity occurs in the matrix around the wormhole.

These studies agree on the following: 1) the inlet face of the core is free from residue, indicating that surfactant fluids do not damage injectivity in the cores used; 2) offsets in pressure buildup between the lower permeability core and the higher permeability core were noted for all tests; 3) surfactant-based acid demonstrates superior

diversion capability by its sustained viscosity when pH increases above 2; and 4) surfactants exhibit similar or better cleanup behavior than do polymer-based acid systems.

Many questions remain regarding how diversion occurs as surfactant-based fluids flow inside the porous media and what parameters control the diverting process. Such questions can be addressed by utilizing long cores, and by measuring the concentration of acid, HCl, in the core effluent samples. To the best of the author's knowledge, these measurements were not conducted in previous studies dealing with surfactant-based acids. **Table 1** summarizes the most recent lab work conducted using parallel coreflood to study the flow of surfactant-based acid in porous media.

**TABLE 1-RECENT PUBLICATIONS ON COREFLOOD EXPERIMENTS USED TO STUDY THE BEHAVIOR OF SURFACTANT-BASED ACID IN POROUS MEDIA.**

| Reference | Length (inch) | Diameter (inch) | Aspect Ratio, L/D | Flow Rate ($cm^3$/min) | Temperature ($^oF$) | Lithology |
|---|---|---|---|---|---|---|
| Frank *et al.* 2001 | 4 | 1 | 4 | 5 to 10 | 150 | Indiana Limestone |
| Lungwitz *et al.* 2006 | 5 to 6 | 1 or 1.5 | 4.4 | 1 | Up to 240 | Indiana Limestone |
| Nasr-El-Din *et al.* 2006 | 2 | 1 | 2 | 5 | Up to 220 | Indiana Limestone |
| Tardy *et al.* 2007* | 6 | 1.5 | 4 | 13 | 150 | Indiana Limestone |
| Alghamdi *et al.* 2009 | 20 | 1.5 | 13 | 1.5 to 50 | Up to 180 | Pink desert limestone |

* In addition to linear core-flood, Tardy *et al*. (2007) conducted radial core-flood experiments

### 1.1.2 Optimum Injection Rate for Wormhole Propagation

The wormhole process is consistently a subject of interest for scientists, who put a great deal of effort toward understanding the process and describing the best design treatment to maximize the efficiency of the wormhole process and the overall acidizing treatment. Over the past 40 years, numerous studies that have addressed this subject can be classified into six categories (notice the citations include work by the earliest authors) : 1) understanding reactive dissolution in carbonate reservoir when acid is injected for stimulation purpose (Williams *et al.* (1979); Lund *et al.* (1973,1975); Daccord and Leonormand (1987)); 2) studying the influence of reaction and transport mechanisms on wormhole formation and optimum conditions for injection (Fredd and Fogler (1998); Buijse (1997); Bazin (2001)); 3) investigating the dependency of pore volume to breakthrough on acid concentration, temperature, porosity, and permeability (Talbot and Gdanski (2008)); 4) studying reactive dissolution in radial geometry (Daccord and Leonormand (1987); Frick *et al.* (1994)); 5) modeling the linear flow of acid under contained conditions by understanding the complexity of the dissolution phenomenon pattern (Daccord and Leonormand (1987) ; Williams *et al.* (1979); Hoefner and Fogler (1985, 1988)); 6) modeling wormhole formation under radial flow conditions (Daccord and Leonormand (1987); Pichler *et al.* (1992); Gdanski (1999)) ; 6) predicting the optimum injection rate under field conditions by extending the results from laboratory scale experiments and models to reservoir scale (Fredd and Fogler (1999); Bazin (2001)).

To obtain deep penetrating wormholes, three important parameters that can be controlled must be considered, as summarized by Glasbergen and Kalia (2009): fluid volume, injection flow rate, and fluid type.

The importance of fluid volume is realized from the fact that a larger amount leads to deeper fluid invasion and consequently deeper wormhole penetration. Lab work has shown that, when acid is injected at very low injection rate, no wormhole is observed, but the acid dissolved part of the rock, a phenomenon known as face dissolution. On the other hand, when acid is injected at an extremely high flow rate, such a strategy will result in a highly branched wormhole pattern known as ramified wormhole. It is believed that between these two extreme scenarios, an optimum injection rate exists that will lead to the deepest wormhole penetration, taking into consideration the acid volume to be injected. Plotting the $PV_{bt}$ verses injection rate shows a minimum number of $PV_{bt}$,which corresponds to optimum injection rate. Other factors affecting the wormhole propagation are based on the fluid types used in the acidizing job. Some will behave better for wormhole propagation under known reservoir conditions, such as temperature, mineralogy, and permeability. Therefore, an important step in the designing process includes selecting the acid type, concentration, and additives needed.

Most lab experiments published on this subject concern HCl in limestone cores. Further tests are required to understand the behavior of other fluids that retard acid spending, such as emulsified acids, surfactant-based acids and so on. The preliminary conclusions by Glasbergen *et al.* (2009) and Bazin (2001) indicated that for emulsified acids, no optimal wormhole injection rate exists in linear-core tests for plain HCl, but

not necessarily for more complex fluids under conditions that can be measured in the laboratory.

Another parameter increasing the complexity of understanding the mechanism of wormhole propagation is the fact that most laboratory wormhole tests utilize controlled conditions in linear cores. However, under field conditions, several other factors will play roles, as summarized by Abou-Sayed *et al.* (2005). Some of these factors are: radial flow instead of linear flow, injection flow rate limitation, heterogeneities in permeability, variation in reservoir pressure, heterogeneities in mineralogy, and variation in injection temperature. For example, in the case of radial flow, constant injection rate has been found to be inefficient for the wormhole-growth rate. This is because there is not a single optimal-pump rate, but it continues to increase with wormhole penetration depth (Tardy *et al.*(2007)).

## 1.2 Carbonate Acidizing and Acid Placement

### 1.2.1 Stimulation Technique

One of the most common reasons for a decline in oil production is “damage” to the formation that plugs the rock pores and acts as a barrier to the oil flow. Examples of the formation damage include: spent drilling fluid, fines migration, paraffin, mineral precipitation (scale). Another reason is that the formation is naturally tight (low permeability formations) which will result in a very slow movement of oil toward the wellbore.

In order to increase the net permeability of the reservoir and overcome the problems mentioned earlier, stimulation techniques can be applied. There are basically

three stimulation techniques: (1) injecting chemicals into the wellbore to react with and dissolve the damage (e.g., wellbore coating); (2) injecting chemicals through the wellbore and into the formation to react with and dissolve small portions of the formation to create alternative flow paths for the hydrocarbon; or (3) injecting chemicals through the wellbore and into the formation at pressures sufficient to actually fracture the formation. The subject of this study is related to the second stimulation technique and has some application to the third type. Abou-Sayed *et al.* (2005), Hutchins *et al.* (1996), Moradi-Araghi *et al.* (1988)

### 1.2.2 Geometry of the Wormhole and Pore Volume Breakthrough Concept

Two parameters control the reaction rates which result in dissolving rock formation when an acid, such as HCl, contacts the rock. These two parameters are the acid transport rate to the rock surface and the intrinsic reaction kinetics once acid reaches the rock surface. Several authors (William *et al.* (1979) and Hung (1987)) have investigated the nature of the reaction between HCl and calcite. The result shows that due to the fast reaction as acid contacts the rock, the reaction rate can be controlled by the rate of acid transfer to the reactive surface.

In matrix treatments, formation properties, such as permeability and porosity, determine the direction and magnitude of fluid flow, but these properties are continuously altered as a result of acid-rock dissolution.

Wormhole is a result of two physically distinct, but intrinsically connected, processes (Buijse *et al.* (1997), and Fredd and Fogler (1999):

1) The chemistry of acid reaction and acid spending in the tock pores and in wormholes, and
2) The physics of fluid loss from wormhole to formation and fluid distribution in a multiple wormhole geometry

Acid propagation can be described in three dissolution regimes, characterized by low injection rate (compact dissolution), optimum injection rate, and high injection rate (uniform dissolution). The three dissolution types are described below.

*Low injection rate and compact dissolution*: At a very low injection rate, or high diffusion rate, all acid will be spent on the wormhole wall before it reaches the tip. The wormhole propagation rate is zero and compact dissolution is the result. Compact dissolution must be avoided in matrix acid treatment in the field because it enlarges the wellbore diameter.

*Optimum injection rate*: The optimum injection rate is reached when the reduced wormhole propagation rate is at maximum. Also, the optimum rate depends on wormhole length. As the wormhole length increases, a higher injection rate is required to maintain sufficient live acid at the tip of the wormhole.

*High injection rate*: At a higher injection rate, only a small fraction of acid will be spent on the wormhole wall and a large fraction of acid will reach the tip. The result will be a highly branched, high-density wormhole pattern, comprising a thin wormhole.

Another concept used significantly in this study to describe the efficiency of the wormhole process is pore volume breakthrough. The pore volume to breakthrough (PVBT) ratio represents the volume of acid required for breakthrough to the pore volume

of the core. Two velocity components can be described in two wormhole process: wormhole velocity and interstitial velocity. Wormhole velocity is the ratio of interstitial velocity to PVBT, which is a measure of the velocity of the improved permeability front. Interstitial velocity is a measure of the velocity of the fluid front. Note that for most of the experiments in this study, the improved permeability front moved much faster than the fluid front. However, generally, the improved permeability front can be ahead of or behind the fluid front, depending on the type and concentration of acid used and injection rate.

### 1.2.3 Technique to Control Acid Placement

The techniques to control acid placement can be divided into either mechanical or chemical techniques. Mechanical techniques include ball sealers, packers and bridge plugs, coiled tubing and bull-heading.

The idea of ball sealers is to drop a ball into the wellbore to plug the perforations in the well casing, which will act as a sealant against fluid entry. An example of packers and bridge plugs, in particular, is straddle packers which is a mechanical device that plugs a portion of the wellbore and thereby inhibits fluid entry into the perforations around that portion of the wellbore. Coiled tubing is described as a mechanized reel, through which the acid can be delivered more precisely to locations within the wellbore. The last mechanical technique is bull-heading, which essentially depends on pumping the acid at the highest possible injection rate keeping in mind the injection pressure will not exceed the fracture pressure of the formation. **Fig.1** shows the classification of techniques to control acid placement.

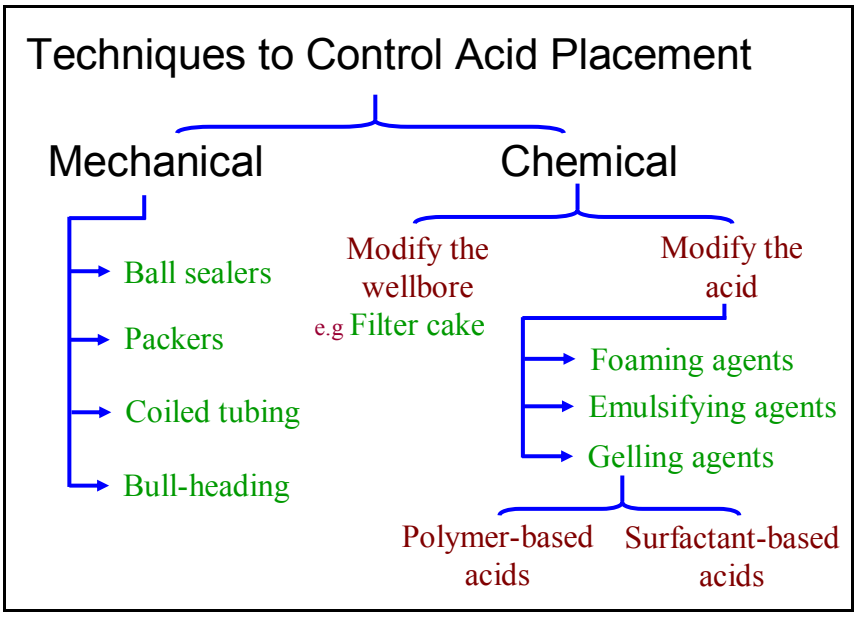


**Fig. 1— Techniques to control acid placement: 1) Mechanical; 2) Chemical. Surfactant-based acid is one method among several other techniques.**

Chemical techniques can be further divided into ones that chemically modify the wellbore, and ones that modify the acid-containing fluid itself. The first type involves materials that form a reduced-permeability cake on the wellbore face which, upon contact with the acid, will divert it to higher permeability regions. The second type includes foaming agents, emulsifying agents, and gelling agents.

The primary fluid used in acid treatments of chemical diversion systems directed at modifying the acid is hydrochloric acid. Emulsified acid systems and foamed systems are other commercially available responses to the diversion problem, the operational complexity of both systems and the limitation of the applications drive researchers to develop more sustainable systems with better operational capability. This leaves gelling agents as the class of diverters which this research studies. The principle behind this

system is to increase viscosity to makes it more difficult for the fluid to invade more permeable zones and push toward un-invaded zones. Depending on the viscosifiying agent, these systems can be divided into two main categories: polymer-based acids and surfactant-based acids. The present study is related to the second type of gelling agent. Lockhart and Albonico (1992), Sydansk (1995), Nasr-El-Din *et al*. (2004), and Shimizu *et al.* (2005).

To overcome potential problems associated with polymer-based acids, surfactant-based acids were introduced over the last 10 years. These systems are easy to mix in the field, and use fewer additives than those utilized in polymer-based acids. Surfactant-based acids have been extensively used in both matrix stimulation, and acid fracturing. Field application using surfactant-based acids have been very positive, as highlighted by several authors (Nasr-El-Din *et al.* (2008).

**1.3 Objectives**

The objectives of this work are to: 1) examine the propagation of surfactant-based fluids in carbonate cores, 2) conduct parallel coreflood experiments using 20 inches core length, 3) identify main parameters that affect the characteristics of generated wormholes, and (4) identify the conditions under which surfactant-based acids work as diverting agents. These objectives were achieved by conducting experiments using long cores, monitoring the pressure drop across the cores, and measuring the concentration of calcium ions and acid concentration in the core effluent. In addition, the cores were scanned with X-rays before and after injecting the subject acids into the core. Both regular and surfactant-based acids were tested.

# CHAPTER II

# EXPERIMENTAL STUDIES

## 2.1 Material

Two acid systems were used to conduct the acidizing experiments: regular and surfactant-based acids. Both acids contained 15 wt% HCl and a corrosion inhibitor (main components: methanol; aliphatic amide; and quaternary ammonium compounds). The surfactant-based acid contained 7.5 vol% of an amphoteric surfactant. Hydrochloric acid and water (total dissolved solids, TDS = 500 ppm) were used to prepare the acid solutions. The mixing procedure started by adding 0.3 vol% corrosion inhibitor to the water. Then, the surfactant was added at 7.5 vol%, followed by concentrated acid added to the mixture such that the final concentration was 15 wt% HCl. During the mixing procedure, a magnetic stirrer was used, which allowed working with small volumes without trapping air bubbles.

Based on the permeability requirement, three calcite rock types were used in this study: Austin cream chalk, Edward limestone , and Pink Desert. The cream chalk core samples had permeabilities around 5 md (within ±3 md). The Edward limestone cores had permeabilities of 20 to 60 md. The Pink Desert cores had permeabilities of 50 to 150 md. Since both cream chalk and Edward limestone are used extensively in the industry, I will keep the geological description limited to the Pink Desert type of rock. **Table 2** summarizes the geologic properties for the pink desert formation including the geology classification.

| TABLE 2— GEOLOGIC DESCRIPTION OF THE PINK DESERT FORMATION USED IN THE STUDY. | |
|---|---|
| **Parameter** | **Description** |
| **Rock type** | **Limestone** |
| **Color** | **Light pink** |
| **Bedding & sedimentary structures** | **No visible original depositional texture.** |
| **Dunham classification** | **Grainstone** |
| **Main grain types** | **Non skeletal/ peloid and crystalline. Dendritic growth forms of the widespread calcimicrobe organism (Epiphyton) are present in some places.** |
| **Visible porosity** | **Intercrystal and moldic** |
| **Cement matrix** | **Calcite as cement and matrix** |
| **Genetic classification of carbonate porosity** | **Hybrid 1 (hybrid of depositional and diagenetic processes)** |

CT imaging was conducted with a 4$^{th}$ generation CT scanner. In this technique, an X-ray beam from the CT scanner is attenuated when it passes through the carbonate sample. The attenuation depends on the density of the minerals and is calibrated to the bulk density if the rock. Volume unit in tomogarph are called voxels. In this work, the voxel size in the x- and y- directions (in-slice) is 0.48 mm and the slice distance in the z-direction was fixed at 2 mm. X-Ray CT scans were taken along the core. The cores were scanned from the inlet to the outlet of the core. The slice thickness and separation distance between slices were 2 mm and 5 mm, respectively. Auzerais *et al.* (1991), and Akin *et al.* (2003) provided more details on the CT scanning.

**2.2 Experiment Work Flow**

**Fig. 2** illustrates the sequence of the lab work followed to generate the necessary data. The procedure began by preparing the core sample, this include measuring the core weight before and after saturation, to measure the porosity and verify the value with the value measured using the CT. To ensure an adequate homogeneity of the core sample,

early in this study, a procedure was put in place to scan the core before the acidizing experiment. At this stage, the core sample was ready and the acidizing experiment performed. During the acidizing experiment , an automated fraction collector was attached to the outlet of the core–holder to allow the user to automatically collect the effluent samples as frequently as needed. This procedure was mainly applied if calcium analysis was part of the experimental procedure or in the case of parallel coreflood experiments, where the flow rate entered in each core was monitored to track the fluid distribution. During the test, $\Delta p$ was measured continuously. By this stage, the experiment was over and the effluent samples were used to measure volume and calcium using Atomic Absorption Spectroscopy. Also, HCl concentration can be measured. For image processing, both VoxlCalc and AVS software can be used to generate a cross sectional area for each slice along the core and a 3-D image for the wormhole. Other plots, such as pore volume breakthrough and pressure date analysis, were prepared for further discussion.

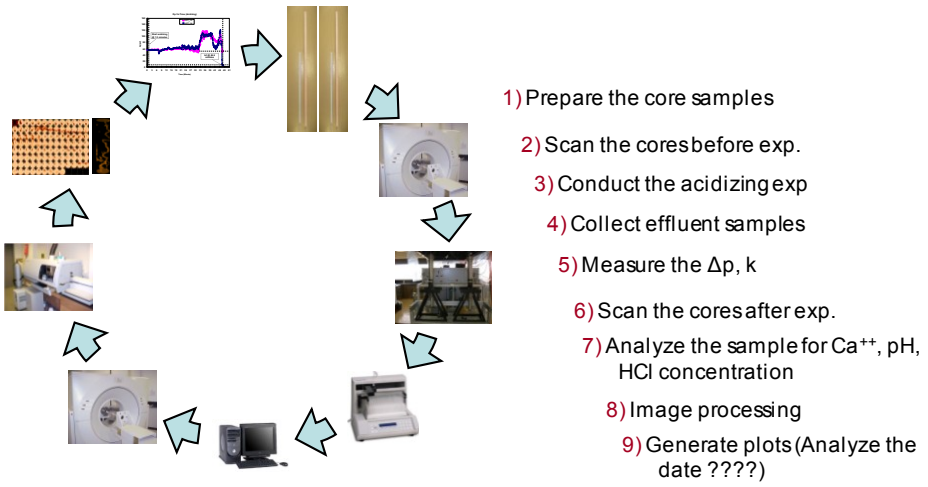


**Fig. 2—The flow work from sample preparation through final results.**

## 2.3 Surfactant Based-Acid System

### 2.3.1 Mechanism

The viscoelastic surfactant system used is a blend of an amphoteric surfactant and solvents. This surfactant is carboxybetaine with a general formula of R-CO-NH-$(CH_2)_n$-$N^+$-$(CH_3)_2$-$(CH_2)_P$-$COO^-$, where R = a hydrocarbyl group. The quaternary group carries a positive charge (cationic) in live acids. Once the acid reacts with carbonate rocks (Eqs. 1 and 2) and the pH increases to a value greater than the isoelectric point, pH 2 to 3, the carboxylic group carries a negative charge and the surfactant acts as a zwitterionic surfactant (i.e., carries positive and negative charges at the same time).

$CaCO_3 + 2\ HCl \rightarrow CaCl_2 + CO_2 + H_2O$.....(1)

$CaMg(CO_3)_2 + 4\ HCl \rightarrow CaCl_2 + MgCl_2 + 2\ CO_2 + 2\ H_2O$.....(2)

One possible explanation for the viscosity build-up is that surfactant molecules form rod-shaped micelles when the pH values increase to a value greater than 2 and the

concentration of divalent cations ($Ca^{2+}$ and $Mg^{2+}$) increases in the spent acid. The rod-shaped micelles will significantly increase the viscosity of the spent acid. Entanglement of these micelles results in a 3-D structure, which will further increase the apparent viscosity of the solution. In-situ build-up of apparent viscosity will divert the acid into tight un-stimulated and/or highly damaged zones.

To break the surfactant gel, one must convert the micelles from their rod-shaped structure into spherical ones. This can be done in water injectors by reducing the concentration of the surfactant and/or salts by dilution with the injection water. In oil or gas wells, the surfactant gel can be broken by mixing the gel with a hydrocarbon phase (oil or condensate). Pre and post flushes that include a mutual solvent (e.g., ethylene gylcol monobutyl ether) can be used in all wells to break the surfactant gel. Even though the system has been proven to be a self breaker, there have been recent improvements in developing internal breakers that can break gels with high surfactant concentrations. (Nasr-El-Din *et al.* (2008); Chang *et al.* (1999)).

There are several ways that viscoelastic surfactant can affect the reaction of acid with the rock. The viscoelastic surfactant will increase the viscosity of the acid, which reduces the rate of transfer of $H^+$ from the bulk solution to the surface of the formation. Viscoelastic surfactant molecules can absorb on the rock surface and form a barrier that reduces acid reaction with the rock. Finally, viscoelastic surfactant solutions are non-Newtonian fluids and can change the flow pattern close to surface of the rock, and therefore, affect the way the acid reacts with the rock.

Research on the effects of surfactant on the dissolution rate of calcite and the impact of a surfactant on the diffusion coefficient of $H^+$ was completed by AlMohamed *et al.* 2006. Based on their study the surfactant reduces both the dissolution rate of calcite with HCl acid and the diffusion coefficient for $H^+$.

The physical properties of viscoelastic surfactants are a complex function of surfactant type, concentration, additives, salinity, temperature, and shear rate. These properties are more complicated for betaine surfactants, where the rheological properties, surface tension, and adsorption characteristics depend on the pH level, in addition to the above mentioned parameters. Nasr-El-Din *et al.* (2008) invesigated more in depth how parameters such as concentration, additives, etc., affect the rheological properties of surfactant.

### 2.3.2 Why Surfactant-Based Acid

Chemical diverters can be achieved through placing viscous fluid into the matrix to decrease injectivity, using foam or particulate diverting agents which create a filter cake. This filter cake results in a temporary skin effect that alters the injection profile. For this reason, polymer and surfactant based acids are being used increasingly as a mean of improving acid placement. The polymer-based acid diversion stages provide a means of slowing down the acid reaction and increasing resistance to flow by a particular interval to allow diversion to another zone. This technique has been used successfully in diverting matrix acid treatment. Success has been achieved in controlling fluid loss in carbonates by using special polymer systems which viscosify and weakly crosslink, as the acid spends and pH increases. The cross-linked gel thus created is quite unstable and

begins to break down as the acid neutralizes with exposure to excess carbonate. The crosslink time, however, is generally sufficient to create resistance for the cross-linked, partially spent acid to leak off, thus creating sufficient back pressure to send subsequent volumes of acid to other portions of the interval. These types of polymer systems have been used successfully in a variety of wellbores, including horizontal wells. So, why has surfactant-based acid received considerable attention over the past 10 years?. **Table 3** summarizes the characteristic of each system; clearly, surfactants surpass the use of polymer for several reasons.

TABLE 3— SUMMARY OF POLYMER AND SURFACTANT DIVERTING SYSTEMS.

| Diversion system | Characteristics |
|---|---|
| Polymer-Based Acid | ▪ The in-situ gelled acids cause loss of core permeability in tight carbonate cores.<br>▪ Precipitation of the cross-linker (iron) at high temperature and in sour environment.<br>▪ $H_2S$ scavengers may interact with the polymer and lose their ability to remove hydrogen sulfide.<br>▪ Large volume normally needed.<br>▪ It could form external filter cake that reduces injectivity |
| Surfactant-Based Acid | ▪ Simple system requires minimum additives.<br>▪ Can be placed using bullheading or CT.<br>▪ Ability to break when coming into contact with hydrocarbons.<br>▪ High level of ferric iron can adversely affect the apparent viscosity.<br>▪ Requires fewer stages compared with other acid systems.<br>▪ Reduces friction loss in CT resulting in high pumping rate ~2.3 bpm.<br>▪ More economical as it can save an average of two days of rig time.<br>▪ Volume needed for the same treatment is less than PBS.<br>▪ Doesn't tolerate hydrocarbons, therefore, spacer needed.<br>▪ Shorter time is needed to lift spent acid due to reduction in surface tension. |

# CHAPTER III

# SINGLE COREFLOOD

## 3.1 Procedure

The sequence of the lab work followed to generate the necessary single coreflood data can be summarized as follows:

- Prepared the core sample including weighing the limestone core dry. Then, the core was saturated using fresh water with a TDS of 500 ppm. The weight measurement was used to calculate porosity and establish a baseline for the porosity estimated from the CT (Computed Tomographic) scans.
- Measured the initial permeability using fresh water.
- Conducted the acidizing experiment at a constant flow rate and monitored the pressure drop across the core.
- Collected effluent samples, using a fraction collector.
- Examined the core using the CT scan to characterize wormholes generated by acids.
- Analyzed the effluent samples for $Ca^{++}$ content, HCl concentration, and pH.

**Fig. 3** is a schematic diagram of the matrix acidizing set-up used in this study. A back pressure was necessary during the experiments in order to keep $CO_2$ in solution. Therefore, a back pressure regulator (model S91-W) was set at 1000 psi. Finally, the pressure drop was sensed with a set of FOXBORO differential pressure gauge models, IDP10-T26(C-D-E) 21F-M2L1. There were three gauges installed with ranges of 0-300 psi, 0-1500 psi, and 0-3000 psi. The calcium concentration in the core effluent samples

was measured by Atomic Absorption Spectroscopy (Analyst 700). To measure density and pH, an Orion model 950 meter and a Parmer NaOH single junction pH electrode were used.

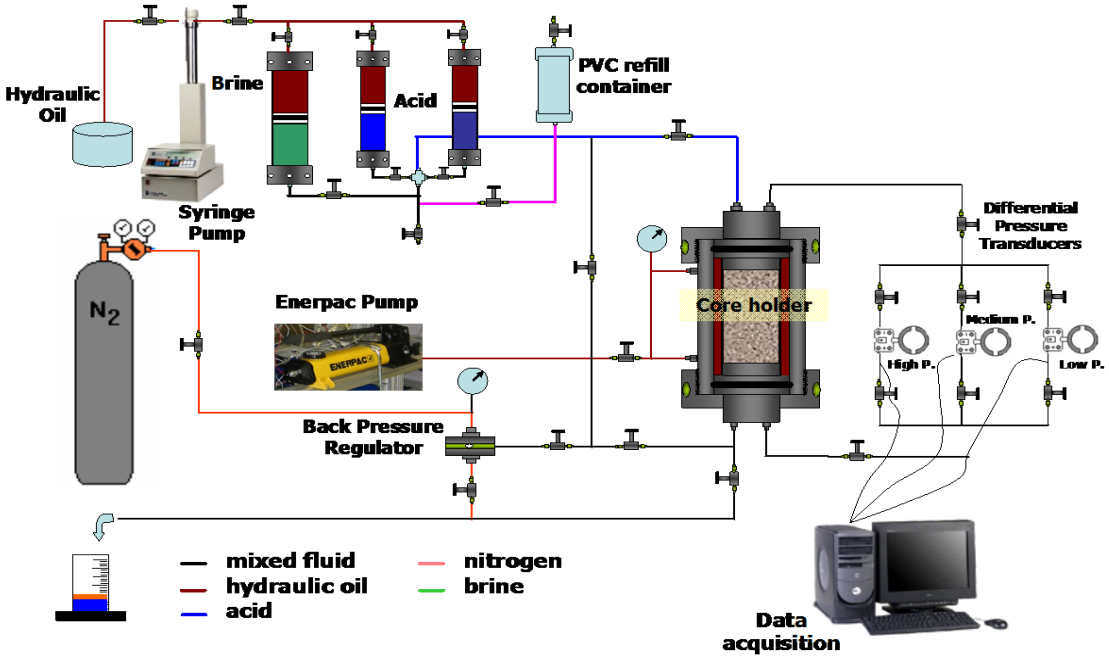


**Fig. 3— A schematic diagram of matrix acidizing set-up.**

The results obtained will be presented in two major parts. First, the flow of regular acid in calcite cores was examined. Second, the flow of surfactant-based acids was investigated.

### 3.2 Propagation of Regular Acid in Carbonate Cores

In section 3.2, four experiments conducted with regular acid at four different flow rates are presented. The flow rate was kept constant during each experiment, and the pressure drop across the core was monitored. A new core was used in each experiment. The four experiments were conducted to validate the experimental procedure, establish a baseline for wormhole characteristics and determine pH, calcium, and HCl concentrations in the effluent samples, which will enable us to gain insight regarding the nature of the chemical reaction takes place inside the core. These values will be compared later with those obtained when surfactant-based acid was used.

*Experiment #1 (Low injection rate)*

In experiment #1, the injection rate was 3 $cm^3$/min in order to establish a longer acid front. Therefore, calcium concentration was measured during the acidizing process for all effluent samples. **Table 4** gives the permeability, porosity, flow rate, and pore volume to breakthrough for this experiment and other experiments included in Chapter III.

| TABLE 4— SUMMARY OF COREFLOOD EXPERIMENTS; SINGLE COREFLOOD. | | | | | |
|---|---|---|---|---|---|
| **Experiment #** | **Acid System** | **Initial Permeability (md)** | **Initial Porosity (vol%)** | **FlowRate ($cm^3$/min)** | **$PV_{bt}$** |
| **1** | **Regular Acid** | **66** | **23** | **3** | **1.32** |
| **2** | | **101** | **30** | **6.75** | **1.45** |
| **3** | | **95** | **28** | **15** | **0.97** |
| **4** | | **85** | **23** | **20** | **0.84** |
| | | | | | |
| **5** | **surfactant Acid** | **57** | **13** | **5.5** | **1.82** |
| **6** | | **73** | **20** | **15** | **1.23** |
| **7** | | **83** | **25** | **3** | **1.22** |

During the experiment, the pressure drop across the core was monitored. The pressure drop slightly decreased upon acid injection for long periods then started to decrease almost linearly with time, until acid breakthrough, **Fig. 4**. As expected, at acid breakthrough in the core, a sudden increase in the calcium concentration in the effluent sample was noted. Calcium levels reached an average of 120,100 g/l, as shown in **Fig. 5,** which is more than double that measured when the acid injection rate was 15 $cm^3$/min. The amount of calcium measured in the effluent samples suggests that as acid injected below the optimum rate allows the acid filtrate to extend further ahead of the wormhole. This is indicated by a significant increase in the amount of calcium measured in the effluent samples as the wormhole approaches the other end of the core. This observation proves to be an important aspect when surfactant-acid system is used, as demonstrated in section 3.3.

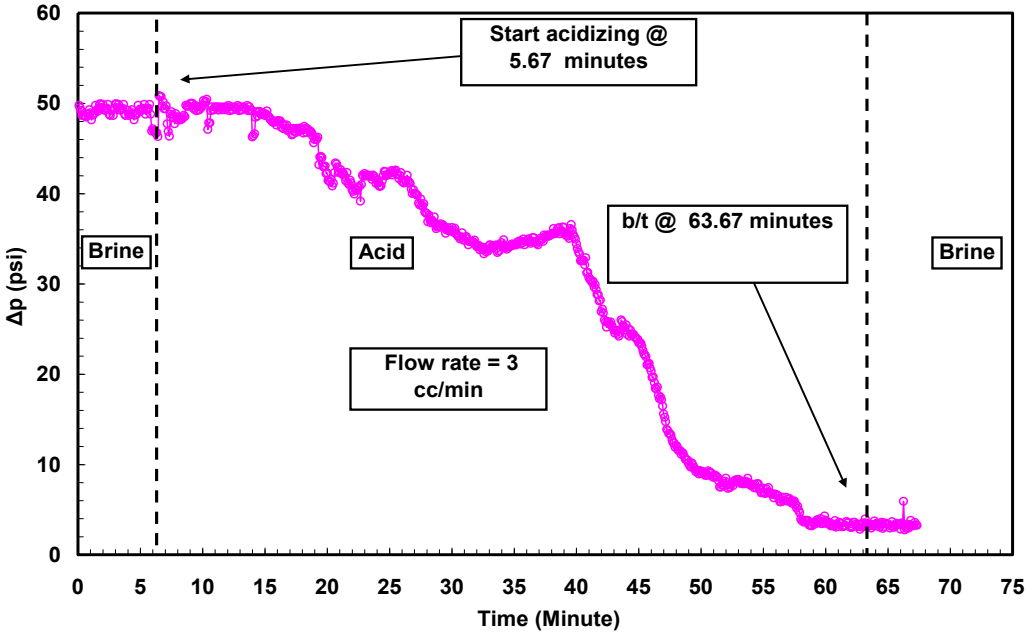


**Fig. 4— Pressure drop across the core; 15 wt% HCl; experiment (1).**

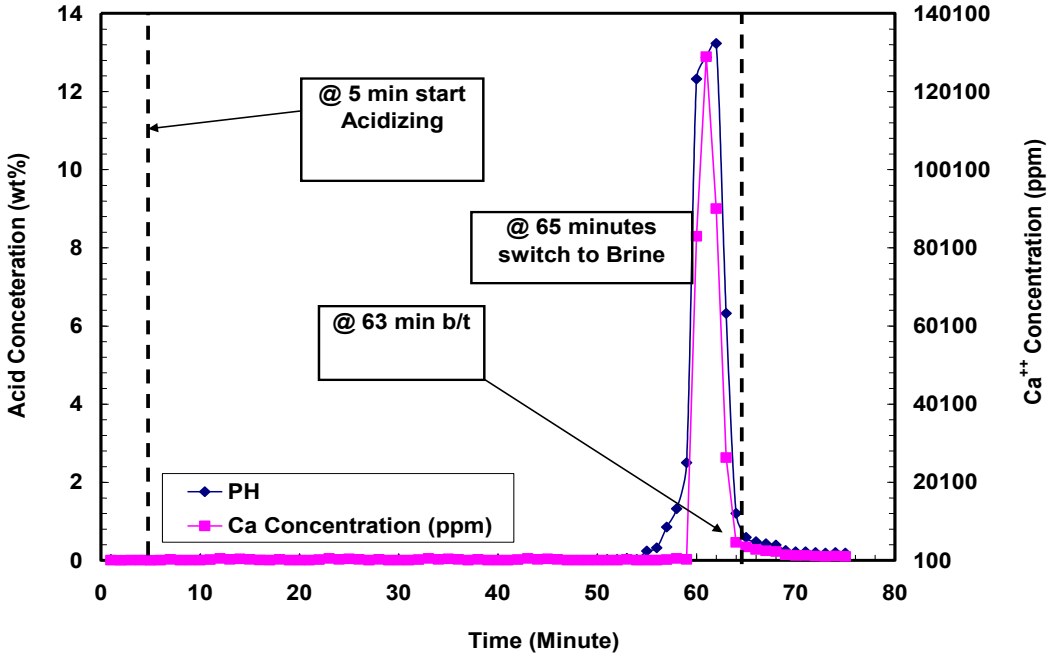


**Fig. 5—Acid concentration and calcium content (ppm) in the core effluent; experiment (1).**

**Fig. 6** shows a cross-sectional area for each slice along the core length after acidizing, combined with a 3-D visualization image for the wormhole. The spacing between each slice is set at 2 mm, which makes 100 slices per 20-inch single core. Notice that the diameter of the wormhole in the second half of the core was significantly smaller compared with the diameter of the wormhole in the first half of the core; this was not observed at the higher flow rate. The diameter of the wormhole in the second half of the core at an injection rate of 3 $cm^3$/min was 0.11 inch compared with 0.22 inch at an injection rate of 15 $cm^3$/min.

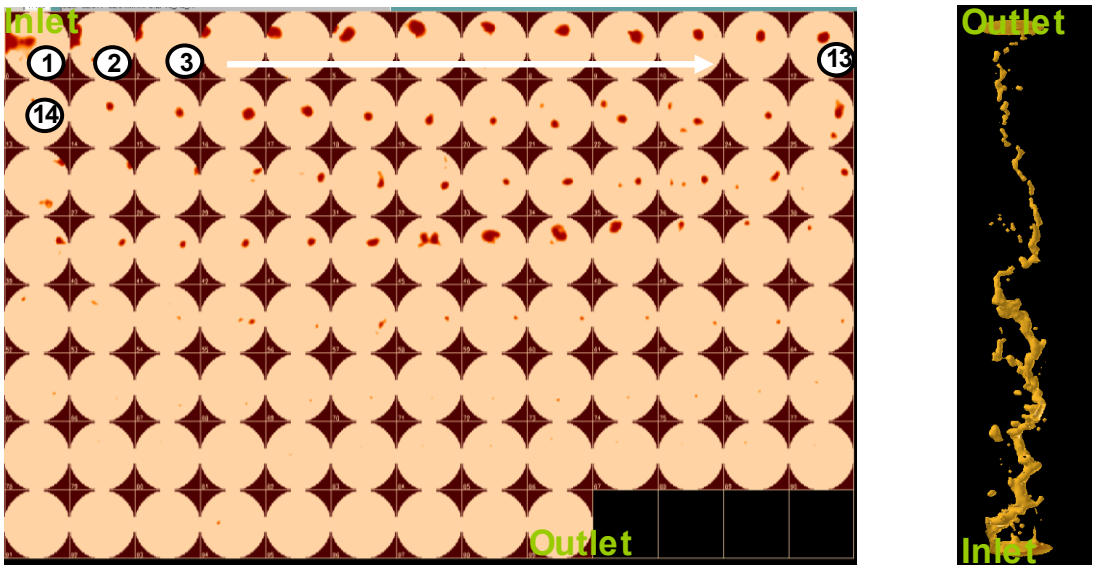


**Fig. 6— A cross sectional area for each slice along the core length after acidizing combined with a 3-D visualization image for the wormhole for experiment (1).**

*Experiment #2 (moderate injection rate)*

In experiment #2, acid was injected at a flow rate of 6.75 $cm^3$/min. During the experiment, the pressure drop across the core was monitored. The pressure drop slightly decreased upon acid injection, then started to decrease almost linearly with time, until acid breakthrough, **Fig. 7.** After acid breakthrough, the pressure drop across the core was nearly zero.

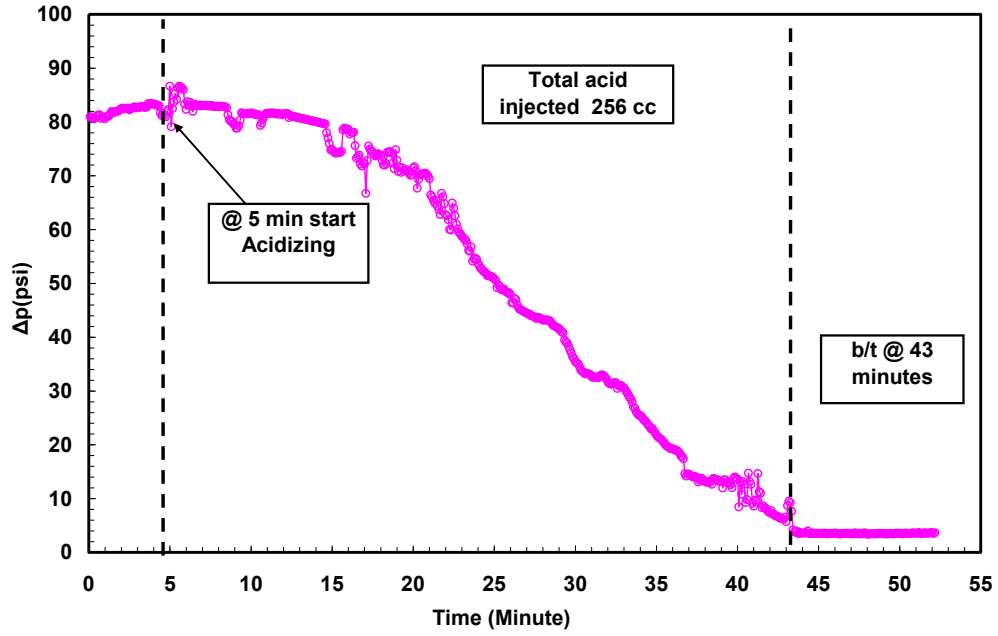


**Fig. 7— Typical pressure drop response during injection of regular 15 wt% HCl in limestone cores at 6.75 $cm^3$/min at room temperature, experiment (2).**

**Fig. 8** shows a cross-sectional area for each slice along the core length after acidizing, combined with a 3-D visualization image for the wormhole.

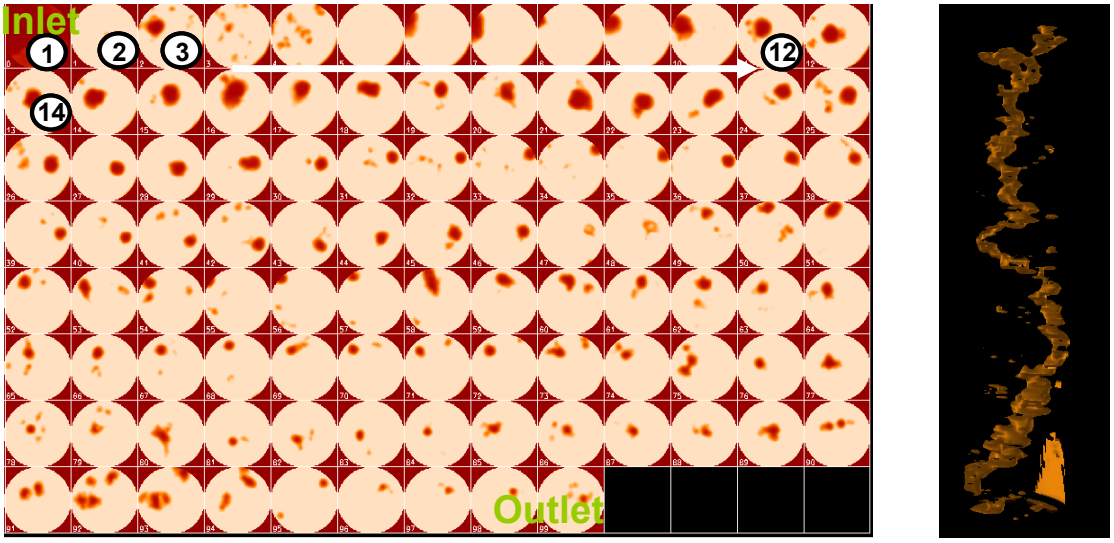


**Fig. 8— A cross sectional area for each slice along the core length after acidizing combined with a 3-D visualization image for the wormhole for experiment (2).**

*Experiment #3 (high injection rate)*

In the third experiment, the acid injection rate was increased to 15 $cm^3$/min. The pressure drop across the core changed with time in a manner similar to that noted at the lower flow rate. However, the initial period where the pressure slightly declined was much shorter. This period represents the time for the acid to initiate the wormhole and consequently, pressure drop occurred thereafter. The higher the injection rate the faster the wormhole can be initiated, **Fig. 9**. In this experiment, it took less time for the acid to break through the core compared to the lower injection rate. Acid breakthrough occurred

after 15 minutes of acid injection. Acid continued to be injected for another five minutes before switching to brine.

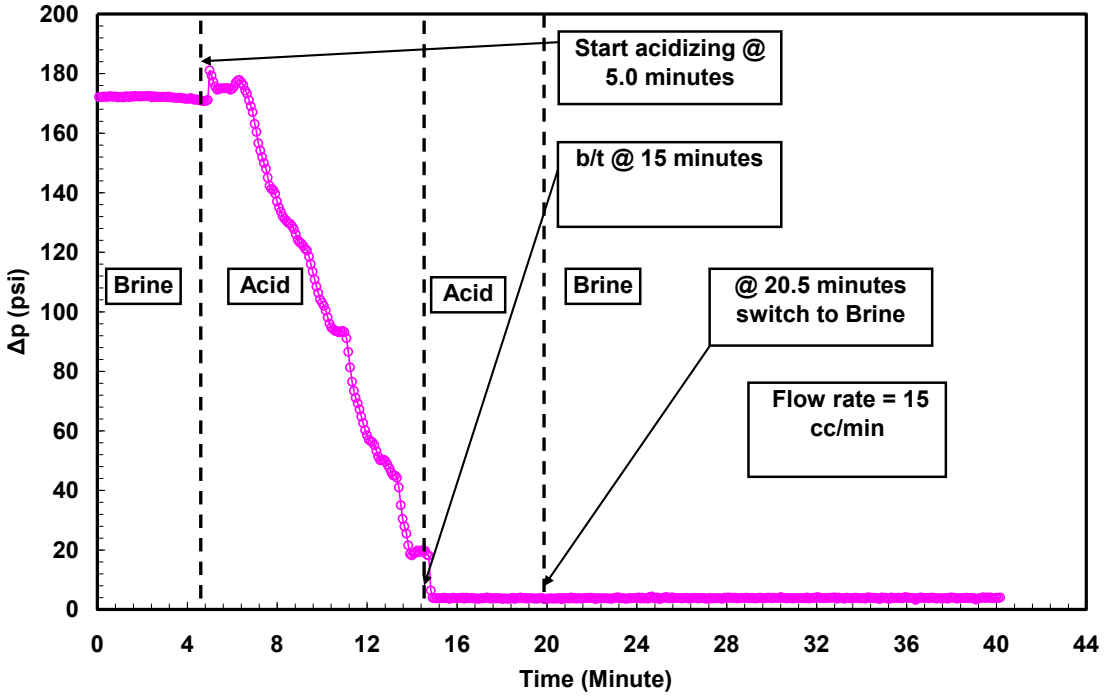


**Fig. 9— Pressure drop across the core. Acid injection continued after breakthrough to confirm the acid strength as wormhole propagated inside the core; 15 wt% HCl; experiment (3).**

Calcium concentration was measured in the core effluent samples before acid breakthrough and was found to be ~ 2,000 ppm. With acid breakthrough from the core, a sudden increase in the calcium concentration in the effluent sample was noted. Calcium levels reached an average of 55,000 ppm, **Fig. 10**. Five minutes after acid breakthrough, the $Ca^{++}$ concentration dropped to the initial value. The HCl concentration in the collected samples was not significant before acid breakthrough, which mainly

represents the unacidized zone followed by the acid filtrate. However, after wormhole breakthrough, the average HCl concentration increased to 8 wt% HCl. This concentration represents acid strength at the tip of the wormhole at acid breakthrough. The pH profile, another indication of acid concentration, was measured during the acidizing experiment, as shown in **Fig. 10**. The pH value was measured as basic in all the effluent samples. However, after acid breakthrough, the pH value was negative until all acid was flushed from the core. At the end of the experiment, the pH value level was nearly 2.

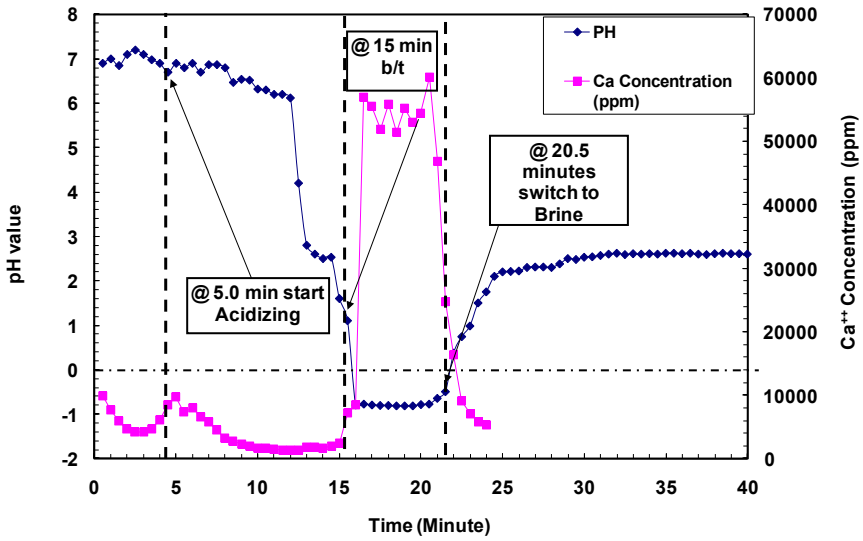


**Fig. 10—The pH and calcium concentration (ppm) in the core effluent; experiment (3).**

**Fig. 11** shows a cross-sectional area for each slice along the core length after acidizing combined with a 3-D visualization image for the wormhole. The wormhole

diameter was observed to be almost constant throughout the core length and measured to be 0.22 inch.

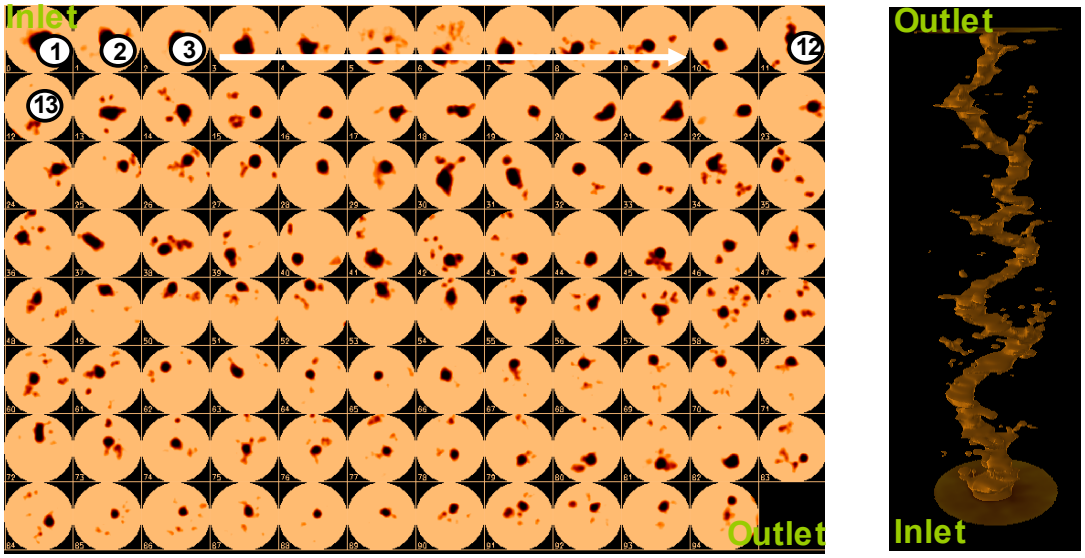


**Fig. 11— A cross sectional area for each slice along the core length after acidizing combined with a 3-D visualization image for the wormhole for experiment (3).**

*Experiment #4 (high injection rate)*

In the fourth experiment, the flow rate was further increased to 20 $cm^3$/min. The period of slight decrease in the pressure drop almost disappeared, and the pressure drop decreased nearly the entire time the acid was being injected, **Fig. 12**. The acid breakthrough occurred after 5.8 minutes of acid injection. **Fig. 13** shows the pH measurements for the effluent sample for a given acid concentration

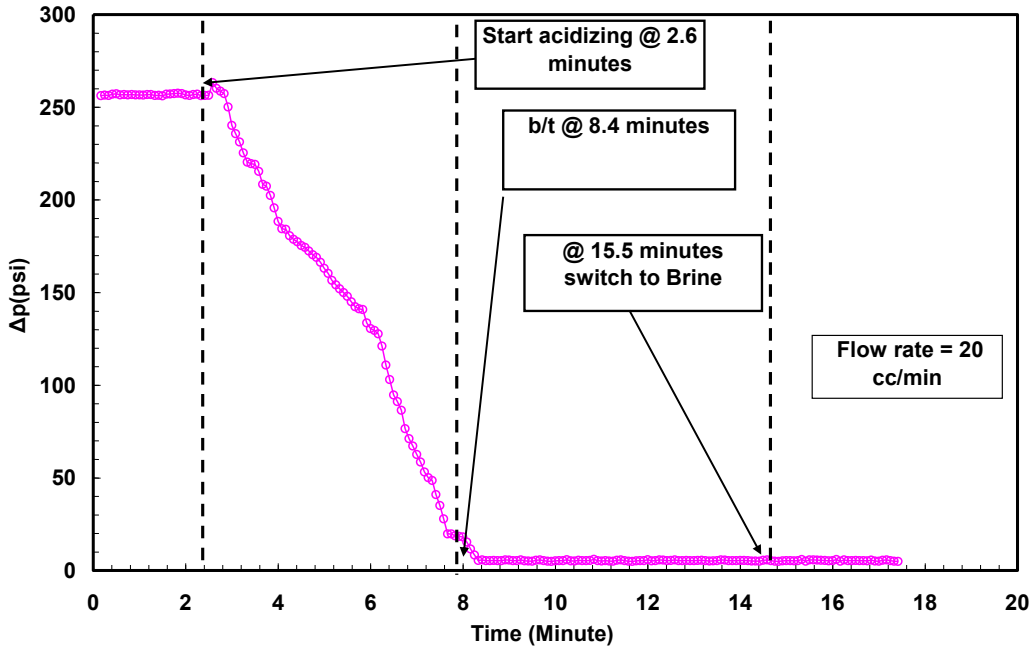


**Fig. 12— Pressure drop across the core. Acid was injected after breakthrough to confirm the acid strength as wormhole propagated inside the core, experiment (4).**

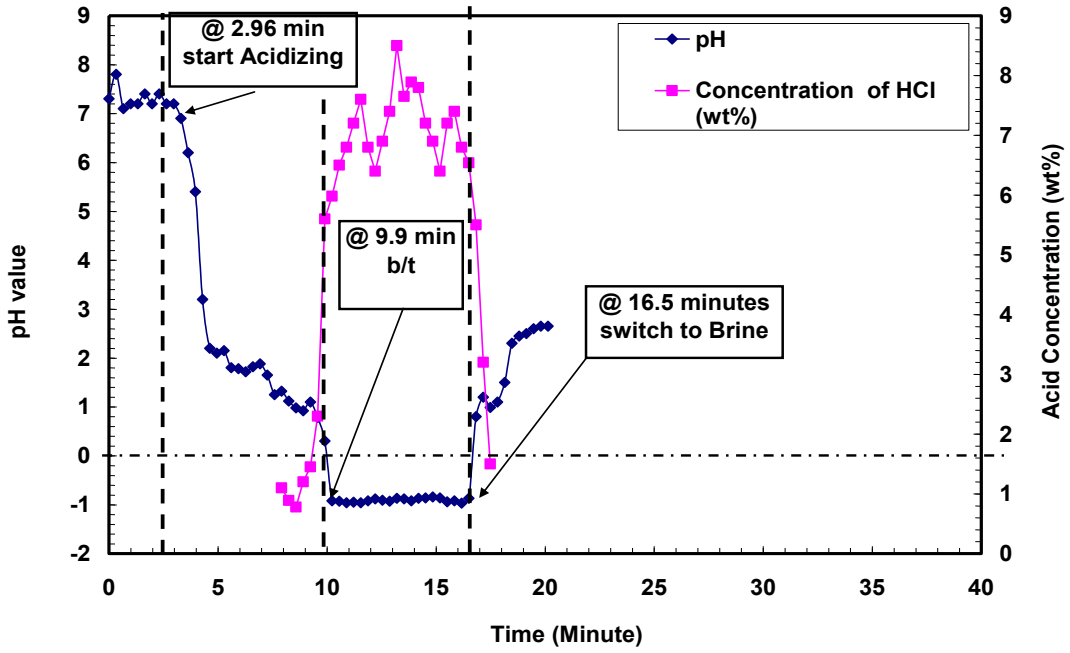


**Fig. 13—pH and acid concentration for the effluent samples.**

**Fig. 14** compares the normalized pressure drop as a function of pore volume injected until acid breakthrough at different rates. At a relatively high injection rate, the pressure drop can be correlated linearly with the pore volume injected. However, as the acid injection decreases to 3 $cm^3$/min, as illustrated in **Fig. 14,** the linear correlation is represented by different slopes. The slope was less steep as the acid injection decreased, which allowed the acid to leak off more in the direction perpendicular to the main acid flow path. This can be represented by different slopes, as well as higher pore volume to breakthrough at a lower injection rate (1.32 compared with 0.97). The pressure decline was noticeably sharper as the wormhole propagated more inside the core. **Fig. 15** shows the shape of the wormhole as the acid injection rate changed. Clearly, at 3 $cm^3$/min, the wormhole tended to be thinner as the wormhole propagated further inside the core until acid breakthrough, as previously discussed. Notice the scale on **Fig. 15** corresponding to different setting during the scanning procedure. To be able to compare the diameter of wormholes at different flow rates, **Fig. 16** shows the first 5 inches of the each wormhole using the same scale.

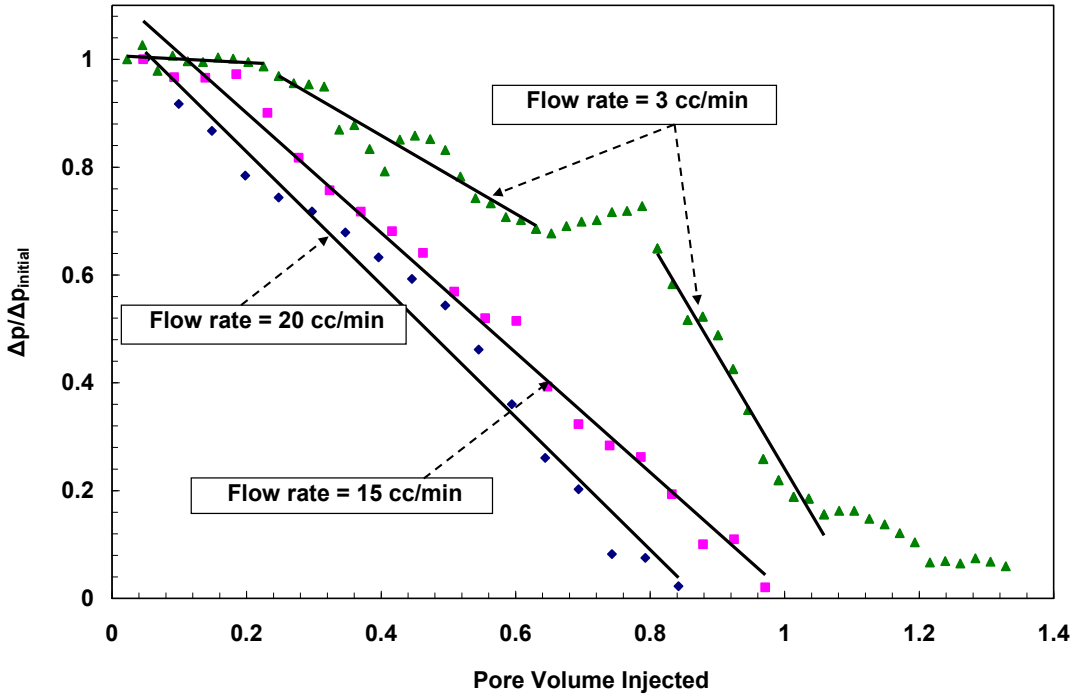


**Fig. 14— Normalized pressure drop as a function of pore volume injected until acid breakthrough; 15 wt% HCl.**

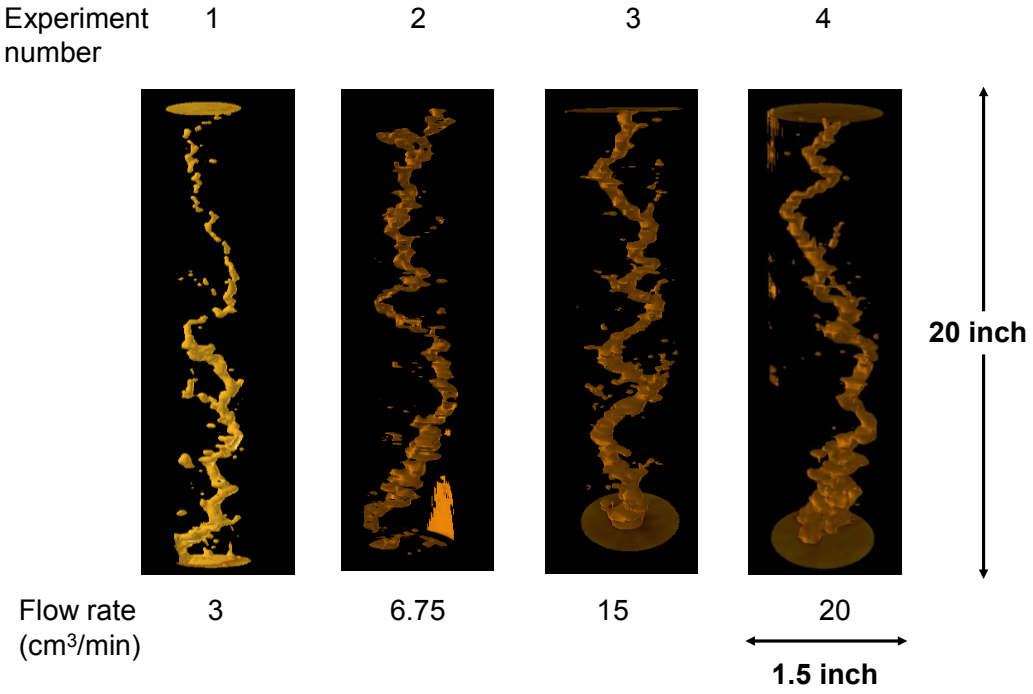


**Fig. 15— Shape of the wormhole at different flow rates; 15 wt% HCl.**

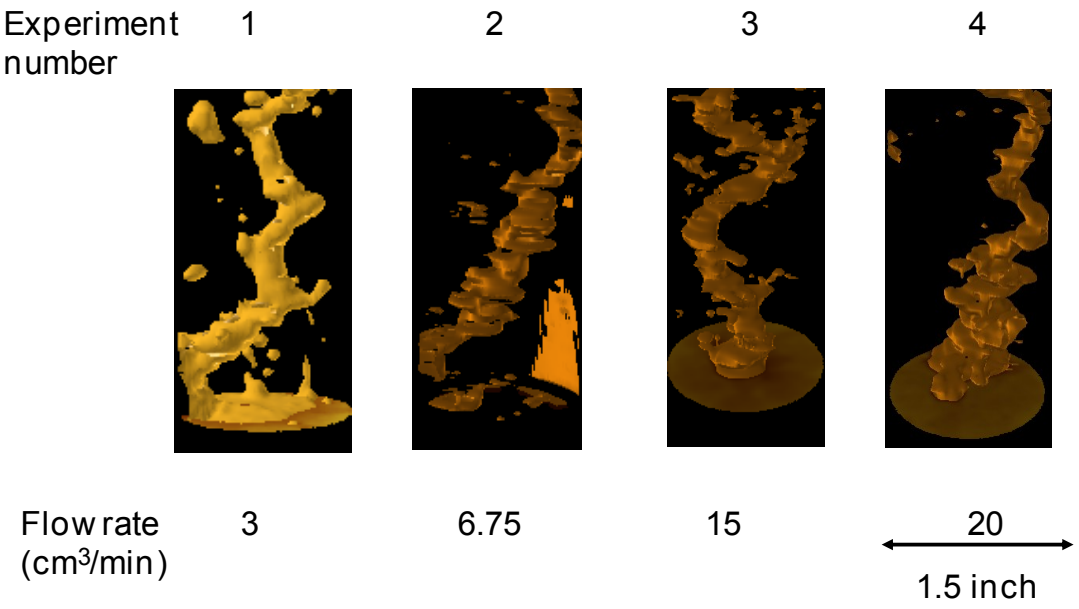


**Fig. 16— Comparing diameter of wormholes at different flow rate on the same scale.**

### 3.3 Propagation of Surfactant-Based Acid in Carbonate Cores

Next, three experiments were performed using 15 wt% HCl + 7.5 vol% surfactant + 0.3 vol% corrosion inhibitor injected into limestone single cores at flow rates of 3, 5.5 and 15 $cm^3$/min, respectively.

Depending on the injection rate, as acid enters the core, the Δp should increase differently, as illustrated in the next three experiments. The duration of this period and the magnitude of its frequency, combined with the maximum resistivity pressure that can be obtained, is crucial behavior to understand as it reflects the efficiency of the diverting material. As more live acid is injected in the core, it will allow the wormhole to propagate inside the filtrate zone causing a sharp reduction in pressure build-up. After reaching a minimum value, the process will repeat itself until wormhole breakthrough.

Clearly, this was not the case when regular acid was used, whereby the pressure drop declined linearly as acid entered the core and wormhole propagation began in the core.

Since the flow rate was kept constant, two mechanisms took place simultaneously while the acid was injected, thus affecting Δp differently.

Darcy's law for a linear flow assuming laminar flow/Newtonian fluid is

$$\Delta p = \frac{q\mu L}{kA} \quad \text{.....(3)}$$

The two mechanisms are in-situ viscosity and effective permeability. First, as the acid was injected, a wormhole was created, which increased the effective permeability of the core and decreased Δp. On the other hand, as the acid propagated in the core and the surfactant entanglement built up viscosity, the pressure drop increased. Now, the apparent viscosity changed according to the effective shear rate, which consists of two parts (Delshad et al., 2008): shear viscosity-dominant part, $\mu_{sh}$, and elongational-viscosity-dominant part, $\mu_{el}$:

$$\mu = \mu_{sh} + \mu_{el} \quad \text{.....(4)}$$

If elongated viscosity is significant, that could explain part of the process. As the elongated viscosity increases, Δp will increase to compensate for the pressure needed for a constant flow rate. The dominant mechanism will reflect Δp more by either lowering or increasing its value. As the acid flows in the wormhole, four periods can be identified as follows:

1. *Period A* ; this period contained the initial plateau expected in an acidizing experiment. The viscosity effect overcame any decrease in the pressure that could

possibly be caused by dissolving the rock matrix. The measured Δp prior to period A corresponded to the brine injection with a viscosity of nearly 1 cp. As self–diverting acid was injected, with a viscosity higher than the brine, Δp was expected to increase to maintain a constant flow rate. Several factors can affect Δp, including the characteristics of the core given by the permeability, flow rate and the acid system properties. Importantly, if the acid injection rate was low enough, this period would be dominant and the pressure build-up would reach the maximum value. The effective shear rate was calculated using Eq. (5), (Delshad *et al.* 2008). After that, the viscosity value was obtained from the corresponding viscosity measurements reported by Nasr-El-Din *et al.* (2008). Based on the effective shear rate and the corresponding measured viscocity, it was found to be 8 cp as the surfactant-acid based system was injected inside the core.

$$\gamma_{eff} = C\left[\frac{3n+1}{4n}\right]^{\frac{n}{(n-1)}}\left[\frac{u_w}{\sqrt{kk_{rw}S_w\phi}}\right] \quad \text{.....(5)}$$

2. *Period B*: as the wormhole propagated further, Δp declined gradually and the pressure response overcame any possible build up in viscosity, which was more dominant in period A.
3. *Period C*: the process repeats itself at this stage, and this stage would only occur if the acid injection rate was not low enough (example; 15 $cm^3$/min) to have period A as the dominant period. On the other hand, a very high injection rate, such as 15 $cm^3$/min, will accelerate wormhole propagation and minimize having enough filtrate ahead of the wormhole. Consequently, no pressure build-up would be expected.

Then the injection rate was between the two levels, more calcium dissolved, which allowed the surfactant to form a gel in-situ. The pressure drop kept increasing until the fluid propagated further.

4. *Period D*: the last stage before acid breakthrough. Δp started to decline as the acid approached the exit end of the core, there was a sharp decline in Δp, and ultimately, Δp approached nearly zero.

*Experiment #5 (Low injection rate)*

In experiment # 5, acid injection rate was 3 $cm^3$/min. The results obtained in this experiment were essential to explaining a critical part of the process. **Fig. 17** shows that the pressure build-up increased by more than 5-fold compared with the initial pressure before acid injection. Period A took more time before it reached the maximum value.

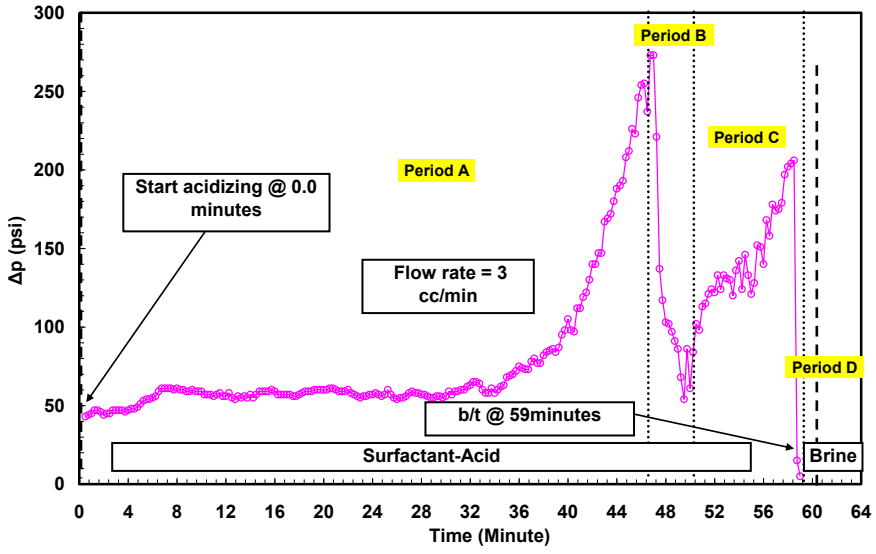


**Fig. 17— Pressure drop across the core. Four periods have been identified as period A, B, C and D; (15 wt% HCl + 7.5 vol% surfactant + 0.3 vol% C.I.); experiment (5).**

**Fig. 18** shows a cross-sectional area for each slice along the core length after acidizing, combined with a 3-D visualization image for the wormhole. The wormhole path observed when surfactant-based acid was injected tended to change direction several times to avoid any possible blockage caused by the diverting material. In the case where conventional acid was used, the wormhole shape did not show a similar pattern and the wormhole shape was less tortuous with the direction of flow.

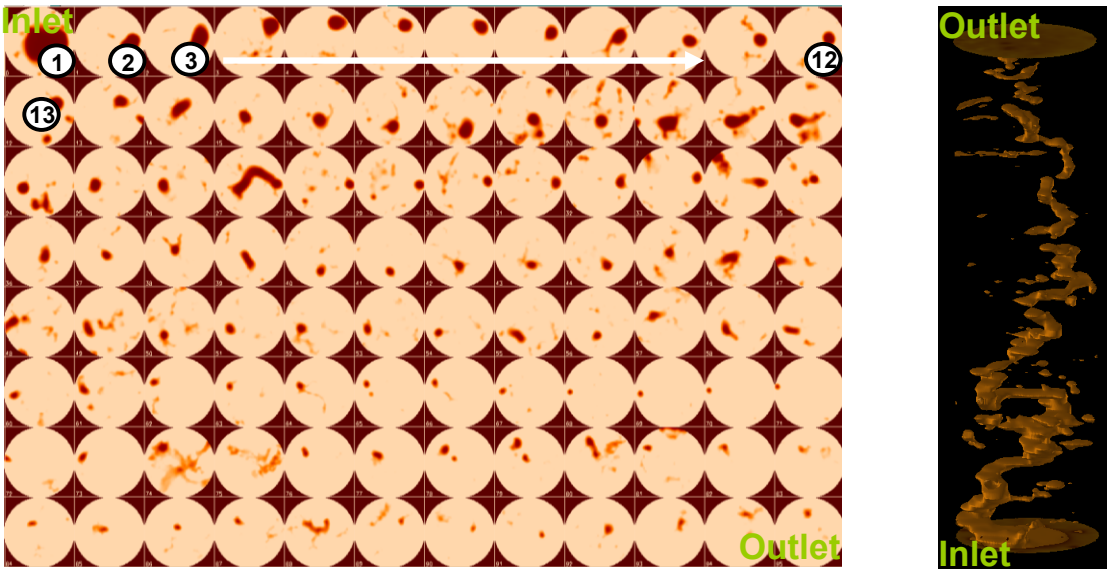


**Fig. 18— A cross sectional area for each slice along the core length after acidizing combined with a 3-D visualization image for the wormhole for experiment (5).**

*Experiment #6 (moderate injection rate)*

In experiment #6, the acid injection rate was 5.5 $cm^3$/min. In this particular experiment, as the acid entered the core, the Δp started to increase gradually and reached

a maximum 9 minutes after the beginning of acid injection. After that, the Δp declined sharply and reached a minimum value of 30 psi. **Fig. 19** shows the measured Δp across the entire core with time until acid breakthrough. In some experiments, period C did not last long as the acid approached the end of the core and the pressure drop suddenly decreased.

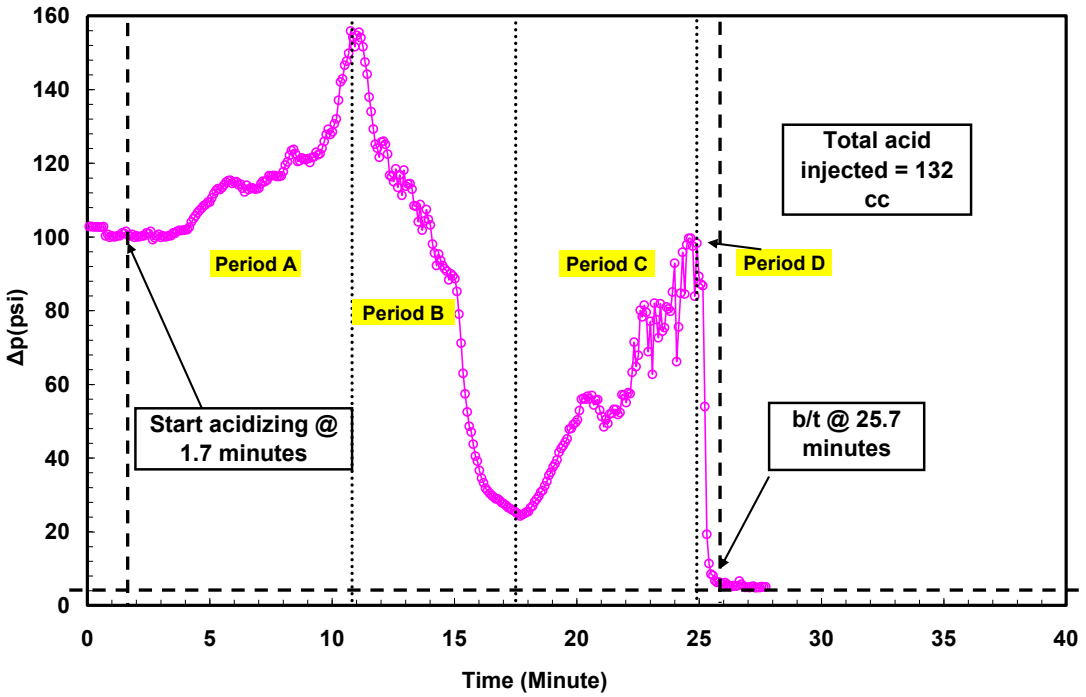


**Fig. 19— Pressure drop across the core. Four periods have been identified as period A, B, C and D, experiment (6).**

**Fig. 20** shows a cross-sectional area for each slice along the core length after acidizing, combined with a 3-D visualization image for the wormhole. The wormhole path observed in the first case changed direction several times as the acid propagated

further and avoided possible blockage caused by the diverting material. In the case where conventional acid was used, the wormhole shape did not show a similar pattern--it was less tortuous.

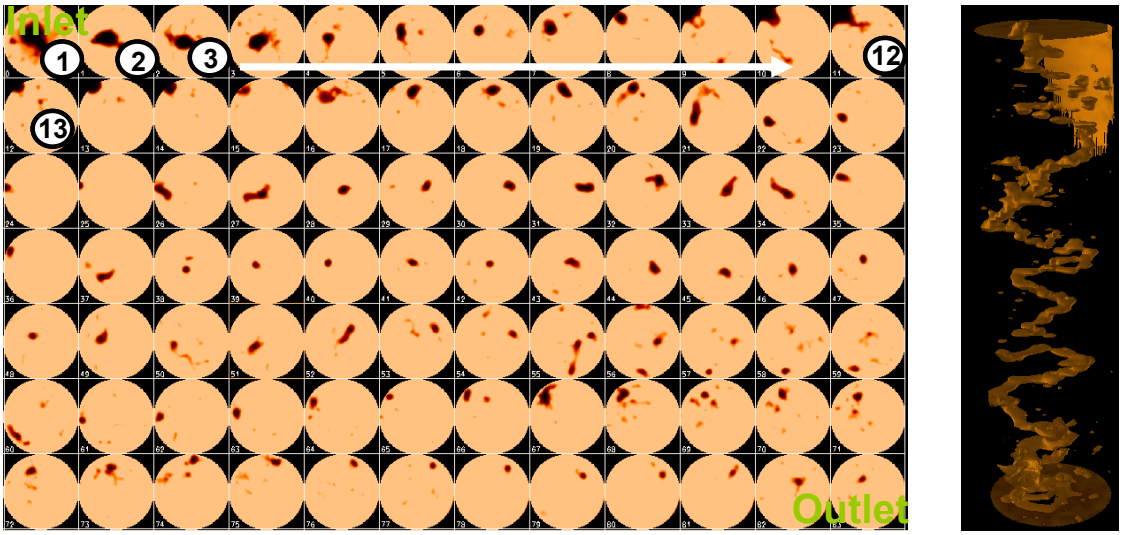


**Fig. 20— A cross sectional area for each slice along the core length after acidizing combined with a 3-D visualization image for the wormhole for experiment (6).**

*Experiment #7 (high injection rate)*

The last experiment using surfactant-based acid had conditions identical to those in experiment #6, except that the flow rate was 15 $cm^3$/min. As described before, period C did not occur at this injection rate, **Fig. 21**. This can be explained by the fact that the amount of calcium dissolved ahead of the tip of the wormhole was not enough to trigger the surfactant to form gel material. This was proven in experiment #3 where only 55,000 ppm of calcium concentration was measured in the effluent sample. Therefore, a high

flow rate will reduce the effectiveness of the surfactant material to form micelles, since the diversion process will not likely take place.

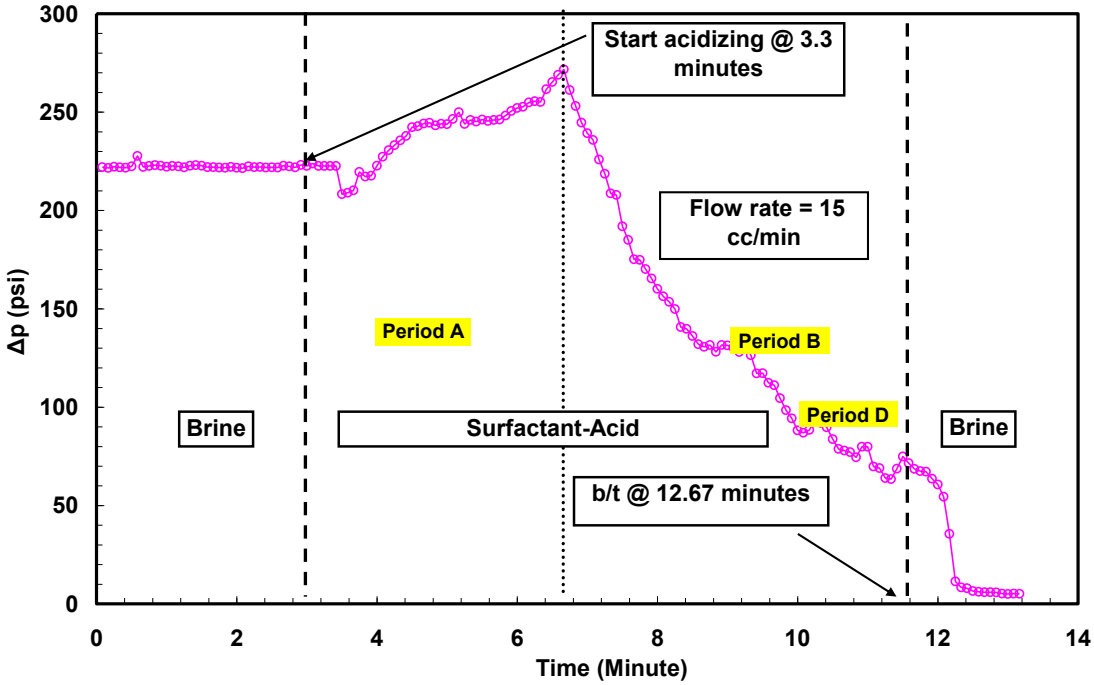


**Fig. 21— Pressure drop across the core. Three periods have been identified as period A, B, and D; (15 wt% HCl + 7.5 vol% surfactant + 0.3 vol% C.I.); experiment (7).**

**Fig. 22** compares the normalized pressure drop as a function of pore volume injected until acid breakthrough at three different flow rates, 3, 5.5 and 15 $cm^3$/min. At 15 $cm^3$/min, no diversion took place at any time during the acidizing process. Also, at a high flow rate, such as 15 $cm^3$/min, the pore volume injected was 20% higher when surfactant-based acid was used compared to the case where 15 wt% HCl was injected. At low flow rates such as 3 $cm^3$/min, two things should be mentioned: first, the viscosity

build-up occurred after the wormhole penetrated more than one foot inside the core; second, the pressure resistivity initiated from the viscosity build-up was very short in time, which limited the efficiency of the diversion process. Because of the large scale of the normalized pressure obtained at low flow rates, **Fig. 23** shows a zoom-in figure of the normalized pressure drop as a function of pore volume injected until acid breakthrough for both 5.5 and 15 $cm^3$/min. **Fig. 24** shows the shape of the wormhole as the acid injection rate changed.

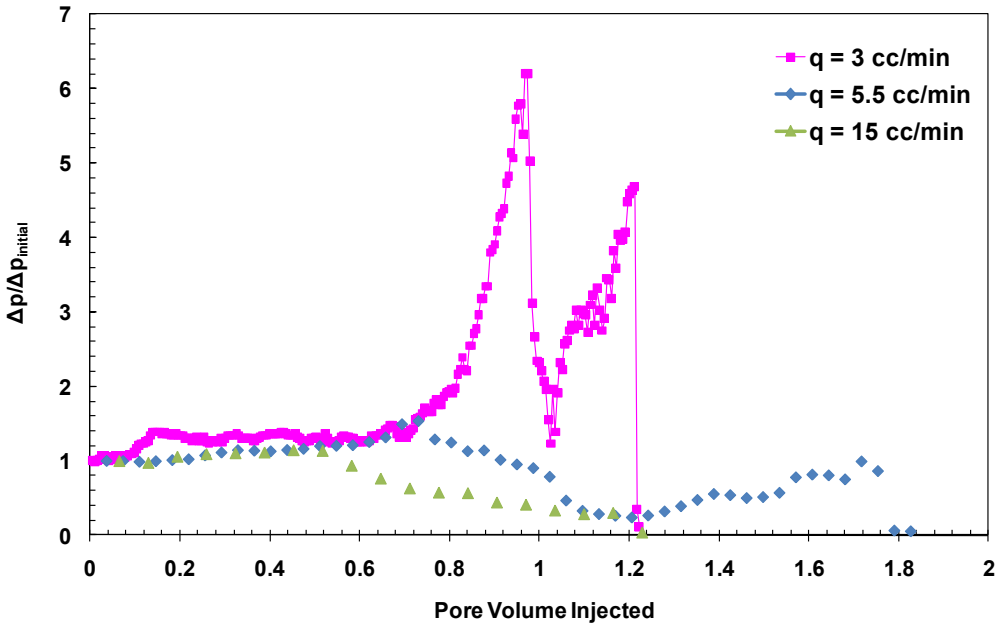


**Fig. 22— Normalized pressure drop as a function of pore volume injected until acid breakthrough; surfactant-based acid.**

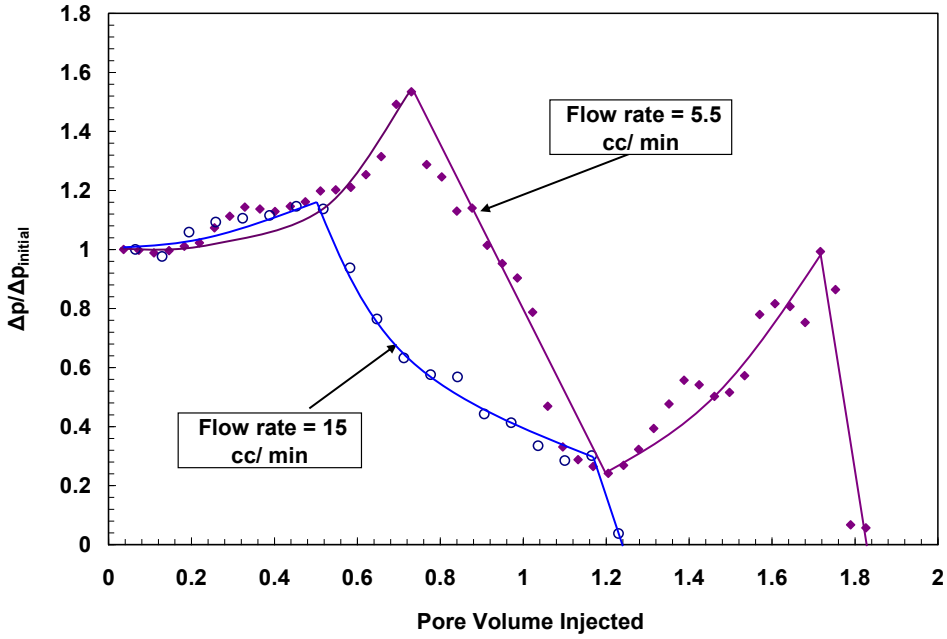


**Fig. 23— Zoom-in normalized pressure drop as a function of pore volume injected until acid breakthrough; surfactant-based acid.**

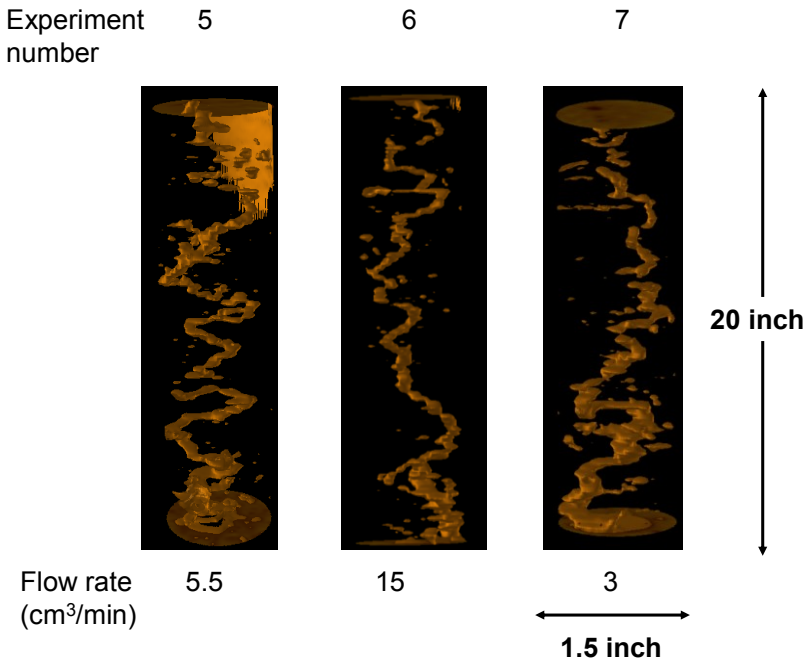


**Fig. 24— Shape of the wormhole at different flow rates; surfactant-based acid.**

# CHAPTER IV

# PARALLEL COREFLOODS

## 4.1 Procedure

The same procedure adopted in performing single coreflood was used with some modifications to allow conducting parallel coreflood tests. The sequence of the parallel coreflood experiments can be summarized as follows:

- Prepared the core sample including weighing the limestone core dry. Then, the core was saturated using fresh water under vacuum. The difference in weight measurement was used to calculate porosity.
- Measured the initial permeability using fresh water for each core.
- Injected fresh water to both cores until pressure stabilized along the parallel core set-up.
- Conducted the acidizing experiment at a constant total flow rate and monitored the pressure drop across the cores.
- Collected effluent samples from each core, using two independent automatic fraction collectors.
- Stopped the flow as soon as breakthrough occurred in one of the cores, as indicated by the differential pressure dropping to zero.
- Examined the cores using the CT scan to characterize wormholes generated by the acid.

**Fig. 25** is a schematic diagram of the parallel core-flood set-up used in this study. The same description of the single coreflood set-up can be applied to the parallel coreflood set-up with slight changes. The modifications include a common back pressure regulator (model S91-W) set at 1000 psi. Also, the inlet line was split with a T-connection to allow fluids to enter each core proportionally to the effective permeability. Finally, the pressure drop was sensed with a set of FOXBORO differential pressure gauges (models IDP10-T26(C-D-E) and 21F-M2L1).The differential pressure was measured across each core separately to ensure both cores sensed the same pressure from both ends.

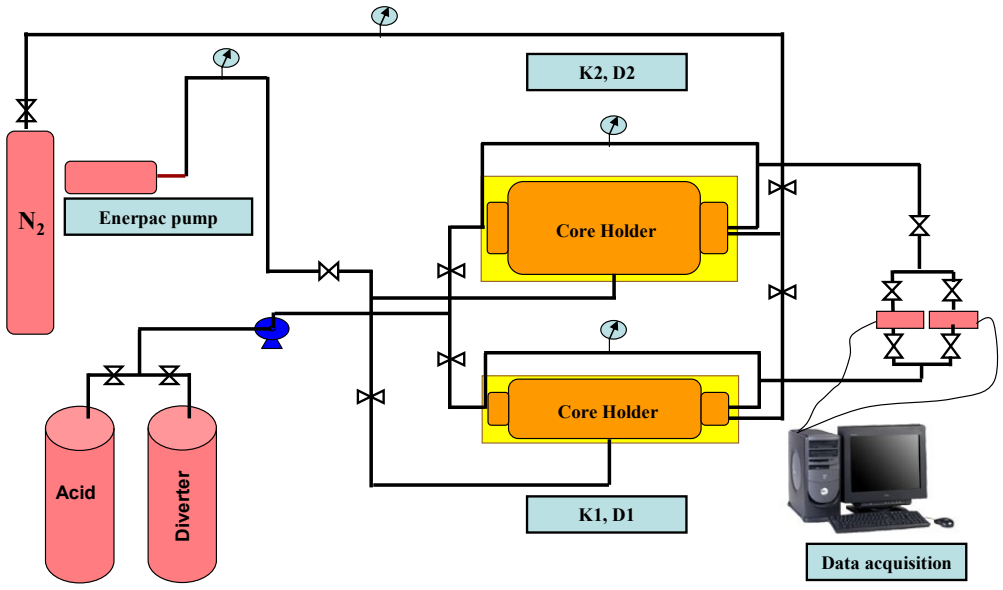


**Fig. 25— A schematic diagram of the parallel core-flood set-up.**

The results obtained will be presented in two parts: regular acid flow in calcite cores, and surfactant-based acid flow.

### 4.2 Propagation of Regular Acid in Carbonate Cores

*Experiment #1 (high contrast in k)*

Experiment #1 illustrates two objectives: 1) validate the experimental procedure followed in conducting the parallel coreflood experiments; 2) magnify the need for diverting material when matrix acidizing is implemented in formations having different permeability layers.

In the first experiment, the acid injection rate was 7 $cm^3$/min. **Table 5** gives the permeabilities, porosities, and flow rates for this experiment and other experiments conducted in this study.

**TABLE 5— SUMMARY OF COREFLOOD EXPERIMENTS; PARALLEL COREFLOOD.**

| Experiment # | Acid System | Initial Permeability $k_1$ (md) | Initial Permeability $k_2$ (md) | Initial Porosity $\Phi_1$ (vol%) | Initial Porosity $\Phi_2$ (vol%) | Flow Rate ($cm^3$/min) |
|---|---|---|---|---|---|---|
| 1 | Regular Acid | 6 | 101 | 11 | 30 | 7 |
| 2 | | 81 | 160 | 26 | 28 | 20 |
| | | | | | | |
| 3 | Surfactant Acid | 6 | 72 | 11 | 17 | 7 |
| 4 | | 96 | 56 | 30 | 12 | 7 |
| 5 | | 74 | 50 | 30 | 12 | 10 |

The contrast in the initial permeability was 16 fold. The pressure drop across the core was monitored as shown in **Fig. 26.** As expected, when HCl was injected into a parallel coreflood, the acid flow moved predominantly into the higher permeability core compared with the lower permeability core. As a result of the high contrast in permeability in this experiment, most of the flow was into the core with a permeability of 101 md leaving the 6 md core almost untreated as indicated by the negligible volume observed in the effluent samples from the low permeability core. A CT scan conducted for both cores indicated no wormholes in the low permeability core in contrast with full penetration observed in the high permeability core.

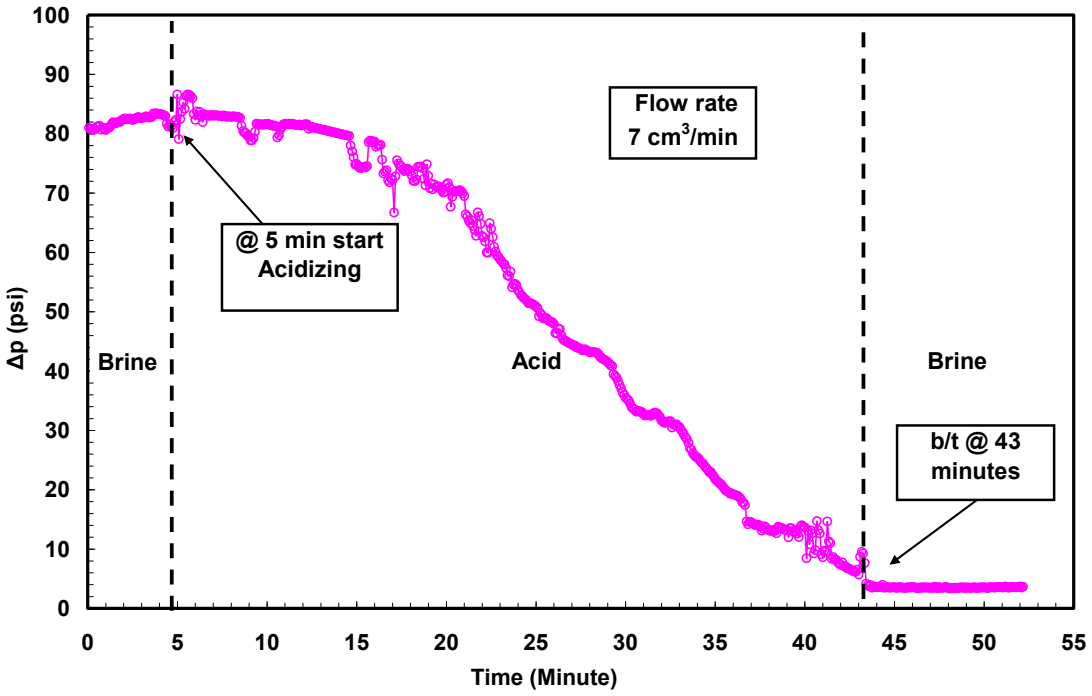


**Fig. 26— Pressure drop across the parallel core; regular acid; experiment (1).**

*Experiment #2 (low contrast in k)*

In the second experiment, the acid injection rate was 20 $cm^3$/min. Two cores with 81 and 160 md were acidized, which made the initial contrast in permeability 2-fold. **Fig. 27** shows the pressure drop across each core, which was the same since both inlet and outlet of each core were exposed to common pressures.

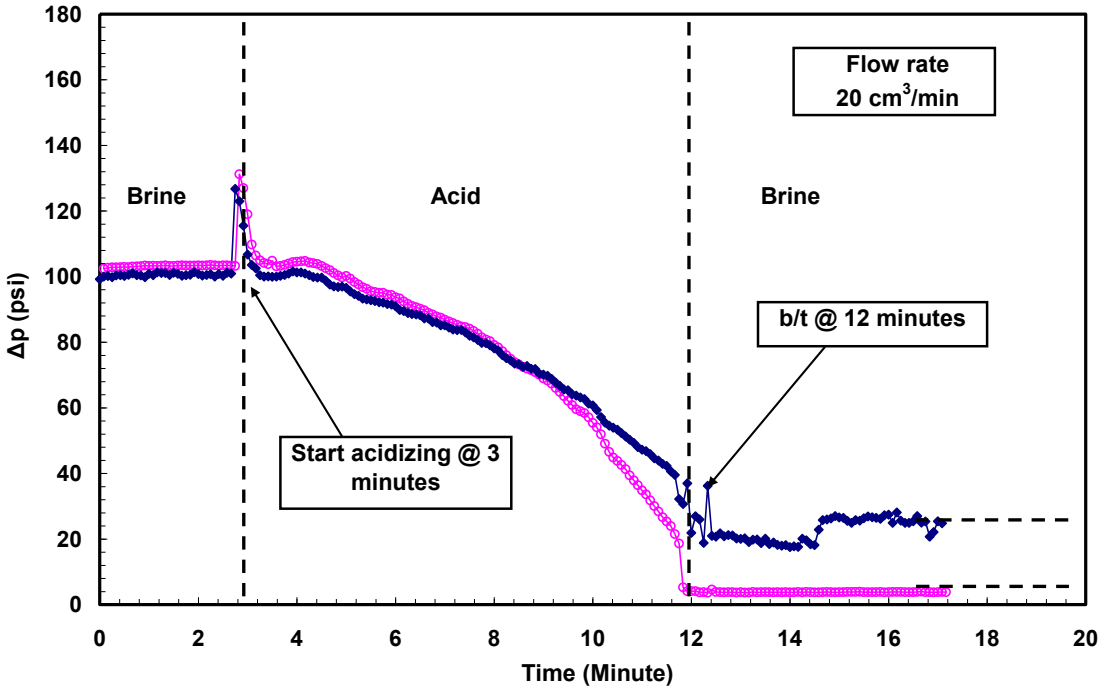


**Fig. 27— Pressure drop across each core; regular acid; experiment (2).**

**Fig. 28** shows the calculated flow rate based on the volume measured in the effluent samples collected from each core. Out of 20 $cm^3$/min, 13 $cm^3$/min entered the high permeability core, leaving 7 $cm^3$/min available for the other core. As acid continued

to be injected to both cores, more acid flowed to the high permeability core until acid breakthrough.

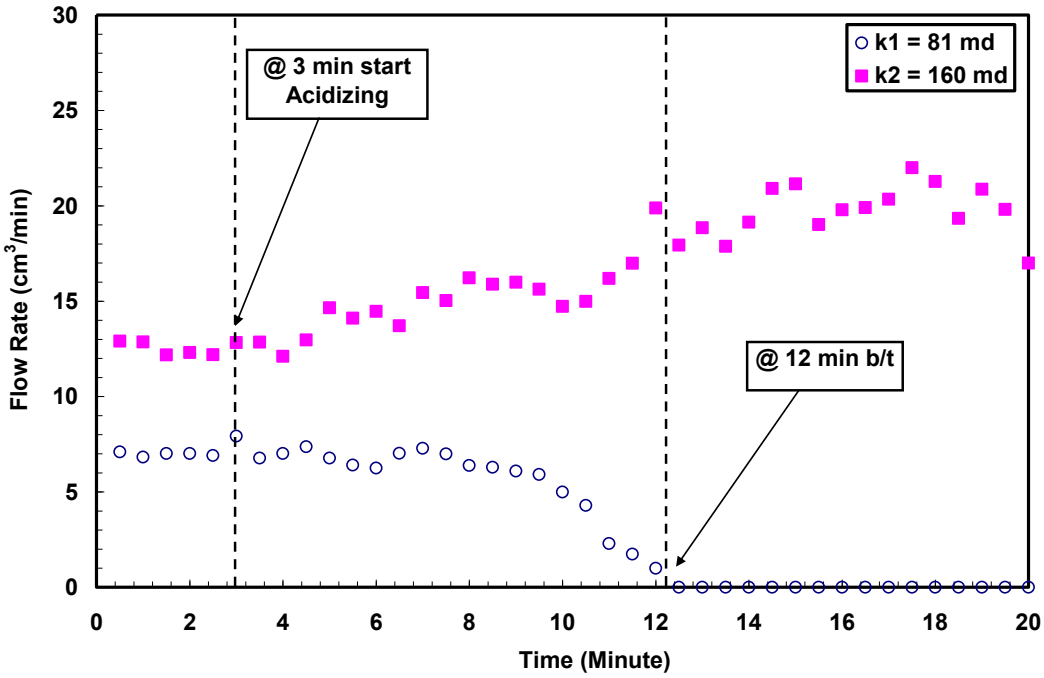


**Fig. 28— Distribution of flow rate in each core; regular acid; acid injection = 20 $cm^3$/min. In this experiment the initial permeability ratio was 12. The flow rate in the high permeability core was predominant over the flow in the low permeability core; experiment (2).**

**Fig. 29** shows a 3-D image for the wormhole created in each core. Only 20% of the low permeability core was acidized compared to the fully penetrated wormhole in the 160 md core. This is another indication for the need to divert material during acid stimulation even with a permeability ratio of 2.

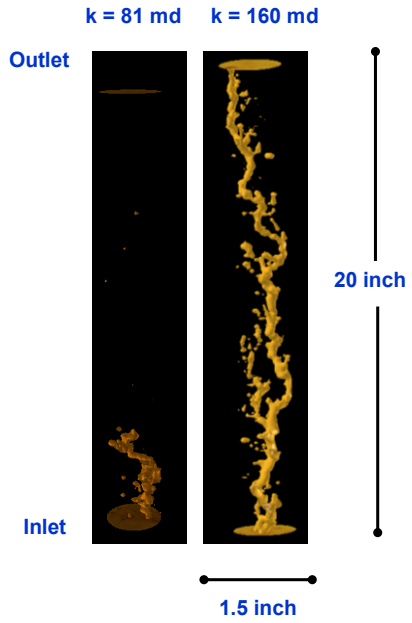


**Fig. 29— 3-D image for the wormholes created in each core; experiment (2).**

### 4.3 Propagation of Surfactant-Based Acid in Carbonate Cores

Next, three experiments were performed using a 15 wt% HCl + 7.5 vol% surfactant + 0.3 vol% corrosion inhibitor injected into parallel limestone cores. Experiment #3 illustrates the flow of diverting material in a high contrast environment ($k_1/k_2$ = 12). Experiments #4 and #5 were conducted at low contrast in permeability ($k_1/k_2$ = 1.7 and 1.5, respectively) at two different injection rates of 7 and 10 $cm^3$/min.

*Experiment #3 (high contrast in k)*

The results presented here belong to the first experiment we conducted using diverting material in a parallel coreflood set-up. The permeabilities selected represent a high contrast in permeability (72 : 6 ).

One major parameter to measure during an acidizing experiment is the differential pressure across the entire core. In this particular experiment, the Δp started to decline gradually 5 minutes after the beginning of acid injection. **Fig. 30** shows Δp, measured across the entire core and over time until acid breakthrough. The pressure decline indicated no major diverting process taking place; otherwise, a build-up in the pressure would have occurred to compensate for the increase in viscosity as gel material started to form. With such a high contrast in the permeability ratio, most of the acid entered the 72 md core, leaving the 6 md uninvaded. Less than 1 $cm^3$/min entered the tight core which was not enough to initiate a wormhole. As a result of the high flow rate entering the high permeability core, viscosity build-up did not occur. Comparing the flow rate distribution between experiment 1 (no diverting material) and this experiment, there is a slight improvement in the fluid distribution but still not as significant as intended, **Fig. 31**. Neither the visual observation nor the CT image showed any wormhole created in the lower permeability core.

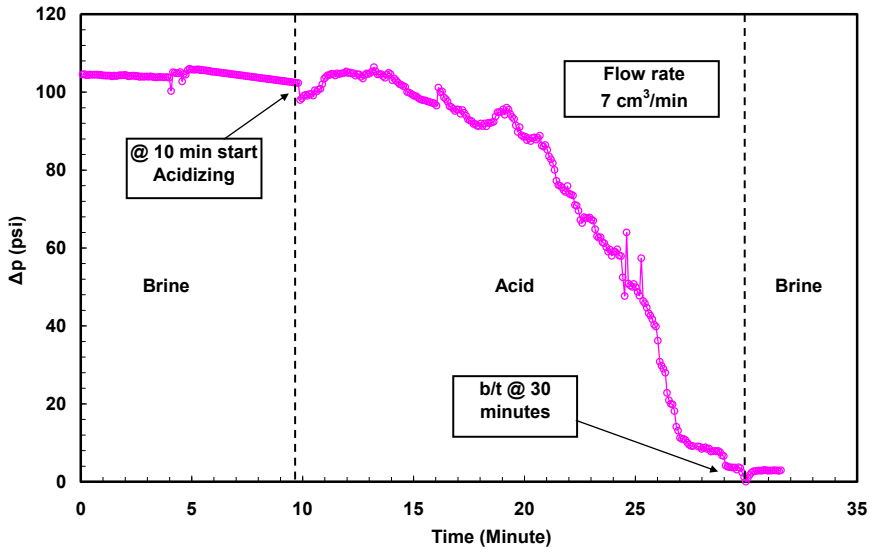


**Fig. 30— Pressure drop across the parallel core; surfactant-based acid; experiment (3).**

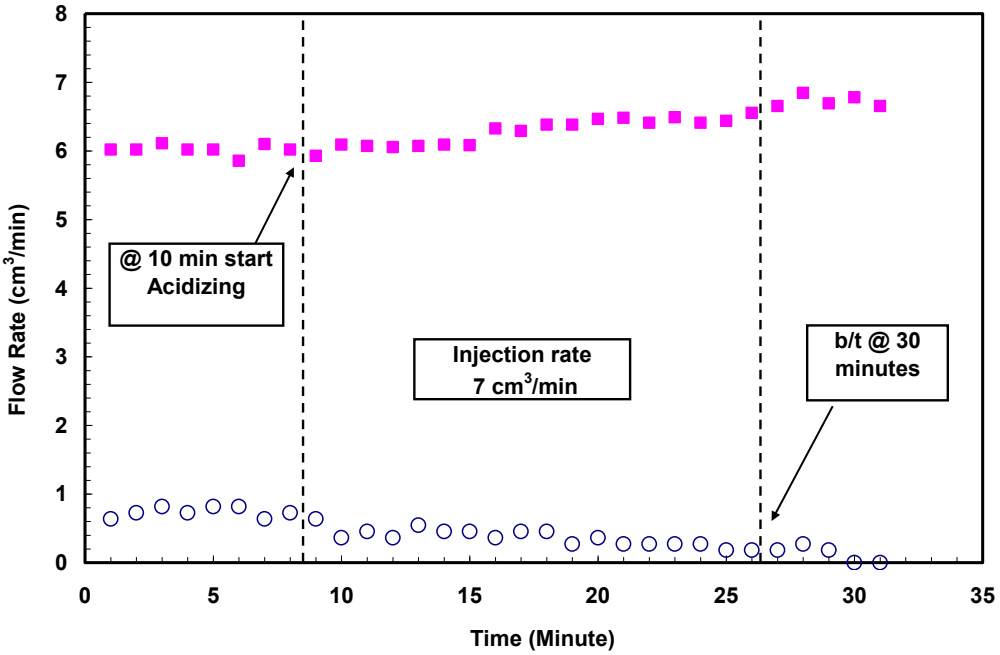


**Fig. 31— Distribution of flow rate in each core; surfactant-based acid; acid injection = 7 $cm^3$/min. In this experiment the initial permeability ratio was 12; experiment (3).**

*Experiment # 4 (low contrast in k + low injection rate)*

Experiment #4 had very similar conditions as experiment #3 except that in experiment #4, the contrast in permeability ratio was 1.7 compared with 12 in the previous experiment. **Fig. 32** shows the Δp, measured across the core and over time until acid breakthrough first in the 56 md core (relatively low permeability). After 27 minutes, the Δp started to increase dramatically as a result of gel formation. This gel forms when the pH value increases above 2 and the concentration of divalent cations ($Ca^{2+}$ and $Mg^{2+}$) increases in the spent acid. At this point, the rod-shaped micelles will significantly increase the viscosity of the spent acid (Nasr-El-Din et al. 2008). The Δp continued to build up until the wormhole propagated further, which caused the Δp to stabilize and decline until acid breakthrough.

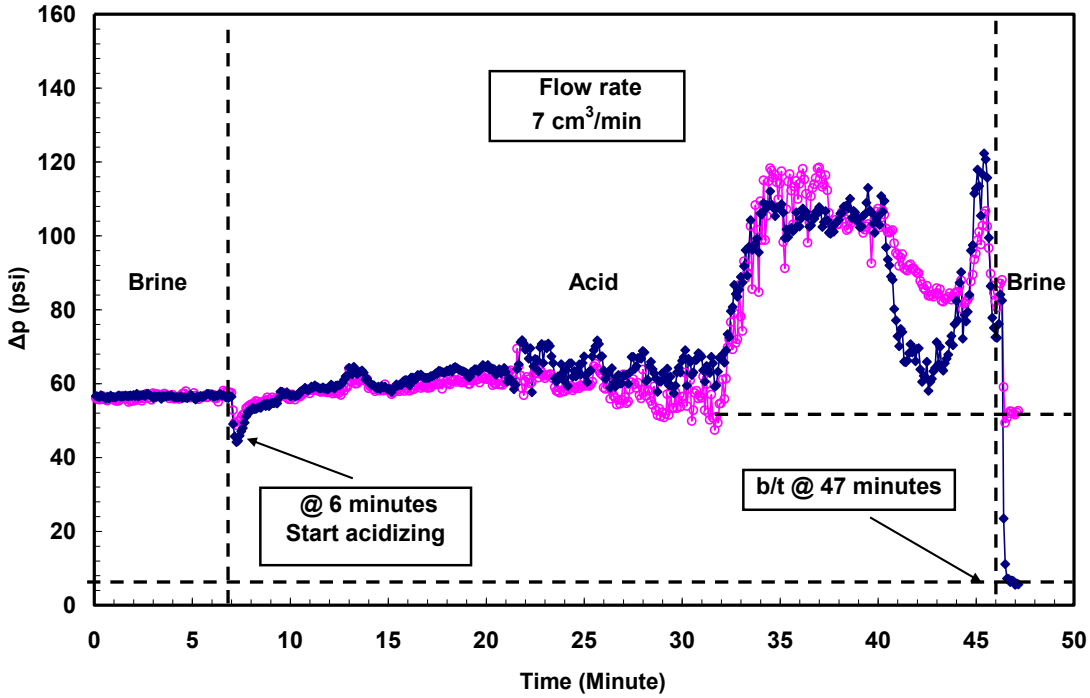


**Fig. 32— Pressure drop across each core; surfactant-based acid; experiment (4).**

Another way to assess diversion is to consider the pressure response in conjunction with the effluent measured from each core (**Fig. 33**). As the acid flows along the core, three periods can be identified as follows:

1. Period I: the distribution of the flow rate remained proportionally constant related to the initial permeability ratio; higher flow rate entered the core with higher permeability and lower flow rate entered the core with lower permeability.
2. Period II: As more live acid entered the higher permeability core, a longer wormhole formed. As a result, the flow rate increased in the higher permeability core. In contrast, less acid was available to the lower permeability core
3. Period III; By the time acid reached this stage, the concentration of divalent cations

($Ca^{2+}$ and $Mg^{2+}$) increased in the spent acid, and the surfactant molecules formed rod-shaped micelles resulting in an increase in apparent viscosity. This mechanism diverted flow from the high permeability core to the lower permeability core. The time observed was 27 minutes, which was the exact time when Δp started to increase significantly.

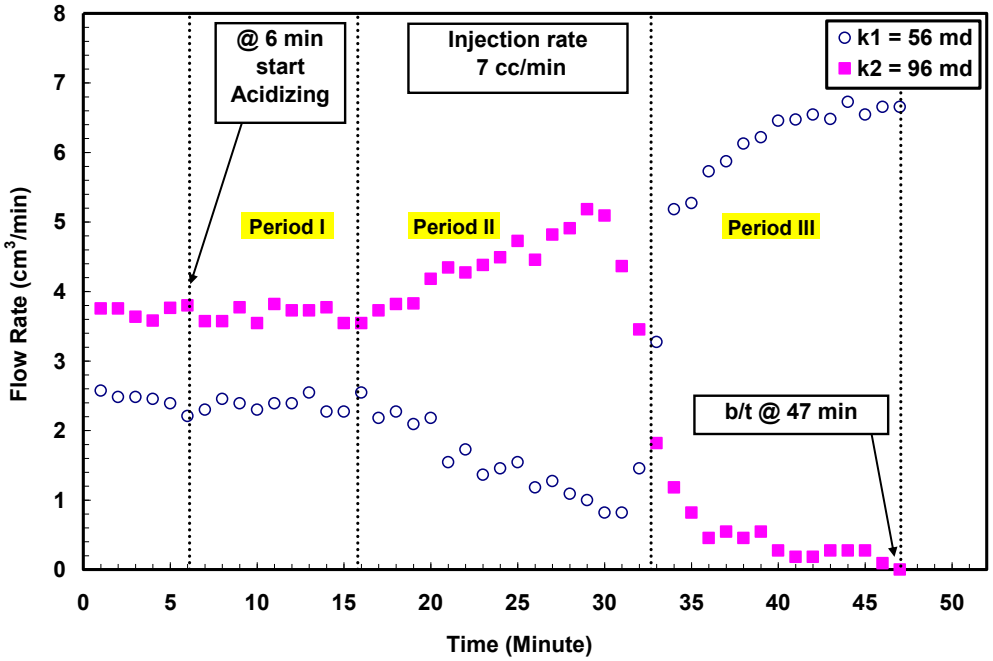


**Fig. 33— Distribution of flow rate in each core; surfactant-based acid; acid injection = 7 $cm^3$/min. In this experiment the initial permeability ratio was 1.7. Adding surfactant material altered the flow rate from the high initial permeability core to the low permeability core; experiment (4).**

Another interesting observation is related to the breakthrough time. Apparently, the diverting material not only diverted the flow from higher to lower permeability, it

also allowed the wormhole to propagate faster in the lower permeability core, as indicated by earlier breakthrough as the differential pressure dropped to zero. **Fig. 34** shows a 3-D image of the wormhole for both cores. In this core, the wormhole propagated more than 80% of the total length of the relatively high permeability core (96 md) before breakthrough occurred in the lower permeability core.

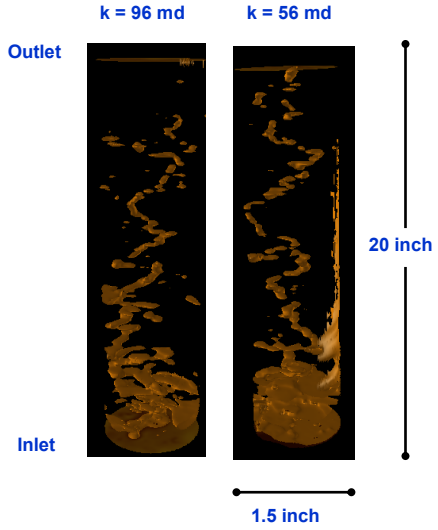


**Fig. 34— 3-D image for the wormholes created in each core. Wormhole propagated more than 80% of the total length of core before breakthrough occurred in the lower permeability core; experiment (4).**

*Experiment # 5 (low Contrast in k + high injection rate)*

Experiment #5 has very similar conditions to those in experiment #4, except that in experiment #5, the injection rate was 10, compared with 7 $cm^3$/min in the previous experiment, an increase of 48%. After acid injection, the average Δp measured for the first 6 minutes was relatively constant. Then Δp started to decline as the wormhole

propagated further, which was not the case in experiment #4. The fast injection rate accelerated wormhole propagation as indicated by the continuous decrease in the Δp until breakthrough occurred. **Fig. 35** shows Δp, measured across the core and over time until acid breakthrough first in the high permeability core.

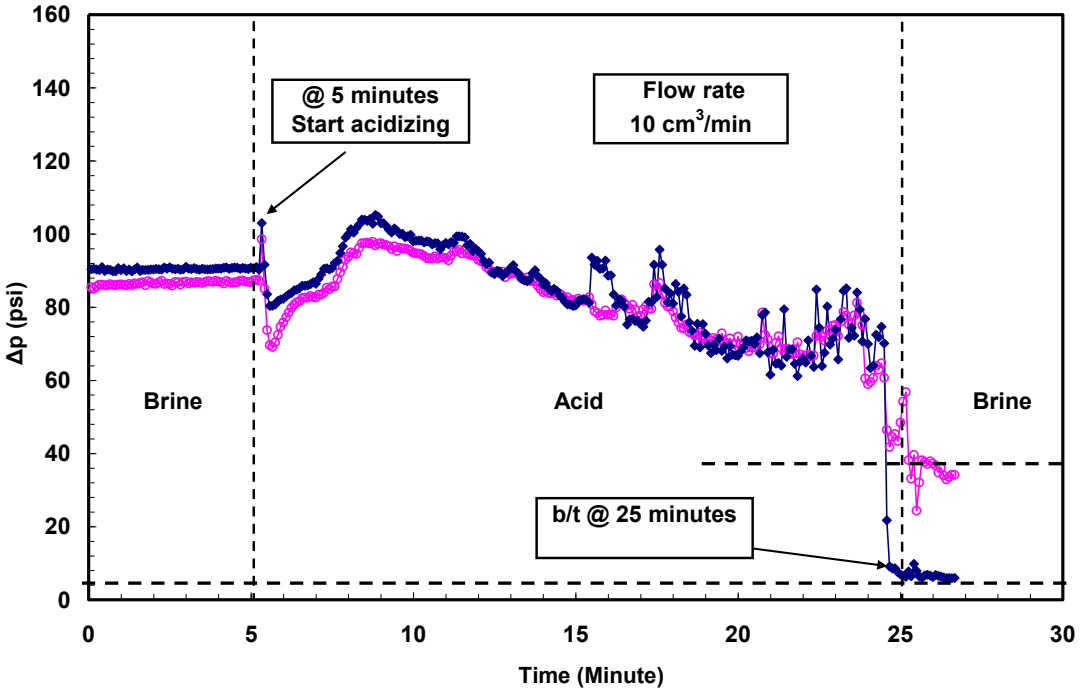


**Fig. 35— Pressure drop across each core; surfactant-based acid; experiment (5).**

Similar to regular acids, periods I and II can be identified. Period III was not observed in this experiment at least until acid breakthrough occurred as shown in **Fig. 36**. The total acid volume injected was 190 $cm^3$ compared with 280 $cm^3$ in experiment # 4. This suggests that the wormhole propagated faster than the spent acid fronts, which

was expected to trigger the surfactant material inside the high permeability core to form gel.

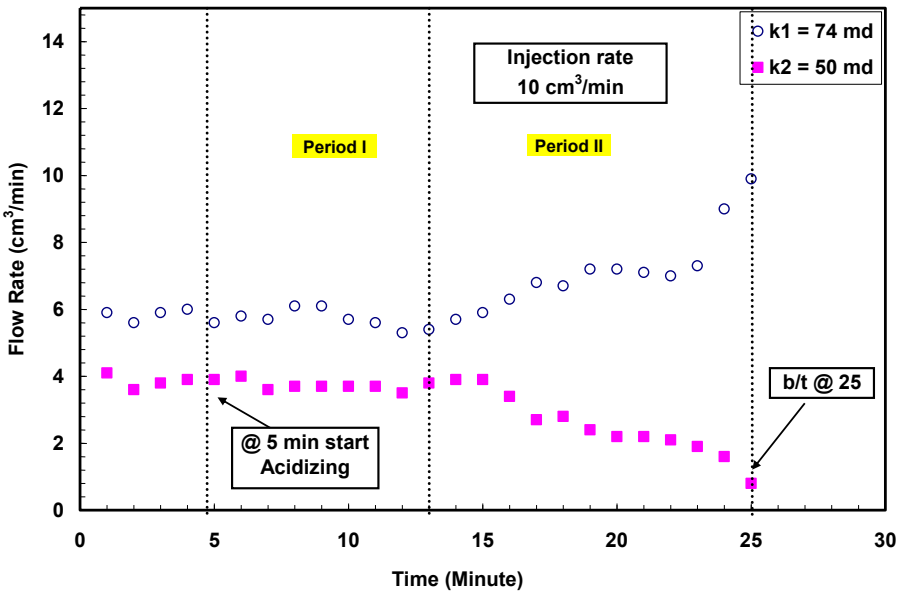


**Fig. 36— Distribution of flow rate in each core; surfactant-based acid; acid injection = 10 $cm^3$/min. Adding surfactant material did not alter the flow rate from the high initial permeability core to the low permeability core; experiment (5).**

The results obtained from Δp measurement and flow rate were in agreement with the CT scan results. **Fig. 37** shows a 3-D image for the wormholes created in both cores. Clearly, the wormhole penetrated the entire high permeability core with 50% penetration in the lower permeability core.

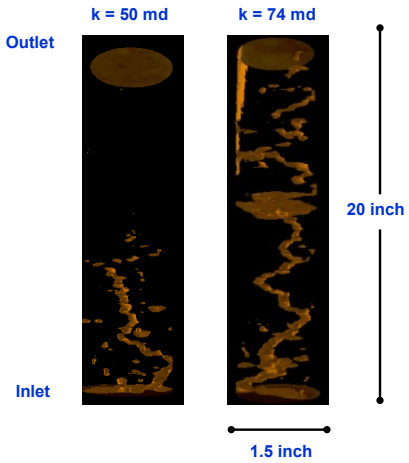


**Fig. 37— 3-D image for the wormholes created in each core. The wormhole penetrated the entire high permeability core with 50 % penetration in the lower permeability core; experiment (5).**

# CHAPTER V

# MODELING

This chapter summarizes the two analytical models used in this study to support some of the arguments made. An acid balance model was presented to investigate acid concentration along a given wormhole length. Also, an analytical solution was derived to match the flow rate distribution in acidizing two cores simultaneously using regular acid.

## 5.1 Acid Balance Model

Measuring the acid concentration at the tip of the wormhole as acid breakthrough formed the basis of the experimental conditions. The acid concentration remained strong and range between 7 and 8 wt% HCl as the acid exited the core. This became an important aspect, when considering whether gel material was formed inside the wormhole or not. To verify the experimental result, one approach is to model the acid profile inside the wormhole. For a gel material to form inside the wormhole, the acid concentration must diminish dramatically so the pH value approaches 2 (Nasr-El-Din et al. 2008). To model the acid concentration, we first consider the acid balance for a small volume element as shown in **Fig. 38.** Assuming steady-state, laminar, incompressible, Newtonian fluid, the general mass conservation equation for the acid can be formulated.

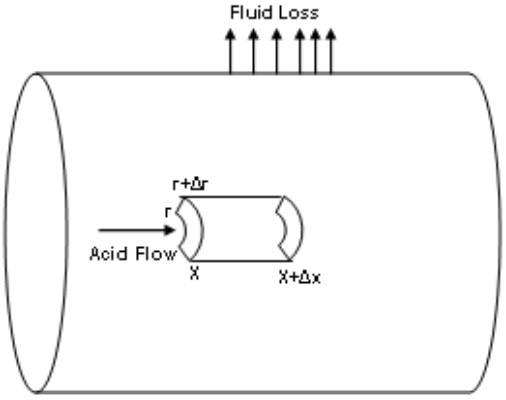


**Fig. 38— Acid balance in a small element of wormhole.**

The acid balance for a small volume element can be written as:

mass in – mass out = mass accumulation……..(6)

$$\pi\left[(r+\Delta r)^2 - r^2\right]\Delta t\left(uC - D\frac{\partial C}{\partial x}\right)\Big|_x + 2\pi r\Delta x\Delta t\left(vC - D\frac{\partial C}{\partial r}\right)\Big|_r +$$
$$\pi\left[(r+\Delta r)^2 - r^2\right]\Delta t\left(uC - D\frac{\partial C}{\partial x}\right)\Big|_{x+\Delta x} + 2\pi r\Delta x\Delta t\left(vC - D\frac{\partial C}{\partial r}\right)\Big|_{r+\Delta r} =$$
$$C\pi\left[(r+\Delta r)^2 - r^2\right]\Delta x\Big|_{t+\Delta t} - C\pi\left[(r+\Delta r)^2 - r^2\right]\Delta x\Big|_t \quad \text{.....(7)}$$

Where, C is the acid concentration, D is the diffusion coefficient as defined by Hung (1987). u and v are the fluid velocity components as defined by Yuan and Finkelstein (1956).

The final form of the acid balance equation is given by Eq. (8)

$$\left(1 - \frac{2\,\mathrm{Re}_w}{\mathrm{Re}}\xi\right)f'(\zeta)\frac{\partial C_D}{\partial \xi} + \frac{2\,\mathrm{Re}_w}{\mathrm{Re}}f(\zeta)\frac{\partial C_D}{\partial \zeta} = \frac{\mathrm{Re}_w}{\mathrm{Re}\,Pe_w}\left(\frac{\partial C_D}{\partial \zeta} + \xi\frac{\partial^2 C_D}{\partial \zeta^2}\right) \quad \text{.....(8)}$$

Where;

$C_D = C/C_o$

Co = acid concentration in the injected acid

$\xi = x/r_{wh}$ $\zeta = r/rwh$

$N_{\mathrm{Re}} = \frac{u(0)r_w}{v}$ (Reynolds number based on the average velocity at the inlet)

$N_{\mathrm{Re},w} = \frac{v_w r_w}{v}$

$N_{Pe,w} = \frac{v_w r_w}{D}$ (Peclet number based on the fluid diffusion coefficient)

With boundary conditions:

$C_D = 1$ $at$ $\xi = 0$

$C_D = 0$ $at$ $\zeta = 1$

$\frac{\partial C_D}{\partial \zeta} = 0$ $at$ $\zeta = 0$

The analytical solution to the acid balance equation is:

$$\bar{C} = -2C_0 \sum_{n=0}^{\alpha} \left[ K_n \left( 1 - \frac{2N_{\mathrm{Re}_w}}{N_{\mathrm{Re}}} \xi \right)^{\frac{\lambda_n^2}{2N_{Pe_w}}} \left[ \frac{\bar{B_n}(1)}{\lambda_n^2 + 2N_{Pe_w}} \right] \right] \quad \text{.....(9)}$$

This solution for the mean acid concentration is restricted to $0.001 < N_{Re} < 1.0$ and $N_{Pe} < 8$. Five terms in the series expressed by Eq. (9) are required for reasonable accuracy (Schechter (1992)).

The analytical solution to the acid balance equation is given by Hung (1987). The solution was obtained by applying the method of separation of variables whereby the

partial differential equation was transformed into two ordinary differential equations, one of which is a simple exponential relation of acid concentration and axial distance. The other is the Sturm-Liouville boundary value equation, and the problem readily reduces to the finding of Eigen values and their corresponding Eigen functions. Equation (9) is the solution to the acid balance equation:

$$\bar{C} = -2C_0 \sum_{n=0}^{\alpha} \left[ K_n \left( 1 - \frac{2N_{\mathrm{Re}_w}}{N_{\mathrm{Re}}} \xi \right)^{\frac{\lambda_n^2}{2N_{Pe_w}}} \left[ \frac{B_n^{-}(1)}{\lambda_n^2 + 2N_{Pe_w}} \right] \right] \quad \text{.....(9)}$$

This solution for the mean acid concentration is restricted to $0.001 < N_{Re} < 1.0$ and $N_{Pe} < 8$. Five terms in the series expressed by Eq. (9) are required for reasonable accuracy (Schechter *et al.* (1992)).

**5.2 Case Study**

The solution given in Eq. (9) can be used to track acid concentration along the wormhole at a given condition. **Table 6** provides the parameters needed to solve the acid balance equation for a given experimental conditions.

TABLE 6— INPUT DATA USED TO EVALUATE THE ACID CONCENTRATION USING THE ANALYTICAL SOLUTION.

| Parameter | Value | Unit |
|---|---|---|
| r | 0.75 | Inch |
| $r_{wh}$ | 0.1 | Inch |
| x | 10 | Inch |
| q | 6.75 | $cm^3/min$ |
| D | $2.4\ 10^{-5}$ | $cm^2/s$ |
| $v_w$ | 0.0075 | cm/s |
| ρ | 1.1 | $g/cm^3$ |
| μ | 1 | Cp |

The core was 1.5 inches in diameter, which makes the radius, r, equal 0.75 inch. The wormhole radius ($r_{wh}$) estimated from the CT scan was 0.1 inch and assumed to be constant to the tip of the wormhole. In this case, the wormhole was assumed to extend for half of the core length, given as x = 10 inches. (q) is the total injection flow rate which was kept constant during the acidizing experiment, in this case 6.75 $cm^3$ /min was used. The diffusion coefficient was measured by Taylor *et al.* (2004) for 15 wt% HCl which was $2.4x10^{-5}$ $cm^2/s$. Fluid loss velocity to the wall ($v_w$) was estimated by analogy with previous work done by Huang et al. (1999) to predict fluid loss in linear core flood experiments. The representative leakoff velocity was estimated to be 0.0075 cm/s.

The dimensionless parameters calculated were $N_{Rew}$ = 0.209; $N_{Re}$ = 0.27; $N_{Pew}$ =80; $\xi(r/r_{wh})$ = 7.5; $\zeta(x/r_{wh})$ ranged from 0 to 60. Since the solution is only applicable for $N_{Pe} < 8$, three values (1.5, 3 and 6) were selected to represent $N_{Pe}$.

To calculate the Eigen values and their corresponding Eigen functions, a mathematical program was written to solve the analytical equation given in Eq. (9).

**Table 7** provides the calculated value. **Fig. 39** shows $C_{avg}/C_o$ represented as a function of $x/r_{wh}$ for the three values of $N_{Pe}$. For $N_{Pe} < 3$, the acid concentration was reduced to small values at small fractional values of the total wormhole length. The effective wormhole length is said to be reaction rate limited. The acid was spent prior to reaching the end of the wormhole and possible gel material formed in the wormhole. On the other hand, when $N_{Pe} > 6$, live acid penetrates to the end of the wormhole. In this case the wormhole is said to be fluid-loss limited since the acid concentration is high at the end of the wormhole. More importantly, gel material will not form inside the wormhole. Notice that the actual Peclet number is calculated to be 80, which makes it far into the fluid-loss limited regime.

**TABLE 7— EIGEN VALUE AND THEIR CORRESPONDING EIGEN FUNCTION CALCULATED USING MATHEMATICA. THIS DATA WILL BE USED IN THE SERIES EXPRESSED BY EQ. (4) TO ESTIMATE THE AVERAGE ACID CONCENTRATION ALONG THE WORMHOLE.**

| $N_{Rew} = 0.209$<br>$N_{Re} = 0.27$ | | | | | |
|---|---|---|---|---|---|
| $N_{Pe} = 1.5$ | | $N_{Pe} = 3$ | | $N_{Pe} = 6$ | |
| $\lambda_n$ | $-K_n B_n'(1)$ | $\lambda_n$ | $-K_n B_n'(1)$ | $\lambda_n$ | $-K_n B_n'(1)$ |
| 1.33 | 1.98 | 0.84 | 2.88 | 0.09 | 7.88 |
| 4.49 | 1.24 | 4.44 | 1.07 | 5.1 | 0.087 |
| 7.40 | 0.98 | 7.39 | 0.87 | 8.11 | 0.15 |
| 10.26 | 0.85 | 10.27 | 0.78 | 10.95 | 0.21 |
| 13.11 | 0.78 | 13.12 | 0.73 | 13.74 | 0.27 |
| 15.96 | 0.72 | 15.97 | 0.69 | 16.53 | 0.31 |
| 1.33 | 1.98 | 0.84 | 2.88 | 0.09 | 7.88 |

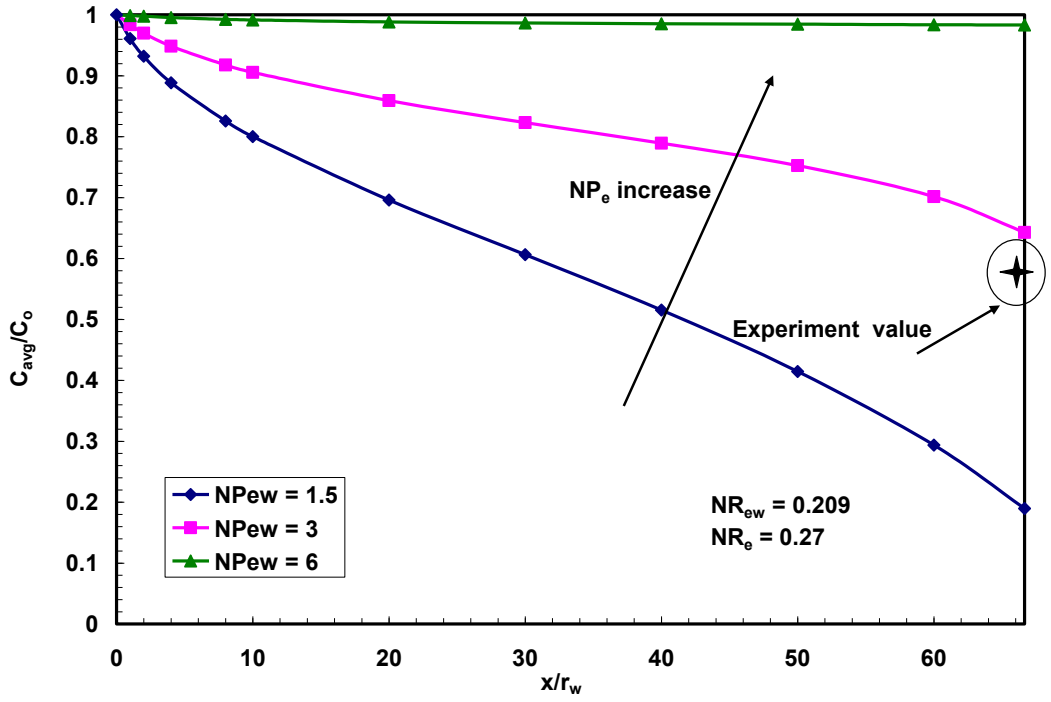


**Fig. 39— Mean concentration profile.**

### 5.3 Flow Rate Model

The results obtained from the acidizing experiments can be modeled mathematically given some input parameters obtained from the experiment. An analytical solution was derived to match the flow rate distribution in acidizing two cores simultaneously. In addition to a known total injection rate, the pore volume to breakthrough in each core serves as an input parameter in the model.

A constant injection rate was split at the face of two linear cores connected in parallel. The pump was adjusted to keep a constant flow rate during the acidizing process, and common back pressure was applied on the outlet of both cores equally and set at 1,000 psi to ensure $CO_2$ remained in solution. This set up ensured $\Delta p$ across each

core to be the same as expected in the real situation except for slight end effects that was observed as wormhole breakthrough first in one of the two cores. The injection pressure changed during the experiment as a function of time. **Fig. 40** shows a diagram illustrating the parameters used to develop the analytical model to match the experiment data of matrix acidizing with a parallel coreflood at a constant acid injection rate.

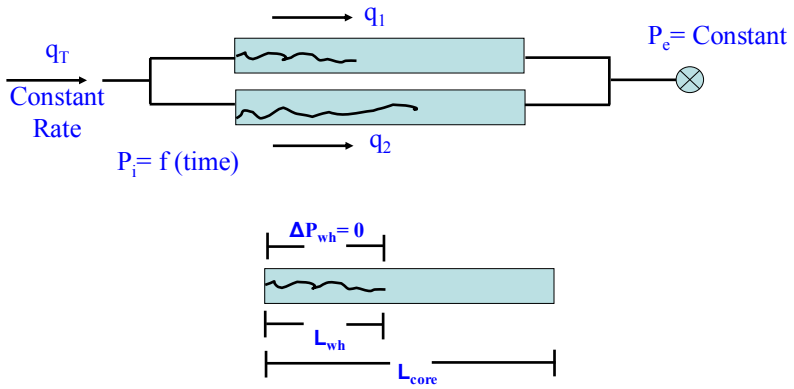


**Fig. 40— A diagram showing the parameters used to develop an analytical model to match the experiment data of matrix acidizing using regular acids with a parallel coreflood at a constant acid injection rate.**

The following equations hold true during the experiment and were used as a starting point in deriving the analytical solution:

$$q_1 + q_2 = q_T \quad \text{.....(10)}$$

$$\Delta p_1 = \Delta p_2 = \Delta p \quad \text{.....(11)}$$

$$p_i = f(time) \quad \text{.....(12)}$$

Assuming that the Δp in the wormhole is approximately zero, the equations can be written to describe a flow system:

Darcy equation for flow in the core ahead of the wormhole:

$$q_1 = \frac{\Delta p(t)\, k_1\, A_1}{\mu_1 (L_{core1} - L_{wh1})} \quad \text{.....(13)}$$

$$q_2 = \frac{\Delta p(t)\, k_2\, A_2}{\mu_2 (L_{core2} - L_{wh2})} \quad \text{.....(14)}$$

Volumetric model equations (Economides *et al.* 1994):

$$V_{wh} = \frac{V_i}{PV_{bt}} \quad \text{.....(15)}$$

$$V_{wh} = \frac{\partial L_{wh}}{\partial t} \quad \text{.....(16)}$$

$$q_i = V_i \frac{\pi}{4} d^2 \phi \quad \text{.....(17)}$$

Both cores have the same cross-sectional area and core length and the same fluid was injected. In addition, for simplification, we will assume both cores have the same porosity:

$$A_1 = A_2 = A; \qquad \mu_1 = \mu_1 = \mu\ ; \qquad L_{core1} = L_{core2} = L_{core}; \qquad \phi_1 = \phi_2 = \phi$$

Substitute eq. (13) & (14) into (11):

$$\frac{q_1\, \mu (L_{core1} - L_{wh1})}{k_1 A} = \frac{q_2\, \mu (L_{core2} - L_{wh2})}{k_2 A} \quad \text{.....(18)}$$

Solve for $q_1 \Rightarrow \quad q_1 = \frac{k_1\, q_2 (L_c - L_{wh2})}{k_2 (L_c - L_{wh1})}$ .....(19)

Substitute eq. (19) into (10):

$$\frac{k_1\, q_2(L_c - L_{wh2})}{k_2\,(L_c - L_{wh1})} + q_2 = q_T \quad \text{.....(20)}$$

Combine eq. (15) & (17) and solve for $v_{wh}$

$$\Rightarrow \quad v_{whi} = \frac{q_i}{PV_{bti}\dfrac{\pi}{4} d_{core}^2 \phi} \quad \text{.....(21)}$$

Rearrange eq. (16) and integrate both sides:

$$L_{wh1} = v_{wh1}\, t \quad \text{.....(22)}$$

Write eq. (21) in term of $v_{wh1}$ $\Rightarrow$ $v_{wh1} = \dfrac{q_1}{PV_{bt1}\beta}$ .....(23)

Where; $\beta = \dfrac{\pi}{4} d_{core}^2 \phi$ .....(24)

Substitute eq. (23) into (22):

$$\Rightarrow \quad L_{wh1} = \frac{q_1\, t}{PV_{bt1}\beta} \quad \text{.....(25)}$$

Similarly; $L_{wh2}$ can be written as $L_{wh2} = \dfrac{q_2\, t}{PV_{bt2}\beta}$ .....(26)

Substitute eq. (25) & (26) into (20):

$$\frac{k_1\, q_2(L_c - \dfrac{q_2\, t}{PV_{bt2}\beta})}{k_2\,(L_c - \dfrac{q_1\, t}{PV_{bt1}\beta})} + q_2 = q_T \quad \text{.....(27)}$$

From eq. (1) $\Rightarrow$ $q_2 = q_T - q_1$ .....(28)

Substitute eq. (28) into (27):

$$\frac{k_1\, q_2(L_c - \frac{q_2\, t}{PV_{bt2}\beta})}{k_2\,(L_c - \frac{q_1\, t}{PV_{bt1}\beta})} + q_T - q_1 = q_T \quad \text{.....(29)}$$

Rearrange eq. (29):

$$\frac{k_1 L_c\,(q_T - q_1) - \left(\frac{(q_T - q_1)^2 k_1\, t}{PV_{bt2}\beta}\right)}{k_2 L_c - \left(\frac{q_1 k_2\, t}{PV_{bt1}\beta}\right)} = q_1 \quad \text{.....(30)}$$

Expand eq. (30) resulting in:

$$k_1 L_c\, q_T - k_1 L_c\, q_1 - \frac{k_1 t\, q_T^2}{PV_{bt2}\beta} + \frac{2k_1 t\, q_1 q_T}{PV_{bt2}\beta} - \frac{k_1 t\, q_1^2}{PV_{bt2}\beta} = k_2 L_c\, q_2 - \frac{k_2 t\, q_1^2}{PV_{bt1}\beta} \quad \text{.....(31)}$$

Eq. (31) can be written in quadratic form:

$$q_1^2\left(\frac{k_2 t}{PV_{bt1}\beta} - \frac{k_1 t}{PV_{bt2}\beta}\right) + q_1\left(\frac{2q_T k_1 t}{PV_{bt2}\beta} - k_2 L_c - k_1 L_c\right) + \left(k_1 L_c\, q_T - \frac{k_1 t q_T^2}{PV_{bt2}\beta}\right) = 0 \quad \text{.....(32)}$$

(32) is a quadratic equation in the form:

$$aq_1^2 + bq_1 + c = 0$$

Where;

$$\text{a}=\left(\frac{k_2 t}{PV_{bt1}\beta} - \frac{k_1 t}{PV_{bt2}\beta}\right); \qquad b = \left(\frac{2q_T k_1 t}{PV_{bt2}\beta} - k_2 L_c - k_1 L_c\right); \qquad c = \left(k_1 L_c\, q_T - \frac{k_1 t q_T^2}{PV_{bt2}\beta}\right)$$

Solving eq. (32); the flow rate is:

$$q_1 = \frac{-\left[\frac{2k_1 t\, q_T}{PV_{bt2}\,\beta} - k_2\, L_c - k_1\, L_c\right] \pm \sqrt{(\frac{2k_1 t\, q_T}{PV_{bt2}\,\beta} - k_2\, L_c - k_1\, L_c)^2 - 4*(\frac{k_2\, t}{PV_{bt1}\,\beta} - \frac{k_1\, t}{PV_{bt2}\,\beta})*(k_1\, L_c\, q_T - \frac{k_1\, t\, q_T^2}{PV_{bt2}\,\beta})}}{2*(\frac{k_2\, t}{PV_{bt1}\,\beta} - \frac{k_1\, t}{PV_{bt2}\,\beta})}$$

The flow rate through the other core, $q_2$, is then simply $q_T - q_1$.

### 5.4 Model Validation

To validate the model presented above, experiment #2 data was used to match parameters. The input data needed for the analytical model is summarized in **Table 8**.

**TABLE 8— INPUT PARAMETERS DESCRIBING EXPERIMENT # 2 THAT WERE USED TO VALIDATE THE ANALYTICAL MODEL.**

| Parameter | Value | Unit |
|---|---|---|
| Permeability ($k_1$) | 81 | md |
| Permeability ($k_2$) | 160 | md |
| Porosity ($\Phi$) | 28 | vol% |
| Total Flow Rate (q) | 20 | $cm^3$/min |
| $PV_{tb1}$ | 0.7 | --- |
| $PV_{tb2}$ | 0.8 | --- |
| Core Length (Lc) | 20 | inch |

The two parameters from the experimental data used to match the flow rate were pore volume to breakthrough in each core, calculated to be 0.7 and 0.8. A very reasonable match was obtained with the model as presented in **Fig. 41**.

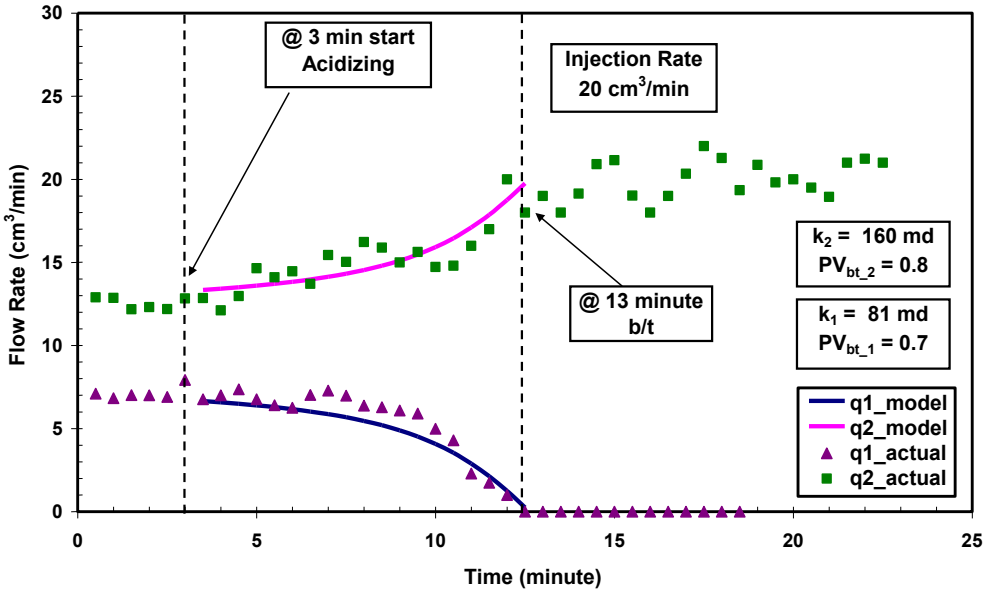


**Fig. 41— Results obtained from the analytical model to simulate the flow rate distribution in a parallel core-flood experiment. The initial permeability was 160 and 81 md; experiment (2).**

# CHAPTER VI

# SUMMARY

This chapter offers a comprehensive discussion of the overall results obtained in this study. For completeness, some of the experiments discussed in previous chapters will be included in this chapter, and not necessarily to have the same experiment number. The results will be presented in two parts: single coreflood experiments and parallel coreflood experiments. Both the flow of regular-based acids in calcite cores, and the flow of surfactant-based acids were investigated. Notice, in all figures presented in this chapter, the dashed line corresponds to the time when the wormhole breakthrough occurred and the numeric value highlighted with a circle indicates the time when acid entered the core and subsequently when wormhole breakthrough occurred.

## 6.1 Regular Acid (Single Coreflood)

Several experiments were conducted with regular acid at different flow rates. The flow rate was kept constant during each experiment, and the pressure drop across the core was monitored. The injection rates were selected to cover a wide range of flow rates. For single coreflood experiments, **Table 9** includes the permeability, flow rate, acid flux, and pore volumes to breakthrough.

| TABLE 9— SUMMARY OF SINGLE COREFLOOD EXPERIMENTS, BOTH REGULAR-BASED ACID AND SURFACTANT-BASED ACID. | | | | | |
|---|---|---|---|---|---|
| **Experiment #** | **Acid System** | **Initial Permeability (md)** | **FlowRate ($cm^3$/min)** | **Acid Flux (m/hr/ $cm^2$)** | **$PV_{bt}$** |
| **1** | **Regular Acid** | **100** | **1.5** | **8** | **2.5** |
| **2** | | **66** | **3** | **16** | **1.9** |
| **3** | | **101** | **7** | **36** | **1.45** |
| **4** | | **95** | **15** | **79** | **0.97** |
| **6** | | **85** | **20** | **105** | **0.84** |
| **6** | | **68** | **30** | **158** | **0.87** |
| **7** | | **62** | **40** | **211** | **1.1** |
| **8** | | **81** | **50** | **263** | **1.3** |
| | | | | | |
| **9** | **Surfactant Acid** | **50** | **1.5** | **8** | **1.94** |
| **10** | | **83** | **3** | **16** | **1.45** |
| **11** | | **57** | **5.5** | **29** | **1.58** |
| **12** | | **73** | **15** | **79** | **1.36** |
| **13** | | **89** | **20** | **105** | **1.21** |
| **14** | | **126** | **30** | **158** | **1.29** |
| **15** | | **90** | **40** | **211** | **1.53** |
| **16** | | **75** | **50** | **263** | **1.54** |

The objectives of performing this particular set of experiments can be summarized as follows: (1) describe the efficiency of the wormhole process in terms of pore volume to breakthrough and pressure drop measured across the coreholder; (2) describe the velocity of the fluid front relative to the improved permeability front (to investigate this issue, calcium concentrations were measured in the effluent samples, which will offer insight regarding the nature of the chemical reaction that took place inside the core); (3) establish the pore volume to breakthrough curve as a function of acid flux to determine the optimum injection rate and the critical rate (rate corresponding

to maximum viscosity build up); and (4) describe qualitatively the shape of the wormhole based on a 3-D image for the wormhole. This analysis will be used for later comparison when surfactant-based acid is used as the stimulation fluid.

### 6.1.1 Pore Volumes to Breakthrough and Pressure Response

**Fig. 42** compares the normalized pressure drop as a function of pore volume injected until acid breakthrough at different injection rates. As the acid injection was lowered to flow rates such as 3 or 1.5 $cm^3$/min, the linear correlations took different slopes. At the injection rate of 1.5 $cm^3$/min, the slope was less steep as the acid leaked off more in the direction perpendicular to the main acid flow path. This resulted in higher pore volume to breakthrough. For example, when the acid injection rate was 1.5 $cm^3$/min, the pore volume to breakthrough was measured as 2.5, compared with 1.24 at an injection rate of 7 $cm^3$/min. The pressure decline was noticeably sharper later, as the wormhole propagated more inside the core. At a high injection rate, the pressure drop can be correlated linearly with the pore volume injected. The pressure drop across the core changed with time in a manner similar to that noted at the lower flow rate. However, the initial period where the pressure slightly declined was much shorter. This period represents the time for the acid to find its preferential path among other tiny wormholes and dissolve enough minerals and eventually become the leading wormhole; as a result, an effective permeability was created inside the core, which caused pressure drop simultaneously. Therefore, the higher the injection rate, the faster the wormhole can be initiated. Daccord *et al.* (1993) discuss this phenomenon relative to rock homogeneity in addition to effective permeability.

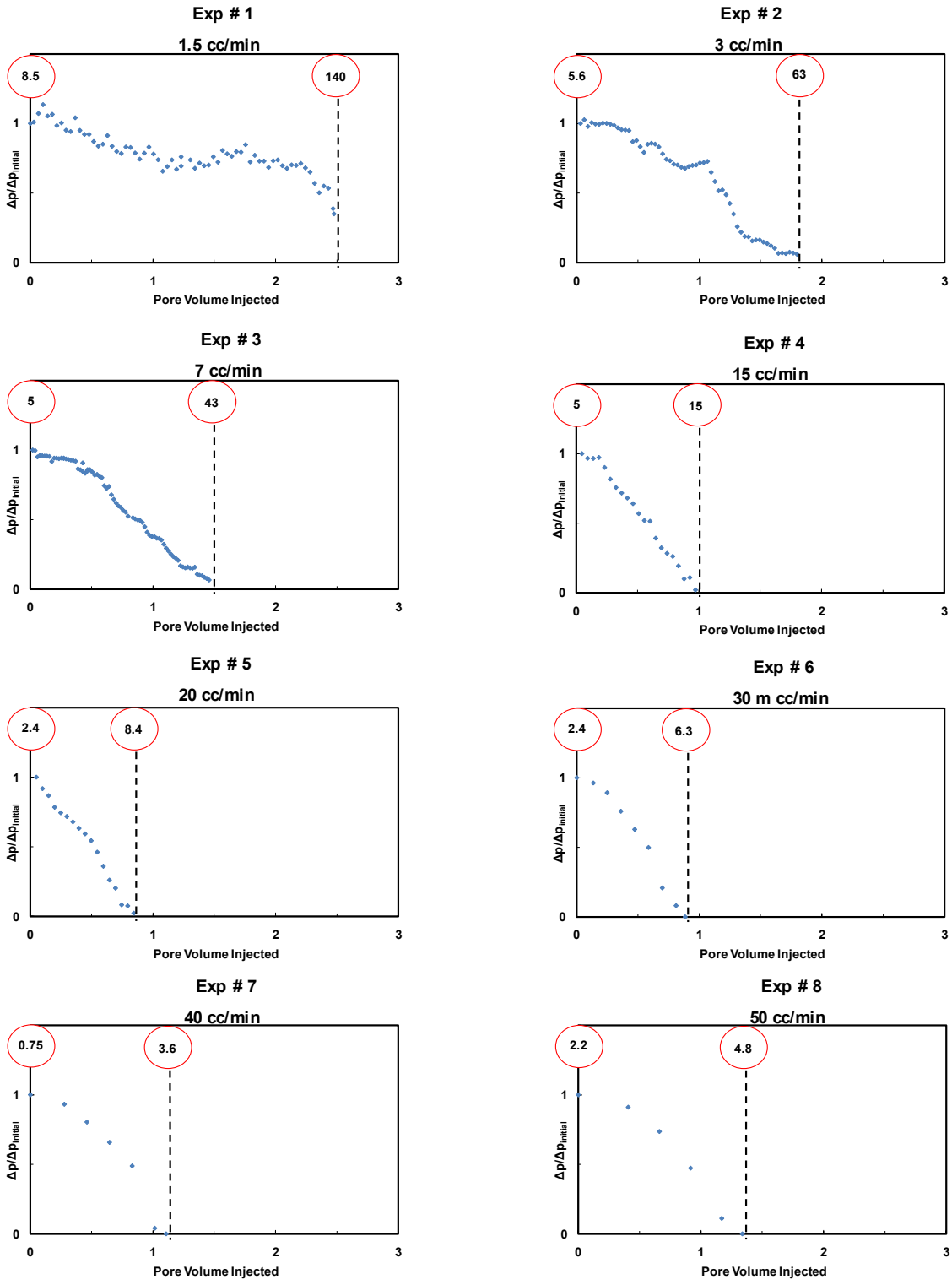


**Fig. 42— Normalized pressure drop as a function of pore volume injected until acid breakthrough; regular acid.**

### 6.1.2 Spent Acid Front Relative to the Wormhole Front

Typically, two velocity components can be described in the wormhole process: wormhole velocity and interstitial velocity. Wormhole velocity is the ratio of interstitial velocity to PVBT, which is a measure of the velocity of the improved permeability front. Interstitial velocity is a measure of the velocity of the fluid front, which can be calculated as ($q/A\Phi$). Interstitial velocity is a theoretical value, which implies that the rock was homogenous and no dissolution is occurring. Usually, such flow is referred to as piston-like displacement.

Another velocity component that was a critical parameter to evaluate in this study is the spent acid front. Note that for most experiments in this study, the improved permeability front moved much faster than the fluid front (these include any acid injection rates at optimum and beyond optimum). Generally, the improved permeability front can be ahead of or behind the fluid front. However, this depends on the type and concentration of acid used and, more importantly, on the injection rate. In this set of experiments, the injection rate is the changing variable that proves to be an important factor in describing how the spent acid front moves relative to the permeability front.

At a high injection rate, such as 15 $cm^3$/min, the concentration of calcium was not significantly present in the effluent samples until acid breakthrough, indicating no spent acid front ahead of the wormhole. With acid breakthrough from the core, a sudden increase in the calcium concentration in the effluent samples occurred. Calcium levels reached an average of 51,770 ppm, (see **Fig. 43)**.

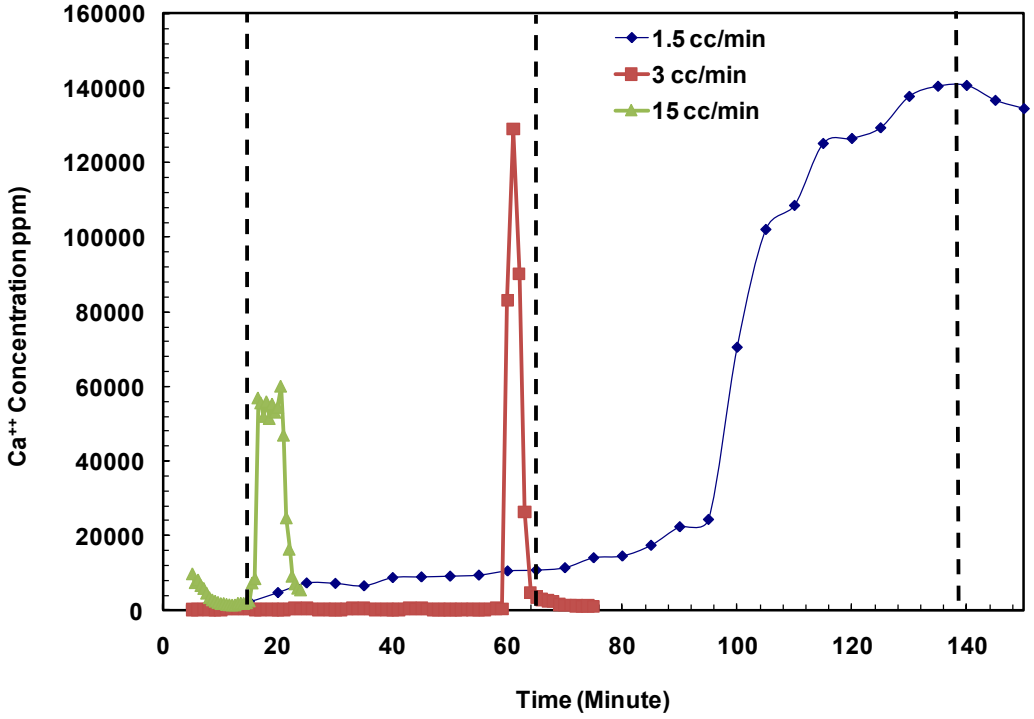


**Fig. 43— Calcium concentration measured in the effluent samples at three injection rates. Notice: dash lines corresponding to acid breakthrough time.**

Now the question to answer: what is the injection rate that will result in a faster acid front? In this study, 3 $cm^3$/min was found to be low enough to allow the spent acid front ahead of the improved permeability front. The calcium concentration was measured during the acidizing process for all effluent samples. Five minutes before acid breakthrough from the core, a sudden increase occurred in the calcium concentration in the effluent samples. Calcium levels reached an average of 82,130 ppm as shown in **Fig. 44,** which is 58% more than the calcium measured at 15 $cm^3$/min. More importantly, the calcium product appeared in the bulk solution before wormhole breakthrough. The amount of calcium measured in the effluent samples suggest that, if acid is injected

below the optimum rate, it will allow the acid filtrate to extend further ahead of the wormhole. This observation proves to be important when a surfactant-acid system is used, as demonstrated in the next section 6.2.

When the acid injection rate was lowered further to a value of 1.5 $cm^3$/min, the spent acid front developed in more progressive fashion and the calcium concentration was more significant, continuing to increase until wormhole breakthrough. A significant amount of calcium was measured in the effluent sample 40 minutes before acid breakthrough. The maximum calcium concentration was measured to be 140,640 ppm, which indicated a long spent acid front ahead of the wormhole.

For comparison, **Fig. 44** plots the average calcium concentration corresponding to the spent acid front as injection rate increased. In addition to what was explained earlier, as far as calcium content in the effluent samples, notice that as the injection rate continues to increase far from the optimum injection rate, the calcium content in the bulk solution levels out to an average of 40,000 ppm.

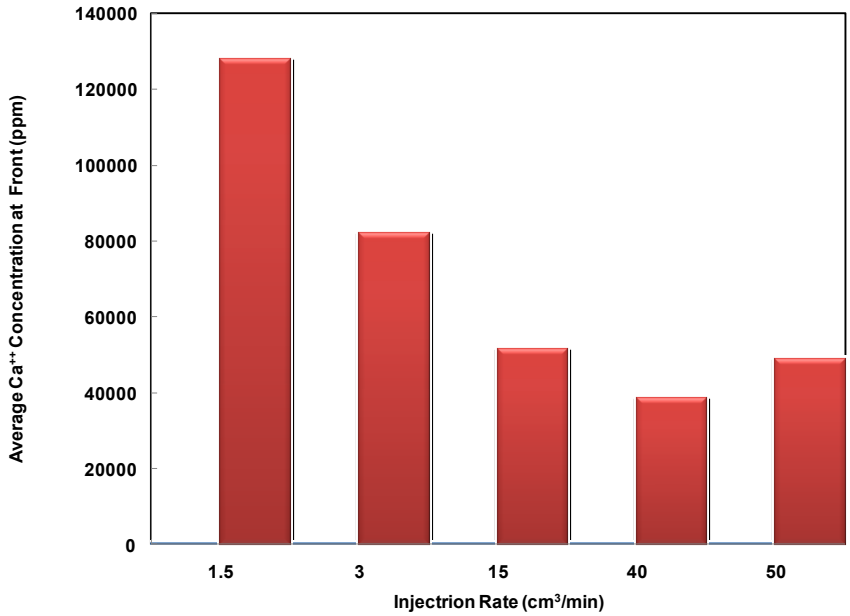


**Fig. 44— Average calcium concentrations measured in the spent acid zone as injection rate increases.**

## 6.2 Surfactant-Based Acid (Single Coreflood)

The same experiments performed for regular acid was repeated using surfactant-based acid. The objectives for performing this particular set of experiments can be summarized as follows: (1) describe the efficiency of surfactant-based acid in generating enough resistance to divert fluid; (2) investigate how the fluid front movement is critical to the gel formation; (3) establish the pore volume to breakthrough curve as a function of acid flux to determine the critical rate (rate at which maximum resistance is measured) relative to optimum injection rate; and (4) describe qualitatively the shape of the wormholes based on a 3-D images of the wormholes.

### 6.2.1 Efficiency of Diverting and Pressure Response

One major parameter to measure during an acidizing experiment is differential pressure across the entire core. Depending on the injection rate, as the acid enters the core at some point, Δp will increase as gel material forms inside the core. As pressure continue to increase, acid will be forced to change path and continue the wormhole process until faced with further resistance. Based on the pressure data collected in our study, this process will repeat itself as long as acid keeps being injected into an uninvaded zone.

Since the flow rate was kept constant in these experiments, two simultaneous mechanisms (in-situ viscosity and effective permeability) took place while acid was injected and they affected Δp differently. First, as the acid was injected, a wormhole was created, which increased the effective permeability of the core and decreased Δp. Second, as the acid propagated in the core and the surfactant entanglement built up viscosity, the pressure drop increased. Typically, the dominant mechanism will better reflect Δp by either lowering or increasing its value.

**Fig. 45** compares the normalized pressure drop as a function of pore volume injected until wormhole breakthrough for different injection rates. At a low injection rate, such as 3 $cm^3$/min, the results obtained in this experiment are essential to explaining a critical part of the process. The pressure drop increased by nearly 6-fold, compared with the initial pressure drop before acid was injected. Because of the large scale of the normalized pressure obtained at low flow rates (1.5 and 3 $cm^3$/min), the scale of the y-axis extended to a possible value of 10. Two things should be mentioned in terms of the pressure drop observed at 3 $cm^3$/min: first, the viscosity build-up occurred later, after the wormhole penetrated more than one foot inside the core; second, the pressure resistivity initiated from the viscosity build-up was very short in terms of time, which limits the efficiency of the diversion process. When the injection rate was decreased to 1.5 $cm^3$/min (experiment # 9), the pressure climbed almost 10-fold and the progression was more gradual. **Fig. 46** shows the calcium concentration measured in the effluent samples at a given injection rate.

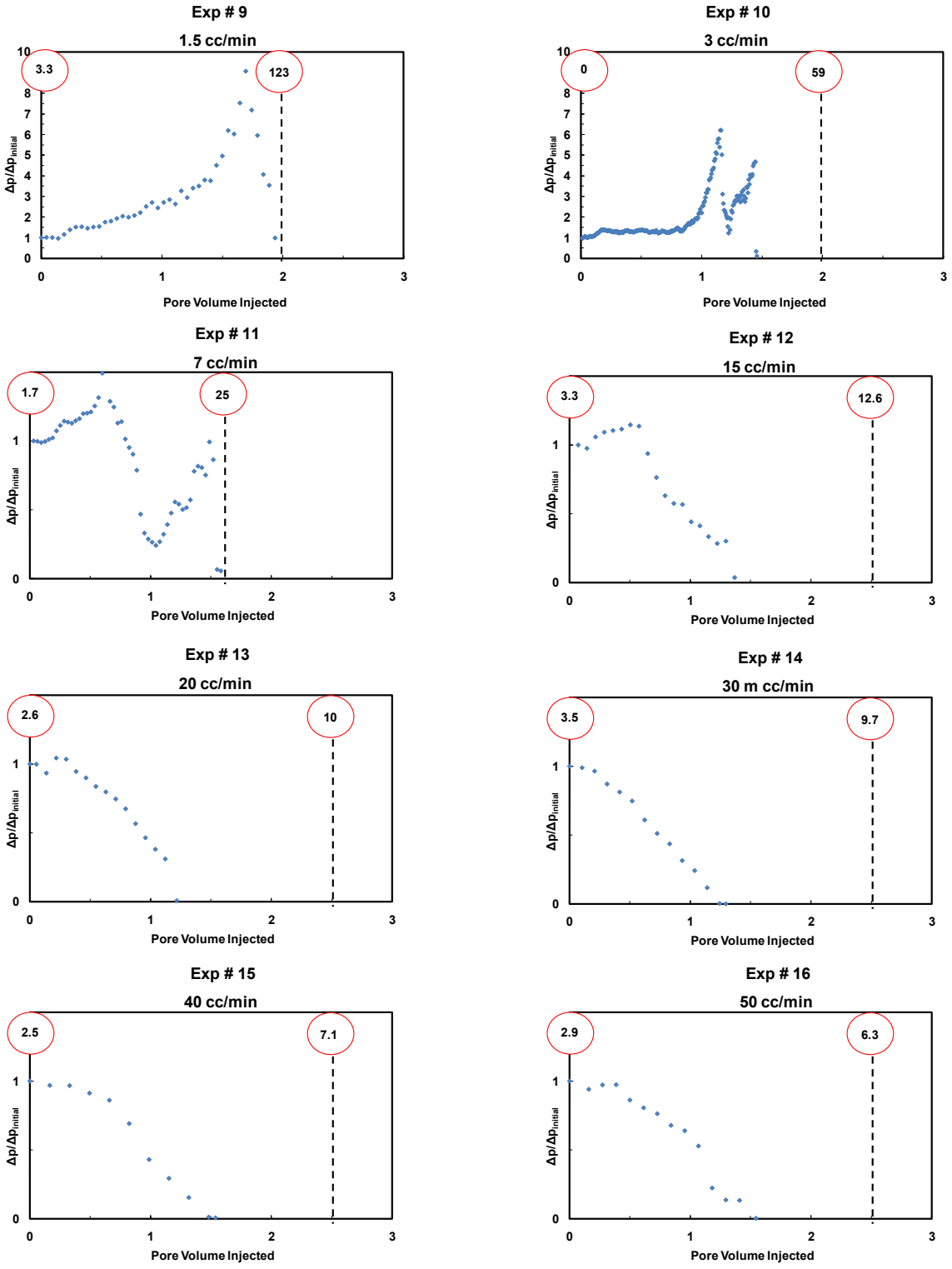


**Fig. 45— Normalized pressure drop as a function of pore volume injected until acid breakthrough; surfactant-based acid.**

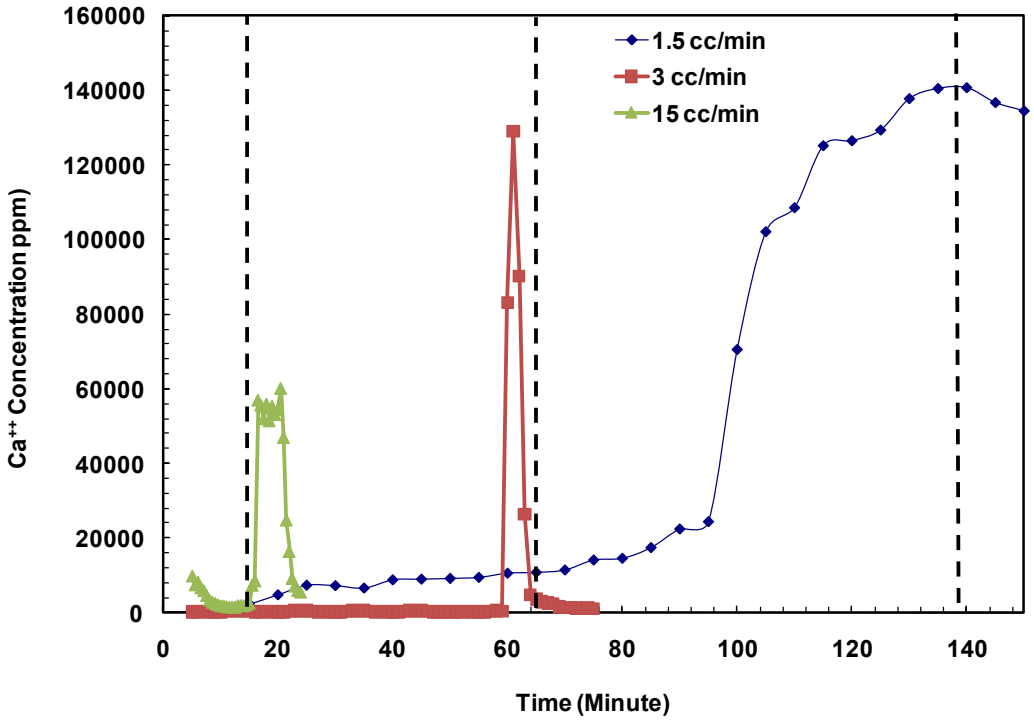


**Fig. 46— Calcium concentration measured in the effluent samples at three injection rates. Notice: dash lines corresponding to acid breakthrough time.**

At a high injection rate, such as 7 $cm^3$/min, there was slight increase in pressure drop observed after one pore volume of acid injection. Such increase in pressure drop can cause diversion to acid flow. However, to see the magnitude of the diversion, the scale of the pressure drop can be compared with previous experiments (experiments # 9 &10) were more pressure drop observed. Higher injection rates, including 15 and 20 $cm^3$/min and higher, resulted in no diversion taking place at any time during the acidizing process and the $\Delta p$ was similar to the one observed with regular acid.

### 6.2.2 Spent Acid Front Relative to the Gel Formation

In experiment #12, the acid injection rate was 15 $cm^3$/min. As described before, there was no pressure build-up observed at this injection rate. This can be explained by the fact that the amount of calcium dissolved ahead of the tip of the wormhole was not enough to trigger the surfactant to form gel material. This was proven in experiment # 4 where only 51,470 ppm of calcium concentration was measured in the effluent samples after wormhole breakthrough, which puts the fluid front behind the improved permeability front. Therefore, a high flow rate will reduce the effectiveness of the surfactant material to form micelles and no diversion will take place. Also, given that the in-situ viscosity is shear thinning, a higher injection rate will reduce the viscosity of any gel material that might form.

In the case where the acid injection rate was enough to allow the fluid front ahead of the improved permeability front, gel material formation was more effective. Obviously, the lower the injection rate, the better the diversion, as long as the acid injection rate is enough to create an effective wormhole.

## 6.3 Miscellaneous

### 6.3.1 Pore Volume to Breakthrough as a Function of Acid Flux

Plotting pore volume to breakthrough as a function of acid flux is an essential curve as it shows the optimum injection rate corresponding to minimum acid volume to be used in acid stimulation treatment. This curve is used widely in the petroleum industry as a guideline for optimizing acidizing treatments and is repeatedly reported as a concave up curve shape with an optimum injection rate for which the acid volume is a minimum.

Based on core geometry and the acid solution, the optimum injection rate for these experiments was estimated to be around 15 $cm^3$/min. **Fig. 47** compares both curves for each acid system. For flux above the optimum injection rate, and to some extent below the optimum injection rate, a greater quantity of surfactant-based acid, compared to regular acid, was needed to achieve the same wormhole penetration. For example, at a high flow rate, such as 15 $cm^3$/min, the pore volume injected was 20% higher when surfactant-based acid was used, compared to the case when 15 wt% HCl was injected. This can be explained by the fact that, at a higher injection rate, only a small fraction of acid will be spent on the wormhole wall and a large fraction of acid will reach the tip. The result will be a highly branched, high-density wormhole pattern, comprising a thin wormhole, eventually more acid required. On the other hand, at very low injection rates, such as 3 or even 1.5 $cm^3$/min--which correspond to acid fluxes of 16 and 8 ($cm^3$/hr/$cm^2$) respectively--less surfactant-based acid is required to achieve the same wormhole penetration. This can be correlated to the viscosity build-up observed at low injection rates, which reduces the leak-off perpendicular to the main flow direction. At the same time, at low injection rate, the wormhole will have less branching compared to highly branched wormhole at high injection, therefore less acid required to reach the same depth of penetration.

At a higher injection rate, only a small fraction of acid will be spent on the wormhole wall and a large fraction of acid will reach the tip. The result will be a highly branched, high-density wormhole pattern, comprising a thin wormhole.

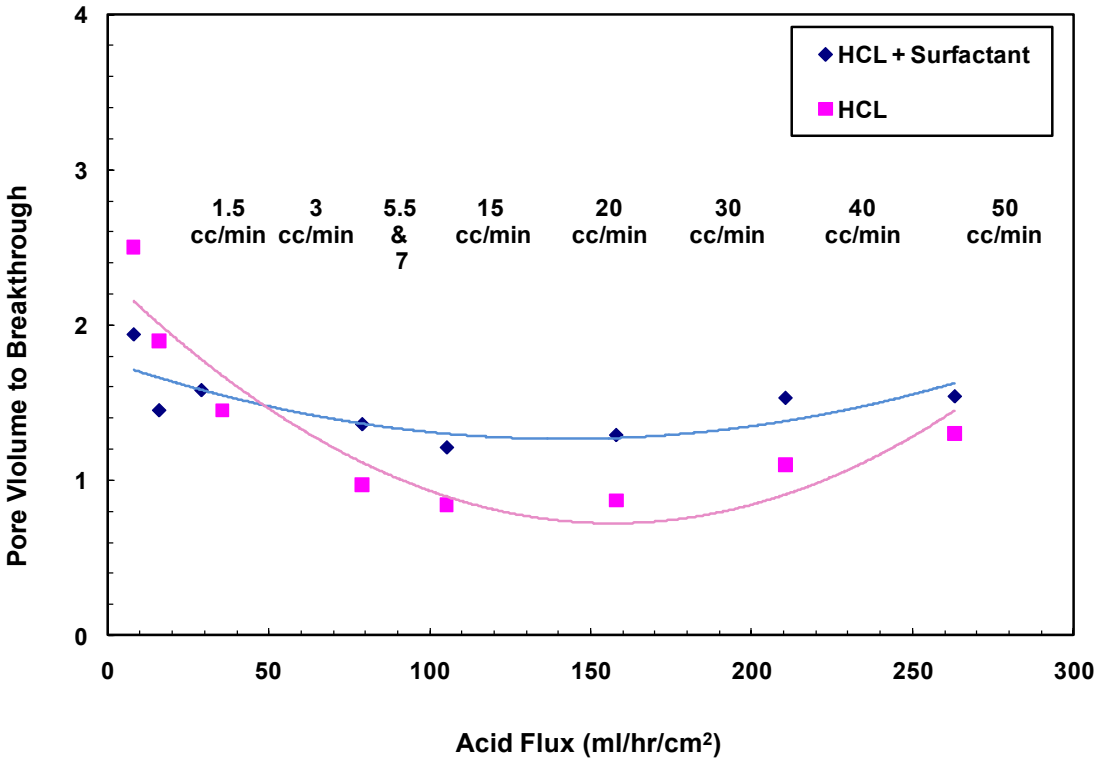


**Fig. 47— Comparing Pore volume to breakthrough as a function of acid flux for both regular acid and surfactant-based acid. Data were fitted using polynomial of order 2.**

### 6.3.2 Shape of the Wormhole

**Fig. 48** shows a 3-D image of the wormhole's shape for each individual core when regular acid is used as the acidizing fluid. As acid injection decreased, the wormhole path became more tortuous, compared with the straighter wormhole path as acid injection rate increased significantly. The diameter of the wormhole was found to be relatively uniform across a wide range of injection rates, with some exceptions. For example, at an injection rate of 3 $cm^3$/min, the wormhole diameter was observed to be almost constant throughout the first half of core length and measured to be 0.22 inches.

However, the diameter of the wormhole at the second half of the core was significantly smaller than the diameter of the wormhole at the first half of the core; this was not observed at higher flow rates. The diameter of the wormhole in the second half of the core at an injection rate of 3 $cm^3$/min was measured to be 0.11 inches. Clearly, at 3 $cm^3$/min, the wormhole tended to be thinner as the wormhole propagated further inside the core until acid breakthrough. This is an example of conical type shape of wormhole. This is because at low injection rates, by the time acid reaches the tip of the wormhole, most live acid has been reacted in earlier stages causing the inlet of the wormhole to enlarge with less reactive acid reaching the tip of the wormhole. Also, a significant amount of acid leaks off as the acid injection decreases.

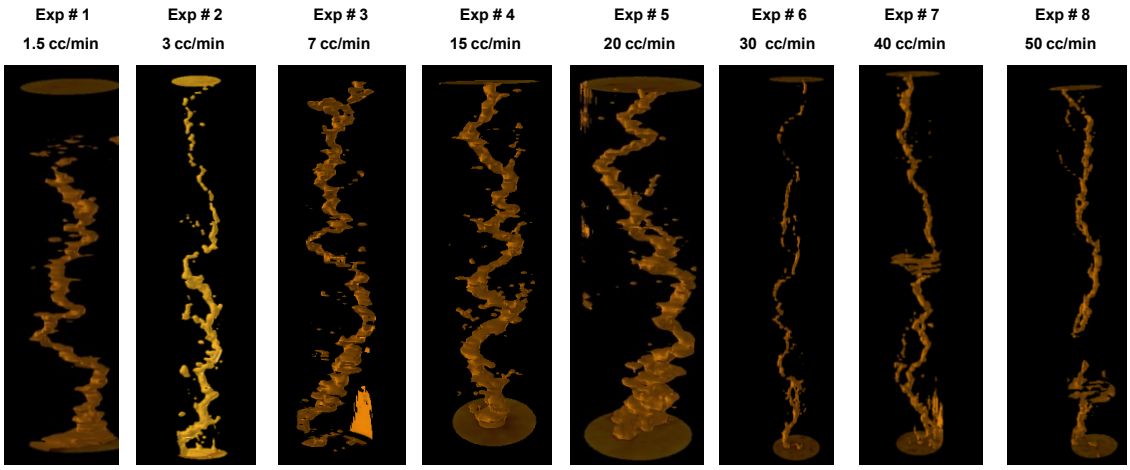


**Fig. 48— Shape of the wormhole at different flow rates; regular acid.**

**Fig. 49** shows a 3-D image for the shape of the wormhole for each individual core when surfactant-based acid is used as the acidizing fluid. The wormhole path observed when surfactant-based acid is injected tended to change direction several times to avoid blockages caused by the diverting material. In the case where conventional acid

was used, the wormhole shape did not show a similar pattern and the wormhole shape was almost linear with the direction of flow except at low injection rates, as explained earlier. The tortuosity was very pronounced at low injection rates where significant pressure build-up was measured across the core. This is another indication of gel formation inside the core.

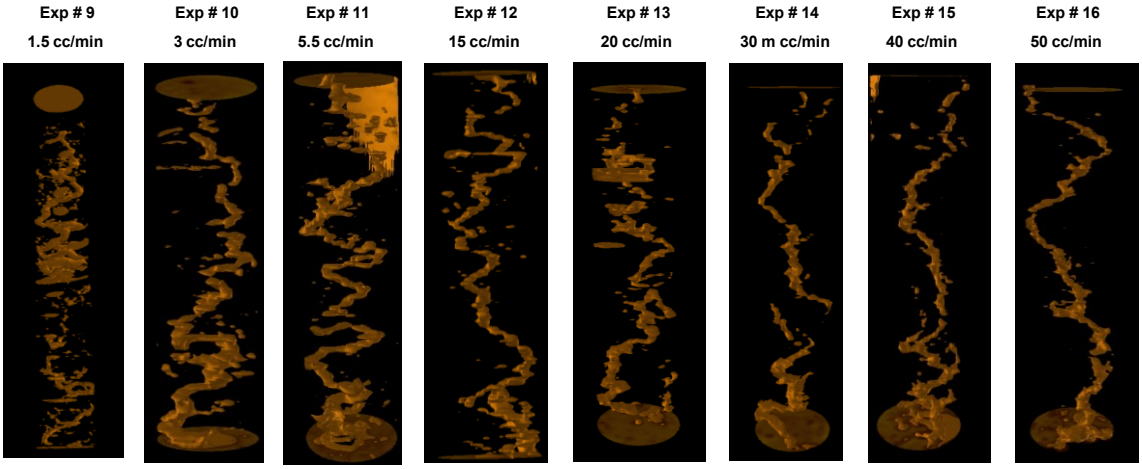


**Fig. 49— Shape of the wormhole at different flow rates; surfactant-based acid.**

The shape of the wormhole for experiment # 9 & 10 was reprocessed using better 3-D image software. **Fig. 50 & 51** shows the shape of the wormhole each experiment respectively. Notice in **Fig. 50** the wormhole stop to grow in the axial direction and any further injection of acid will enlarge the conical shape. However, in our case we have to stop the experiment to prevent any possible collapse in the core. At the same time, **Fig. 51** shows the conical shape observed at low injection rate such as 3 $cm^3$/min.

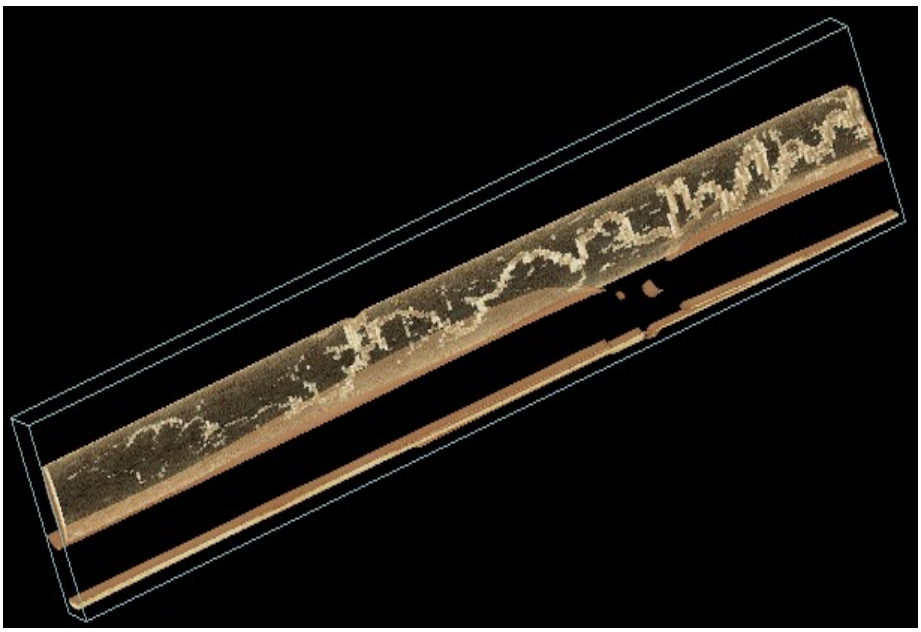

**Fig. 50— Shape of the wormhole at 1.5 $cm^3$/min.**

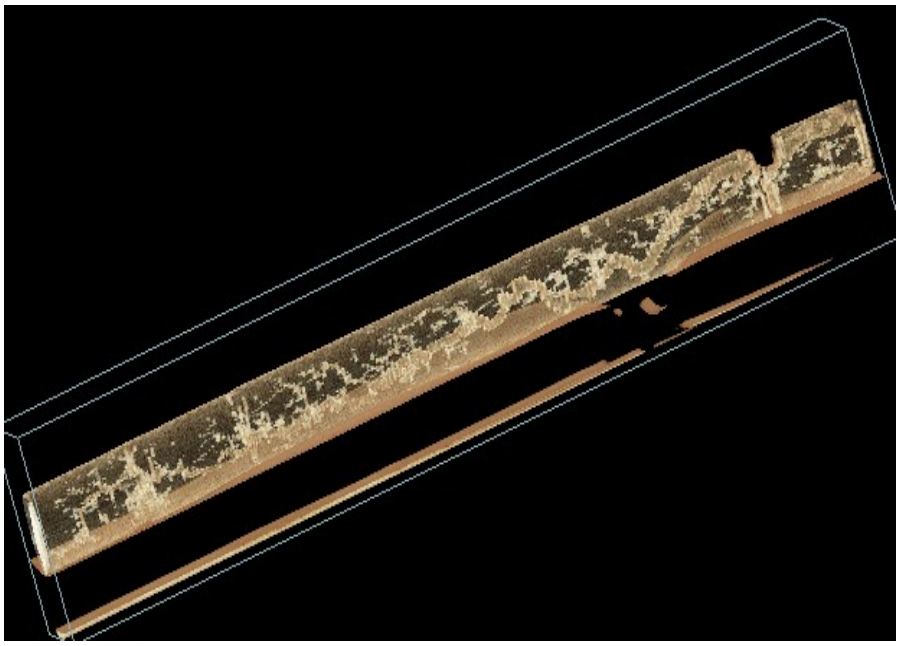

**Fig. 51— Conical shape observed at injection rate of at 3 $cm^3$/min.**

### 6.4 Parallel Coreflood Experiment

Next, five experiments were performed using 15 wt% HCl + 7.5 vol% surfactant + 0.3 vol% corrosion inhibitor injected into parallel limestone cores. The results are presented in two parts. First, two experiments will confirm that no diversion takes place if the injection rate is above the critical rate. Second, three experiments will investigate the effects of the initial permeability ratio on the diversion process when acid is injected at the critical rate. For parallel coreflood experiments, **Table 10** includes the permeability, permeability ratio, total flow rate, and initial flow rate entering each core.

**TABLE 10— SUMMARY OF PARALLEL COREFLOOD EXPERIMENTS, SURFACTANT-BASED ACID.**

| Experiment # | Initial $k_1$ (md) | Initial $k_2$ (md) | Permeability Ratio | Total Injection Rate ($cm^3$/min) | Initial $q_1$ ($cm^3$/mi) | Initial $q_2$ ($cm^3$/mi) |
|---|---|---|---|---|---|---|
| **Acid Injection above Critical Rate** | | | | | | |
| 17 | 74 | 50 | 1.5 | 10 | 6 | 4 |
| 18 | 72 | 6 | 12 | 7 | 6 | 1 |
| **Acid Injection at Critical Rate** | | | | | | |
| 19 | 96 | 56 | 1.7 | 7 | 3.8 | 2.5 |
| 20 | 115 | 26 | 4.4 | 4.5 | 3.5 | 1 |
| 21 | 88 | 7 | 12.5 | 3 | 2.8 | 0.2 |

#### 6.4.1 Acid Injection above Critical Rate

Experiment #17 illustrates the flow of diverting material in a low contrast environment ($k_1/k_2$ = 1.5). Experiment #18 was conducted at high contrast in permeability ($k_1/k_2$ = 12). Notice, in both experiments, the acid flow rate entering the higher permeability core was around 6 $cm^3$/min.

In experiment #17, the total injection rate selected was 10 $cm^3$/min, to magnify the effects of the high injection rate in a low initial contrast in permeability. After acid injection, the average Δp measurement for the first six minutes was relatively constant. Then Δp started to decline as the wormhole propagated further. The fast injection rate accelerated the wormhole propagation, as indicated by the continuous decrease in Δp until breakthrough occurred. **Fig. 52** shows the acid flow rate entering each core and the corresponding Δp measurement across the core as a function of time until acid breakthrough. The results obtained from Δp measurement and flow rate were in agreement with the CT scan results. **Fig. 53** shows a 3-D image for the wormholes created in both cores. Clearly, the wormhole penetrated the entire high permeability core, with 50% penetration in the lower permeability core.

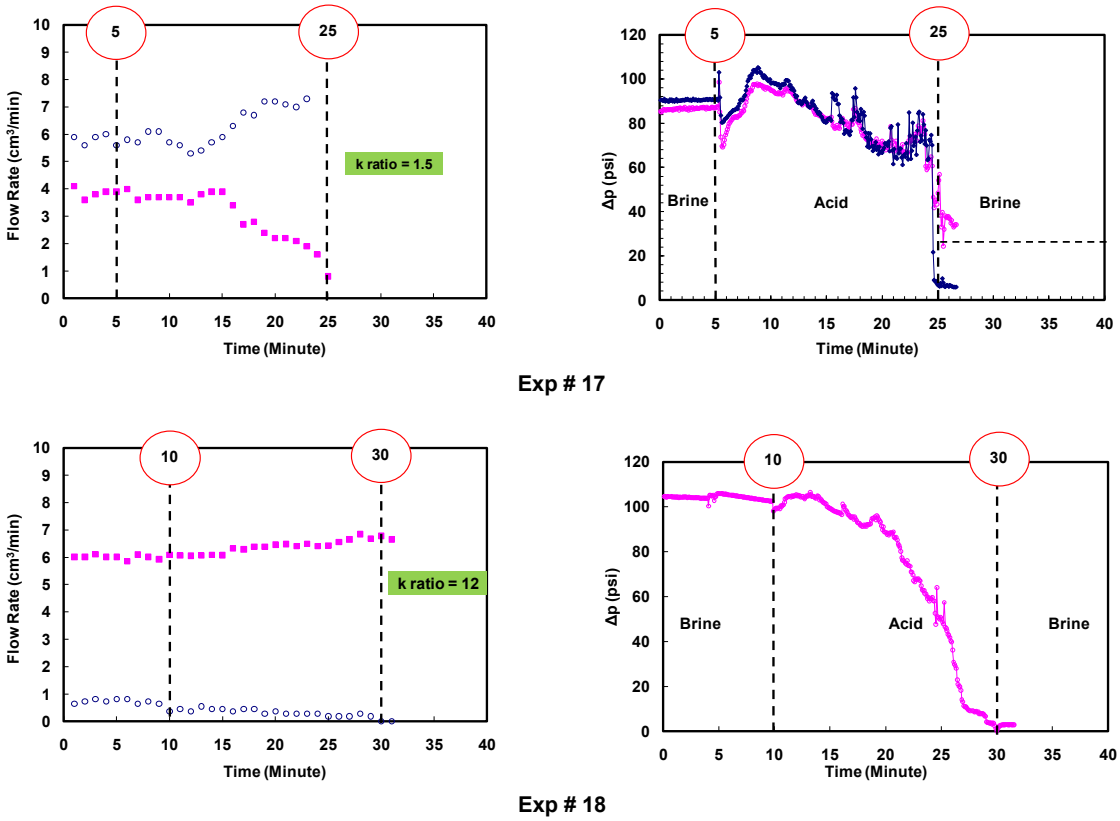


**Fig. 52— Distribution of flow rate in each core; surfactant-based acid combined with the corresponding pressure drop measured across each core.**

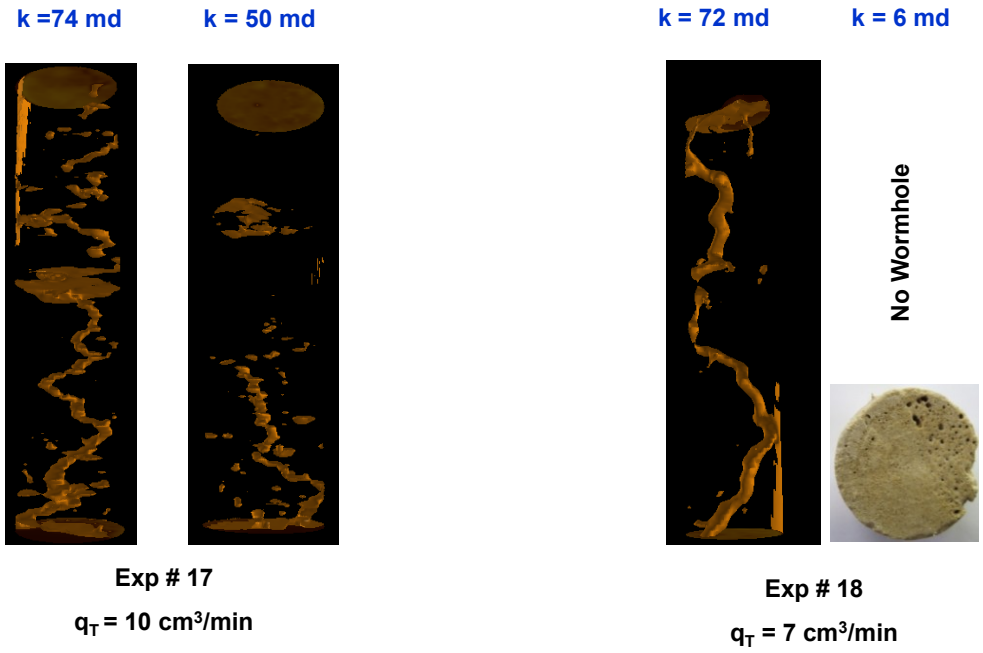


**Fig. 53— 3-D image for the wormholes created in each core.**

Experiment #18 represents high contrast in permeability ratio (72 : 6); the Δp started to decline gradually five minutes after the beginning of acid injection. The pressure decline indicated no major diverting process taking place; otherwise, pressure build-up would be observed, reflecting an increase in apparent viscosity. As a result of the high initial contrast and the absence of a gel formation, most of the acid entered the 72 md core, leaving the 6 md uninvaded. Less than 1 $cm^3$/min entered the tight core, which was not enough to initiate a wormhole. Neither the visual observation nor the CT image showed any wormhole created in the lower permeability core.

### 6.4.2 Acid Injection at Critical Rate

In the next three experiments, the total injection rate was selected to satisfy the condition where around 3 $cm^3$/min enters the higher initial permeability core. The idea was to obtain the maximum possible diversion in each case and be able to compare the results.

Experiment #19 represents low permeability ratio (96:56). Total acid injection rate was 7 $cm^3$/min. **Fig. 54** shows the measured Δp across the core as a function of time until acid breakthrough first in the 56 md core (relatively low permeability). After 27 minutes, the Δp started to increase dramatically as a result of gel formation. The Δp continued to build up until the wormhole propagated further, which caused the Δp to stabilize and decline until acid breakthrough. Another interesting observation is related to the breakthrough time. Apparently, the diverting material not only diverted the flow from the higher to the lower permeability core, it also allowed the wormhole to propagate faster in the lower permeability core, as indicated by earlier breakthrough. This was not surprising, considering the low initial permeability contrast. The real challenge was to divert the fluid, given the higher initial permeability contrast, to be discussed in the next two experiments. **Fig. 55** shows a 3-D image of the wormhole for both cores. In experiment #19, the wormhole propagated more than 80% in the 96 md core before breakthrough occurred in the lower permeability core.

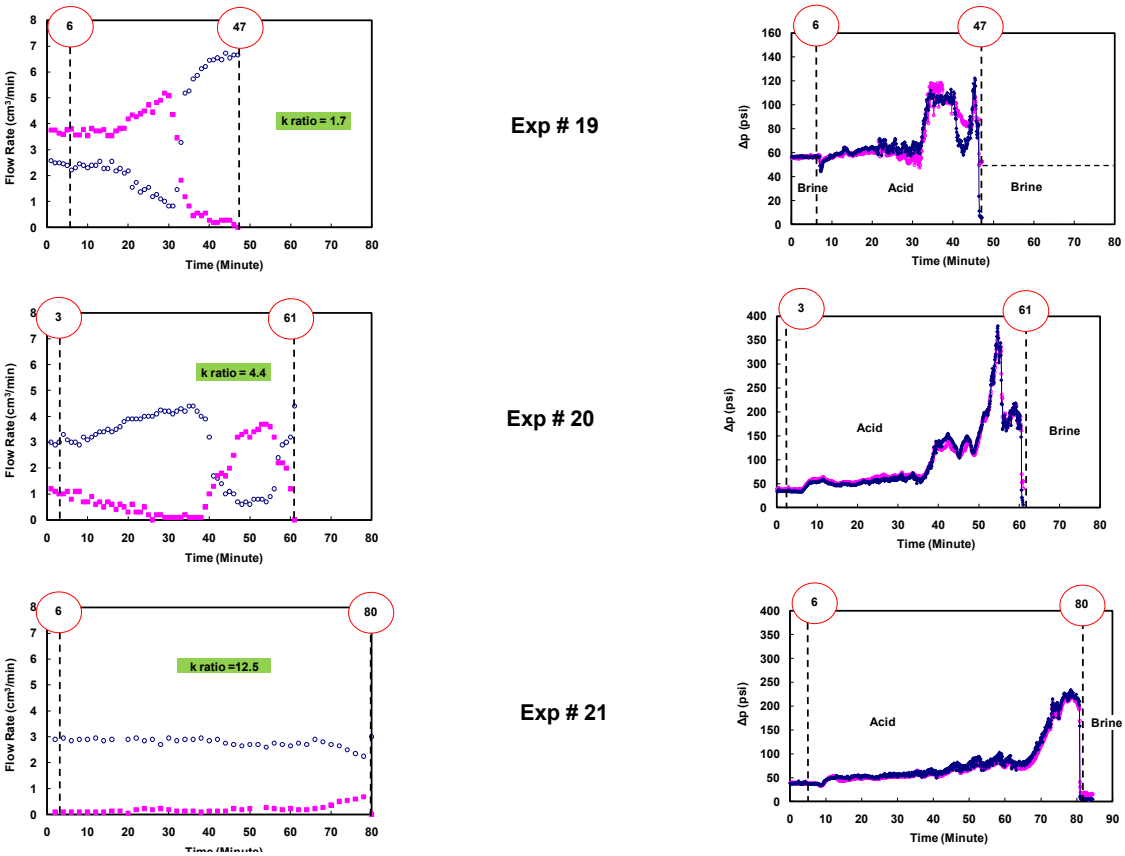


**Fig. 54— Distribution of flow rate in each core; surfactant-based acid combined with the corresponding pressure drop measured across each core.**

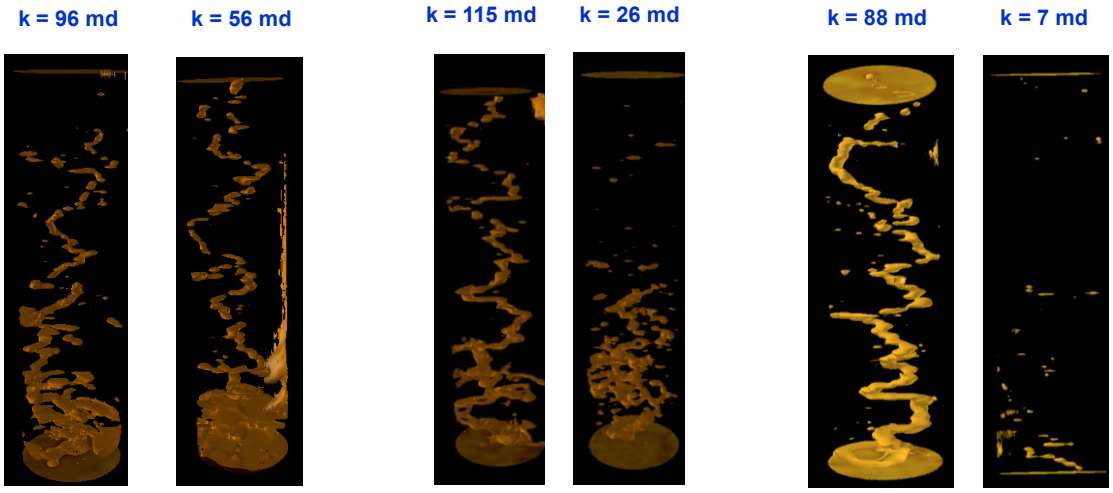


**Fig. 55— 3-D image for the wormholes created in each core.**

As the initial contrast increases, higher Δp is required to alter the tendency of the fluid system to enter the easy path. This was demonstrated in experiment #20 where the core samples were selected for higher initial permeability contrast. The pressure measurement indicates significant pressure build-up that allowed the acid to divert from the 115 md to the 26 md. The CT scan shows that the wormhole penetrated halfway through the 26 md, which still represents significant improvement in the acid diversion process.

The last experiment demonstrates that with very high contrast in initial permeability, even if acid is injected at the critical rate, it will not be sufficient to divert the fluid. During experiment #21, almost the entire amount of acid fluid entered the higher permeability core with limited amount of acid entering the 7 md core. Pressure build-up occurred in the last 10 minutes before wormhole breakthrough. The 7 md core started to accumulate acid fluid at a later time, but it was only enough to create a couple of inches of wormhole inside the core. Due to limited core length, a longer core is required for better understanding about whether there will be diversion if the initial ratio exceeds 10.

# CHAPTER VII

# CONCLUSIONS

During this study, using a longer core was essential to capturing a more realistic picture of the overall process. The acid injection rate was found to be a key parameter for characterizing the correlation between spent acid fronts relative to the improved permeability front. This was evident by measuring calcium content in the effluent samples as acid was injected inside the core. As acid was injected below the critical rate, more calcium was obtained ahead of the wormhole. For example, at 3 and 1.5 $cm^3$/min, the concentration was measured at 82,000 and 127,000 ppm respectively. Several conclusions obtained by performing straight acid experiments include:

- The slope of the linear relationship between $\Delta p$ and time was found to be a function of flow rate.
- Given the experimental parameters applied in this study, 3 $cm^3$/min was found to be a critical rate where the position of the spent acid front comes ahead of the improved permeability front.
- The amount of calcium measured in the effluent samples suggests that, if the acid is injected low enough below the optimum rate, it would allow the acid filtrate to extend further ahead of the wormhole.

Single coreflood experiments were performed using surfactant-based acid to verify certain conclusions reached from performing straight acid experiments. The viscosity build-up was correlated to calcium concentration and the position of the spent

acid front relative to the improved permeability front was delineated. Major findings are summarized as follows:

- Pressure drops across the core show a non-linear relationship between Δp and time when surfactant-based acid flows in porous media, contradicting the linear correlation observed when regular acid is used.
- The build-up in viscosity does not occur immediately, as enough calcium has to be dissolved to form the micelles.
- Acid will remain strong inside the wormhole and that eliminates the possibility for gel to form inside the wormhole. However, it is very important to keep in mind that the acid consumed changes with position.
- The acid injection rate was found to be a critical parameter in maximizing the efficiency of using surfactant-based acids as a diverting chemical.
- The pressure build-up increased by more than 5-fold at low rates such as 3 $cm^3$/min, compared with no pressure build-up at high injection rates.
- The maximum pressure measured across the core was obtained with experiment #9, where the acid injection rate was 1.5 $cm^3$/min, resulting in a 9-fold increase on a normalized scale.
- The maximum apparent viscosity generated during the acidizing process occurred over a narrow range of acid injection rates. Higher injection rates were not effective in enhancing the acidizing process, and the use of diverting material produced results similar to those of regular acids.

To confirm the results obtained from single coreflood experiments, parallel coreflood experiments were conducted using surfactant-based acid:

- Diversion and fluid placement is more important than trying to determine the optimum injection rate.
- The use of surfactant-based acid was also found to be constrained by the scale of the initial permeability ratio. For permeability ratios greater than about 10, diversion was insufficient.
- For permeability ratios greater than 10-fold, acid placement treatment needs to be designed more carefully.

Based on our analysis, surfactant-based acid can be used as a means of diverting material with some precautions depending on the target candidate. Some useful tips can be used as guidelines for achieving more effective diversion, including:

- For permeability ratios greater than 10-fold, there are two ways to obtain diversion:
    1. Inject for a long period at a critical rate, in this case the wormhole target has to be longer than 2 feet (long wormhole).
    2. Inject acid as low as possible but use enough to generate a wormhole; this implies that faster gel formation and maximum resistance can be obtained. However, depth of penetration will be limited to 2 feet.
- At very low permeability contrast, such as 1.5 ~ 2.5, gel is most likely to form in both permeability zones simultaneously. To overcome this problem, alternating

straight acid with surfactant-based acid will create an artificial contrast and result in better diversion.

- Finally, ratios between 2.5 and 8 will be perfect candidates to use surfactant-based acid

There are several ways to improve the use of a surfactant as diverting agent. Considering the limitations observed in this study, any new class of surfactant can be more efficient if at least one of the following criteria improves:

- Surfactants that can be triggered faster;
- Surfactants that form a more sustainable gel that can last longer;
- Surfactants that can provide stronger physical properties, mainly Rheology, so permeability constraints can be overcome; or
- Surfactants that will result in better cleanup.

# NOMENCLATURE

$A$ : cross sectional area, $cm^2$

$B_n$ : Eigen functions

$C$ : acid concentration in the fluid, weight of acid/weight of fluid

$C_{avg}$ : mean acid concentration, weight of acid/weight of fluid

$C_D$ : dimensionless acid concentration, $C/C_o$

$C_o$ : inlet acid concentration, weight of acid/weight of fluid

$d$ : diameter of the core, cm

$D$ : diffusion coefficient, $cm^2/s$

$f$ : function to be determined, Hung (1987).

$k$ : permeability of the core, md

$L$ : length of the core, cm

$L_{wh}$ : length of the wormhole, cm

$N_{Pew}$ : Peclet number = $v_w r_{wh} /D$

$N_{Re}$ : Reynolds number at the wormhole inlet = $u(0) r_{wh} /\nu$

$N_{Rew}$ : Reynolds number at wormhole wall = $v_w r_{wh} /\nu$

$PV_{bt}$ : pore volume at breakthrough

$p_e$ : effluent pressure, psi

$q$ : injection flow rate, $cm^3/min$

$q_T$ : total injection flow rate, $cm^3/min$

$q_1$ : injection flow rate in core-1, $cm^3/min$

$q_2$ : injection flow rate in core-2, $cm^3/min$

r : radius of the core, cm

$r_{wh}$ : wormhole radius, cm

U : fluid velocity in the x direction, cm/s

U(0) : average velocity at the inlet, cm/s

V : fluid velocity in the r direction, cm/s

$\nu_w$ : fluid velocity at the wormhole wall, cm/s

$\mu$ : viscosity, cp

$\beta$ : $(\pi/4\ d^2_{core}\ \Phi)$, $cm^2$

$\phi$ : porosity of the core, percentage

$\zeta$ : dimensionless radial coordinate= $r/r_{wh}$

$\xi$ : dimensionless axial coordinate = $x/r_{wh}$

$\eta$ : $r^2/r^2_w$

$\lambda_n$ : eigen value corresponding to Eigen function $B_n$

$\mu$ : fluid dynamic viscosity, cp

$\nu$ : fluid kinematic viscosity, $\mu/\rho$

# REFERENCES

Abou-Sayed, I. S., C. E. Shuhart and M. Gong, 2005. Well Stimulation for Thick Carbonate Reservoirs. Paper SPE 10647 presented at the 2005 International Petroleum Technology Conference, Doha, Qatar, 21-23 November.

Akin, S., and Kovscek, A.R. 2003. Computed tomography in petroleum research. In: Mees, F., Swennen, R., Van Geet, M., Jacobs P. (eds.), *Application of X-ray Computed Tomography in the Geosciences*, 23-28, Geological Society of London, UK.

Auzerais, F.M., Dussan, E.B., and Reischer, A.J. 1991. Computed Tomography for the Quantitative Characterization of Flow Through a Porous Medium. Paper SPE 22595 presented at the 65th SPE Annual Technical Conference, Dallas, TX, 6-9 October.

Bazin, B., Bieber, M.T., Roque, C., and Boutéca, M. 2001. Improvement in the Characterization of the Acid Wormholing by "In Situ" X-Ray CT Visualizations. Paper SPE 31073 presented at the SPE International Symposium on Formation Damage Control, Lafayette, LA, 14-15 February.

Buijse, M.A. 1997. Understanding Wormholing Mechanisms Can Improve Acid Treatments in Carbonate Formations. *SPEPF* **15**: 168-175.

Chang, F., Qu, Q. and Frenier, W. 2001. A Novel Self-Diverting-Acid Developed for Matrix Stimulation of Carbonate Reservoirs. Paper SPE 65033 presented at the

SPE International Symposium on Oilfield Chemistry, Houston, TX, 13-16 February.

Chang, F.F., Love, C., Affeld, C.J., Blevins, J.B., Thomas, R.L., and Fu, D.K. 1999. Case Study of a Novel Acid-Diversion Technique in Carbonate Reservoirs. Paper SPE 56529 presented at the 1999 SPE Annual Technical Conference and Exhibition, Houston, TX, 3-6 October.

Daccord, G., and Lenormand, R. 1987. Fractal Patterns from Chemical Dissolution. Nature **325**: 41-43.

Daccord, G., Lenormand, R., and Lietard, O. 1993. Chemical Dissolution of a Porous Medium by a Reactive Fluid - I. Model for the "Wormholing" Phenomenon, *Chem. Eng. Sci.* **48**, 169-178.

Delshad, M., Kim, D.H., Magbagbeola, O.A., Huh, C., Pope, G.A., and Tarahhom, F. 2008. Mechanistic Interpretation and Utilization of Viscoelastic Behavior of Polymer Solutions for Improved Polymer-Flood Efficiency. Paper SPE 113620 presented at the SPE/DOE Improved Oil Recovery Symposium, Tulsa, OK, 19-23 April.

Economides, M.J., Hill, A.D., and Ehlig-Economides, C.E. 1994. *Petroleum Production Systems*, NJ: Prentice-Hall.

Fredd, C.N. and Fogler, H.S. 1998. Influence of Transport and Reaction on Wormhole Formation in Porous Media, *AIChE J.*, **44**, 1933-1949.

Fredd, C.N., and Fogler, H.S. 1999. Optimum Conditions for Wormhole Formation in Carbonate Porous Media: Influence of Transport and Reaction, *SPE J.*, **4**, 196-205.

Frick, T. P., Mostofizadeh, B., and Economides, M. J. 1994. Analysis of Radial Core Experiments for Hydrochloric Acid Interaction with Limestones. Paper SPE 27402 presented at the SPE International Symposium on Formation Damage Control, Lafayette, LA, 7-10 February.

Gdanski, R. D. 1999. A Fundamentally New Model of Acid Wormholing in Carbonates. Paper SPE 54719 presented at the European Formation Damage Conference held in The Hague, The Netherlands, May 31-June 1.

Glasbergen, G., and Kalia, N. 2009. The Optimum Injection Rate for Wormhole Propagation: Myth or Reality. Paper SPE 121464 presented at the European Formation Damage Conference, Scheveningen, The Netherlands, 27-29 May.

Hoefner, M.L. and Fogler, H.S. 1985. Effective Matrix Acidizing in Carbonates Using Microemulsions, *Chem. Eng. Prog.*, **40**, 40-44.

Hoefner, M.L. and Fogler, H.S. 1988. Pore Evolution and Channel Formation During Flow and Reaction in Porous Media, *AIChE J.* **34**, 45-54.

Huang, T., Zhu, D. and Hill, A.D. 1999. Prediction of Wormhole Population Density in Carbonate Matrix Acidizing. Paper SPE 54723 presented at the European Formation Damage Conference, Hague, The Netherlands, 31 May-01 June.

Hung, K.M. 1987. Modeling of Wormhole Behavior in Carbonate Acidizing. Ph.D. dissertation. University of Texas at Austin.

Hutchins, R.D., Dovan, H.T., Sandiford, B.B., 1996. Field Applications of High Temperature Organic Gels for Water Control. Paper SPE-DOE 35444 presented at the 10th SPE-DOE Improved Oil Recovery Symposium, Tulsa, OK, April 21–24.

Lockhart, T.P., and Albonico, P., 1992. New Chemistry for the Placements of Chromium (III)/Polymer Gels in High-Temperature Reservoirs. Paper SPE-DOE 24194, presented at the SPE-DOE Eight Symposium on Enhanced Oil Recovery, Tulsa, OK, April 22–24.

Lund, K., H.S. Fogler, C.C. McCune, and Ault, J.W. 1975. Acidization - II. The Dissolution of Calcite in Hydrochloric Acid, *Chem. Eng. Sci.* **30**, 825-835.

Lund, K., H.S. Fogler, and McCune, C.C. 1973. Acidization - I. The Dissolution of Dolomite in Hydrochloric Acid, *Chem. Eng. Sci.* **28**, 691-700.

Lungwitz, B., Fredd, C., Brady, M., Miller, M., Ali, S., and Hughes, K. 2006. Diversion and Cleanup of Viscoelastic Surfactant-Based Self-Diverting Acid. *SPEPO* **22**: 127-121.

Moradi-Araghi, A., Beardmore, D.H., and Stahl, G.A., 1988. "The application of gels in enhanced oil recovery: theory, polymers and cross-linker systems." In: Stahl, G.A., Schulz, D.N. (Eds.), *Water-Soluble Polymers for Petroleum Recovery*. 299–312, Plenum, New York.

Nasr-El-Din, H.A., Chesson, J.B., Cawiezel, K.E. and Devine, C.S. 2006. Field Success in Carbonate Acid Diversion, Utilizing Laboratory Data Generated by Parallel

Flow Testing. Paper SPE 102828 presented at the SPE Annual Technical Conference and Exhibition, San Antonio, TX, 24-27 September.

Nasr-El-Din, H.A., Al-Ghamdi, A.H., Al-Qahtani, A.A., and Samuel, M.M. 2008. Impact of Acid Additives on the Rheological Properties of Viscoelastic Surfactants. *SPEJ*, **13**(1) 35-47.

Nasr-El-Din, H.A., Al-Nakhli, A., Leopoldo, S., Walton, T., and Van Domelen, M. 2009. Optimization of Surfactant-based Fluids for Acid Diversion. *SPEPO*, **24**(1) 124-134.

Pichler, T., Frick, T.P., and Economides, M.J., 1992. Stochastic Modeling of Wormhole Growth in Carbonate Acidizing. Paper SPE 25004 presented at the European Petroleum Conference, Cannes, France, 16-18 November.

Schechter, R.S.1992. *Oil Well Stimulation,* Englewood Cliffs, NJ, Prentice Hall.

Shimizu, I., Itachida, O., Kobayashi, O., Haq, S., Nepia, P., Ajaj, M., and Brady, M. 2005. Surfactant-Based Self-Diverting Acid System Maximizes Acid Coverage and Eliminates Flowback in an Openhole Horizontal Injection Well Offshore Qatar. Paper IPTC 10445 presented at the 2005 International Petroleum Technology Conference, Doha, Qatar, 21-23 November.

Sydansk, R.D., 1995. "Process for Reducing Permeability in a High Temperature Subterranean Hydrocarbon-bearing Formation Utilizing a Decarboxylated Cross-linking Agent." US Patent 5,431,226, July 11.

Talbot, M.S., and Gadanski, R.D. 2008. Beyond the Damkoler Number: A New Interpretation of Carbonate Wormholing. Paper SPE 113042 presented at the Europec/EAGE Annual Conference, Rome, Italy, 9-12 June.

Tardy, P.M., Lecerf, B., and Christanti, Y. 2007. An Experimentally Validated Wormhole Model for Self-Diverting and Conventional Acids in Carbonate Rocks Under Radial Flow Conditions. Paper SPE 107854 presented at the European Formation Damage Conference, Scheveningen, The Netherlands, 30 May-01 June.

Taylor, K.C., Al-Ghamdi, A.H., and Nasr-El-Din, H.A.2004. Measurement of Acid Reaction Rates of a Deep Dolomitic Gas Reservoir. *JCPT* **43** (10): 1-8.

William, B., J. Gidley, and R. Schechter, 1979. *Acidizing Fundamentals*, Richardson, TX: SPE Monograph Series.

Yuan, S.W., and Finkelstein, A.B. 1956. Laminar Pipe Flow with Injection and Suction through Porous Walls. Trans. *ASME* **78**: 1719-1724.

# VITA

Abdulwahab Hussain A. Alghamdi is a petroleum engineer with Saudi Aramco Oil Company at the EXPEC Advance Research Center. He received his B.S. in chemical engineering from King Fahd University of Petroleum & Minerals in 2001. He entered the graduate program at Texas A&M University in September 2004 and received his M.S. in May 2006, and his Ph.D. in December 2010 in petroleum engineering. His research interests include: acid diversion, reaction kinetics, surface tension measurement, Rheology of visco-elastic surfactant, and acid fracturing

Mr. Abdulwahab may be reached at Aramco Oil Company, Dhahran 31311, P.O.BOX 8028, Saudi Arabia. His email is Abdulwahab.Ghamdi@aramcoservices.com